Stratigraphy and Isotope Geochemistry of the pre-Sturtian Ugab Subgroup, Otavi Group, northwestern Namibia

Kelsey G. Lamothe
Department of Earth and Planetary Sciences
McGill University, Montreal

Supervisor: Professor Galen Halverson

April 2018

A thesis submitted to McGill University in partial fulfillment of the requirements of the degree of Master of Science

Table of Contents

Chapter 2

Figures List

Tables List

Abstract

The pre-Sturtian Islay anomaly is a negative carbon isotope excursion that has been documented globally, and recent work in northern Canada and Scotland has led to the suggestion that there may be two distinct negative anomalies, an older one ca. 739 Ma and a younger one ca. 720 Ma, both being assigned to the Islay anomaly. Here we investigate the litho- and chemo-stratigraphy of the pre-Sturtian Ugab Subgroup of the Otavi Group in northwestern Namibia. Carbon isotope data from two separate outcrop belts, the Summas Mountains and the Vrede Domes, indicate that the Ugab Subgroup strata exposed in the former inlier are older than those of the latter, with only approximately 100 metres of stratigraphic overlap. We use detailed measured sections to develop a sequence stratigraphic framework for the Ugab Subgroup in each outcrop belt, and correlate strata across the two exposures to construct a composite $\delta^{13}C$ record. This carbon isotope profile of the Ugab Subgroup shows two separate pre-Sturtian negative anomalies, consistent with the findings in northern Canada and Scotland. Our results are an important contribution to the pre-Cryogenian carbon isotope record, as this data may serve as the first definitive documentation of both anomalies within a single basin.

Abstract (French)

L'anomalie pré-sturtienne d'Islay est une excursion négative du δ^{13}C qui a été documentée à l'échelle mondiale. Des travaux récents dans le nord du Canada et en Écosse ont suggéré qu'il pourrait y avoir deux anomalies négatives distinctes, une plus ancienne d'environ 739 Ma et une plus jeune d'environ 720 Ma, les deux étant attribuées à l'anomalie d'Islay. Cette étude se focalise sur la litho-chimio-stratigraphie du sous-groupe pré-sturtien Ugab du groupe Otavi situé dans le nord-ouest de la Namibie. Les données isotopiques de carbone des strates du sous-groupe Ugab exposées dans les monts Summas indiquent qu'elles sont plus anciennes que celles présentes aux dômes de Vrede avec seulement ~100 mètres de chevauchement stratigraphique. Nous utilisons des sections mesurées de façon détaillée pour développer un cadre de stratigraphie séquentielle pour le sous-groupe Ugab dans chaque bande d'affleurement. Ce cadre de stratigraphie séquentielle a pour but de corréler les deux affleurements afin de construire une courbe composite isotopique de δ^{13}C. Cette courbe isotopique de carbone du sous-groupe Ugab montre deux anomalies négatives distinctes d'âge pré-sturtienne, ce qui appuie les données obtenues dans le nord du Canada et en Écosse. Nos résultats constituent une contribution importante à l'enregistrement isotopique du carbone pré-cryogénien, car ces données représentent la première documentation des deux anomalies au sein d'un même bassin.

Acknowledgements

Firstly and most importantly, I would like to thank my supervisor, Galen Halverson, for the funding he provided for my research, and for his generosity, support, and incredible patience. I also owe a deep debt of gratitude to Paul Hoffman for his guidance in the field and for providing me access to the results of his past work in Namibia. Additionally, I would like to thank Thi Hao Bui for her help with C&O isotope analyses, Samuel LoBianco for his assistance during the 2016 field season, the Geological Survey of Namibia for their aid in acquiring the permits and visas necessary for field work, and the Precambrian Research Office at McGill (Sarah Worndle, Tim Gibson, Peter Crockford, Malcolm Hodgskiss, and Wilder Greenman) for useful discussions.

Contribution of Authors

This thesis was written by K. Lamothe and edited by G. Halverson. Field work in 2015 and 2016 (measuring stratigraphic sections and sampling carbonates) was carried out by K. Lamothe, P. Hoffman, G. Halverson, and S. LoBianco. Data from past seasons was provided by P. Hoffman. Carbon and oxygen isotope measurements were run by K. Lamothe, as taught by T.H. Bui, at McGill University.

CHAPTER 1

1.1 Introduction

The Neoproterozoic Era (1000-541 Ma) was a time of enormous climatic fluctuations that included at least two global glaciations, often termed 'Snowball Earth' events, each followed by extreme greenhouse conditions (Kirschvink 1992; Hoffman et al., 1998; etc.). The Neoproterozoic also records at least six globally correlative negative anomalies in the carbon isotope record, which are superimposed on a long-term baseline carbon isotope enrichment of ~5 ‰ that persisted until the Cambrian Period (~542 Ma) (Halverson et al., 2005) (see ***Figure 1.1***). Additionally, much of the Neoproterozoic is characterized by significant tectonic reorganization, with the lengthy breakup of the equatorially-centered supercontinent Rodinia (ca. 830-720 Ma) and following assembly of Gondwana (Hoffman, 1991, 1999; Meert and Lieberman, 2008; Pisarevsky et al., 2003). Combined with the advances in biological evolution that took place during this eon (Canfield et al., 2007; Gaucher and Sprechmann, 2009), these make the Neoproterozoic a particularly dynamic time in Earth's history.

This thesis focuses on developing the pre-Cryogenian carbon isotope record in northwestern Namibia through studying the Otavi Group's Ugab Subgroup, a mixed carbonate-siliciclastic succession that lies directly beneath glacial deposits from the first Neoproterozoic global glaciation. The late Tonian (ca. 750-720 Ma), when the Ugab Subgroup was deposited, records the break-up of Rodinia and the lead-up to the first Neoproterozoic global glaciation as well as at least one pre-glacial negative anomaly in the carbon isotope record, named the Islay anomaly (Hoffman et al., 2012; Strauss et al., 2015). The carbonate-dominated Neoproterozoic strata of the Otavi Group are well exposed in an arid environment with scarce vegetation and low amounts of rainfall, limiting chemical weathering and making it an appealing target for studies of the Neoproterozoic carbon isotope record. Despite the excellent documentation of the glacial and interglacial deposits in this area, which are the foundation for the original Neoproterozoic Snowball Earth hypothesis (Hoffman et al., 1998), the immediately pre-Cryogenian stratigraphy remains relatively poorly documented.

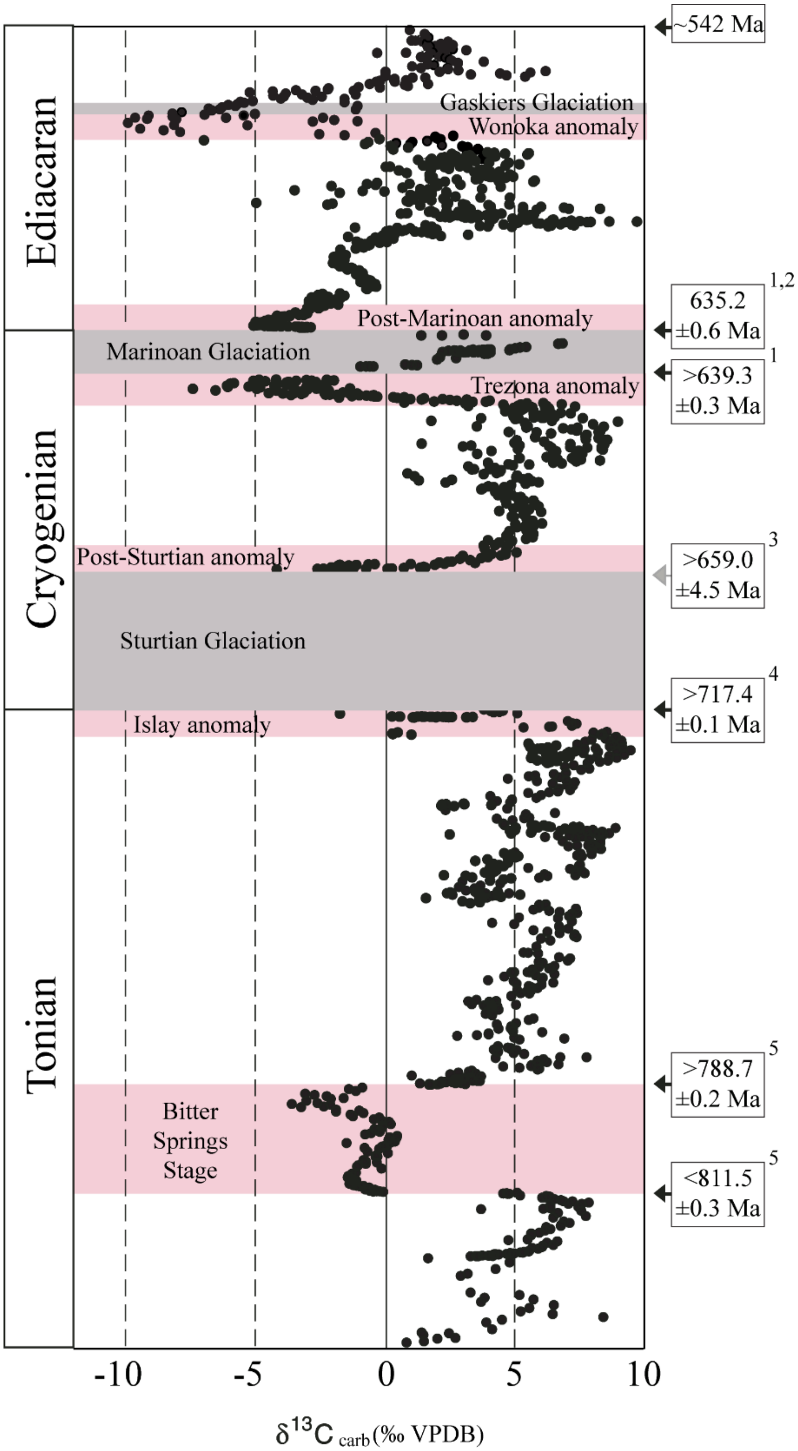

Figure 1.1: *Composite carbon isotope record of the Neoproterozoic, from Halverson et al. (2005). U-Pb dates indicated by black arrows, Re-Os dates indicated by grey arrows. 1: Prave et al. (2016); 2: Condon et al. (2005); 3: Rooney et al. (2015); 4: Macdonald et al. (2010); 5: Swanson-Hysell et al. (2015).*

Though this thesis aims to investigate the late Tonian carbon isotope record in northwestern Namibia and the Islay anomaly hosted therein, an understanding of the changing Earth surface conditions during the Neoproterozoic and how carbon circulates through the Earth's surface environment is important to provide context to the pre-Cryogenian $\delta^{13}C$ record and its possible causal link with the onset of Cryogenian glaciation. This chapter includes an overview of the Neoproterozoic carbon cycle and the carbon isotope fractionations that drive secular variation in in seawater $\delta^{13}C$, followed by a review of the Snowball Earth Hypothesis, the Tonian-Cryogenian boundary, and the global context of the Islay anomaly. Chapter 2 will focus on the Otavi Group of northwestern Namibia, starting with an overview of the paleogeography and stratigraphy. The new contributions in this thesis comprise a sequence stratigraphic interpretation of the Ugab Subgroup as exposed in two separate outcrop belts on the southern, extended margin of the Congo craton, and an accompanying pre-Cryogenian carbon isotope record based on new and previously collected data.

1.2 The Neoproterozoic Carbon Cycle

1.2.1 Background

Sedimentary carbonate rocks are a valuable archive of geochemical signals that reflect conditions on Earth's surface in the deep past. The carbon cycle involves complex interaction between biological and abiotic environmental processes as carbon moves through different reservoirs in the mantle, ocean, continents, and atmosphere. As atmospheric and ocean chemistry, as well as life, have evolved through time, the carbon cycle has also changed. This can be seen through the secular change in dominant styles of carbonate production from the earliest Archean carbonates (ca. 3800 Ma) to those forming today (Grotzinger and James, 2000; Shields and Veizer, 2002).

Throughout most of the Precambrian, life is thought to have been restricted to aquatic prokaryotes and primitive eukaryotes. Cyanobacteria (also known as blue-green algae) were the dominant primary producers in the oceans. The continents were thought to be barren, although some authors have suggested that colonization of the continents in the form of simple bacterial mats may have begun as early as 850 Ma (Kenny and Knauth, 2001; Knauth and Kennedy, 2009; Kump, 2014).

During the Archean Eon (3850-2500 Ma), carbonate sedimentation was mostly characterized by precipitation of cements, encrustations, and crystal fans directly onto the seafloor, suggesting supersaturation of calcium carbonate in seawater (Grotzinger and Kasting, 1993). Minor stromatolites also existed in the Archean, with the earliest documented occurrences ca. 3.45 Ga, and slowly increased in abundance until peaking in the mid-Mesoproterozoic (Hofmann 2000; Riding 2006; Allwood et al., 2009). Direct seafloor precipitation of carbonates gradually declined throughout the late Archean into the Proterozoic (2500-541 Ma), and carbonate precipitation in the water column became more common. This trend suggests that throughout the Proterozoic, a physiochemical change occurred in the ocean that favoured the nucleation of carbonates in the water column, possibly related to a slow rise in oxygen (Higgins et al., 2009; Sumner and Grotzinger, 1996). The mid-Proterozoic (1.8-0.8 Ga) is also believed to be a time when significant diversification of simple eukaryotes began, including the appearance of the first photosynthesizing eukaryotes ca. 1050 Ma, estimated by molecular clock analyses to have evolved as early as 1.25 Ga, and a notable expansion in eukaryotic diversity observed in the fossil record beginning ca. 800 Ma (Knoll, 1994; Porter, 2004; Parfrey et al., 2011; Knoll 2014; Gibson et al., 2017). An increase in abundance of steroid biomarkers suggests that eukaryotes may have taken over from cyanobacteria as the dominant primary producers by the middle of the Cryogenian Period (720-635 Ma) (Brocks et al., 2017). The Ediacaran Period (ca. 635–541 Ma) marked the appearance of the first metazoans in the form of the enigmatic Ediacaran biota, which appeared ca. 575 Ma and disappeared at the Precambrian-Cambrian boundary (Bowring et al., 2003). Although the metazoan affinity of certain Ediacaran fossils is ambiguous, there is growing evidence that the Ediacaran biota included cnidarians, bilaterians, and possible bivalves (Martin et al., 2000; Chen et al., 2002; Ivantsov and Fedonkin, 2002; Van Iten et al., 2006; Gehling et al., 2014). Furthermore, the possible origination of the sponges prior to the Ediacaran (Li et al., 1998; Love et al., 2009) coupled with recent molecular clock results suggest that most if not all animal phyla existed by the end of the Precambrian (Erwin, 2011). When animal life radiated in the Cambrian it resulted in a considerable change in the style of production of marine carbonates from abiotic to biotic. Carbonate biomineralization is believed to have evolved near the end of the Ediacaran Period (ca. 550 Ma) (Grotzinger et al., 1995; Grotzinger et al., 2000; Wood et al., 2002; Zhuravlev et al., 2012; Cortijo et al., 2015a,b), and quickly became responsible for a substantial proportion of carbonate sediments produced in the Phanerozoic Eon (542 Ma – today).

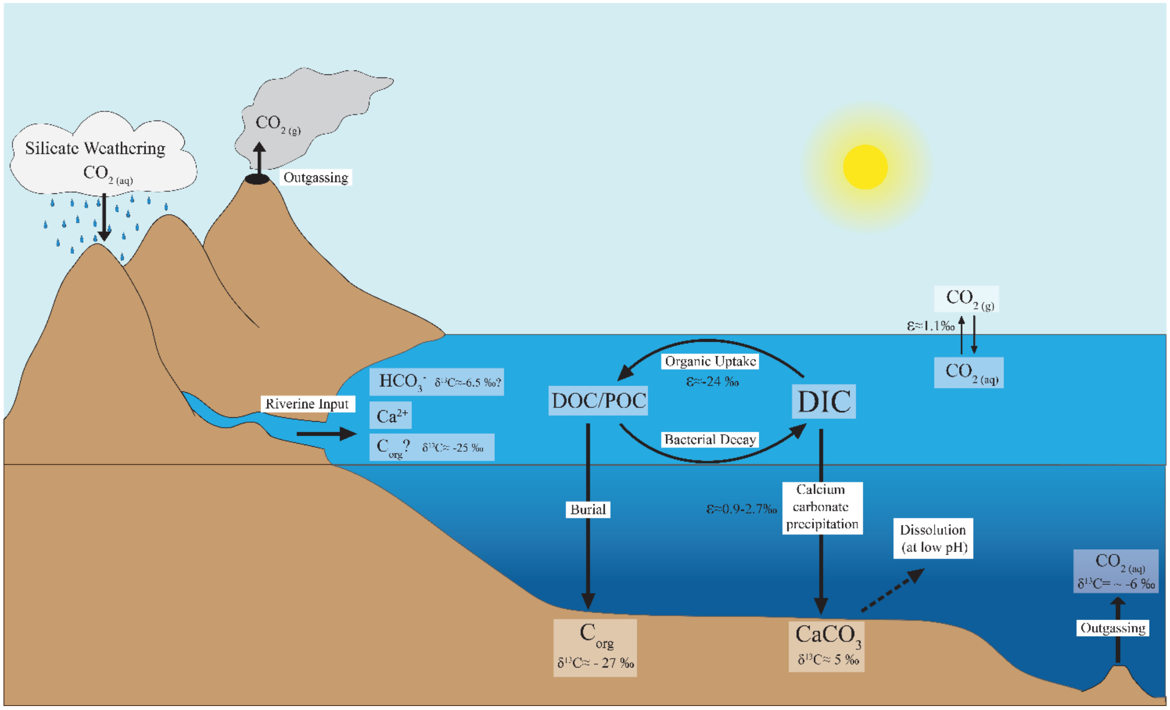

Figure 1.2: *The Neoproterozoic carbon cycle.*

The interval of time of interest for this thesis, the early Neoproterozoic, was a time when cyanobacteria were still the dominant biomass in the oceans, and carbonate nucleation in the water column was the main style of carbonate sedimentation ***(Figure 1.2)***.

1.2.2 Carbon in the atmosphere and ocean

Atmospheric carbon dioxide (CO_2) levels exert a fundamental control on the Earth's temperature and climate system due to the role of CO_2 as the most abundant non-condensing greenhouse gas in the atmosphere (eg. Lacis et al., 2010). CO_2 levels in both the atmosphere and the ocean are dominantly buffered by consumption during silicate weathering reactions and organic uptake by photosynthetic marine organisms, both of which will be discussed further below.

Marine carbon can be viewed as two interacting pools, one consisting of organic carbon, both particulate and dissolved (POC and DOC) and the other much larger pool consisting of the dissolved inorganic carbon (DIC). The organic carbon pool contains the ocean's biota, which drive an organic carbon pump that effectively transfers carbon from the surface ocean to the seafloor and deep oceans. Organisms in the photic zone of the ocean take up CO_2 from the DIC pool during oxygenic photosynthesis according to the following simplified reaction, where CH_2O is used as a general representation of organic matter:

$$CO_2 + H_2O + sunlight \rightarrow CH_2O + O_2 \tag{1}$$

The organic matter produced from this reaction will either sink to the seafloor and become buried in the sediments or will be recycled through bacterial decay back to inorganic carbon (i.e., remineralization), which under aerobic conditions, proceeds according to the following simplified reaction (inverse of photosynthesis):

$$CH_2O + O_2 \rightarrow CO_2 + H_2O \tag{2}$$

Other oxidants, such as sulfate and nitrate, also contribute to the remineralization of organic carbon in the water column or during early diagenesis.

The residence time of the DIC in the ocean is on the order of 10^5 years, exceeding the mixing time of the ocean, which is estimated to be on the order of 10^3 years for the modern ocean.

The sources of carbon to the marine DIC pool include the release of CO_2 during the decay of organic matter, which is generally counterbalanced by the consumption of CO_2 during the silicate weathering process, as discussed in more detail below. Volcanic outgassing at mid-ocean ridges is also a major contributor of inorganic carbon to the ocean. Riverine fluxes transport bicarbonate and cations liberated from minerals during chemical weathering of the continents (discussed below), and may also contain particulate and remineralized organic matter from terrestrial biomass after ~850 Ma (Kump, 2014). Lastly, CO_2 from the atmosphere diffuses into the ocean in areas where seawater is undersaturated with respect to inorganic carbon, such as areas with high rates of primary productivity and regions with cooler surface ocean temperatures which increases CO_2 solubility (Weiss, 1974).

The main flux of carbon directly into the atmosphere during the Precambrian was volcanic outgassing of CO_2, either at volcanic arcs associated with subduction zones or at oceanic island hotspots. Hotspot CO_2 is sourced from the mantle, whereas at subduction-related volcanoes, most of the CO_2 comes from metamorphism of carbonate sediments and organic matter accumulated on the subducted slab, with only approximately one tenth coming from the mantle (Shaw et al., 2003).

1.2.3 Silicate weathering

Silicate weathering acts as an important buffer for CO_2 in the atmosphere during continental weathering and the ocean during alteration of newly formed oceanic crust at mid-ocean ridges. During silicate weathering, CO_2 reacts with seawater in the ocean or meteoric water on the continents (to form carbonic acid—H_2CO_3) which then reacts with silicate rocks, summarized as follows:

$$CO_2 + 2\,H_2O + silicate\ minerals \rightarrow HCO_3^- + cations + clay\ minerals \tag{3}$$

The bicarbonate and cations produced from continental weathering are generally transported to the ocean through rivers. Silicate weathering is enhanced during times of heightened tectonic activity that result in uplift or volcanism associated with rifting. This may increase the draw-down of atmospheric CO_2 or shift where it occurs on the continents, impacting the delivery of important nutrients (eg. P, Fe, N) to the ocean. Consequently, silicate weathering is linked to primary productivity, creating a link between the supercontinent cycle and the carbon cycle. The breakup of Rodinia during the early Neoproterozoic was associated with extensive volcanism including the eruption of flood basalts (Harlan et al., 2003; Heaman et al., 1992), and corresponding volcanic outgassing of CO_2. This likely stimulated silicate weathering due to both the widespread production of fresh volcanic material to be weathered and the increased greenhouse effect invigorating the hydrological cycle (Goddéris et al., 2003; Trenberth, 1999).

1.2.4 Calcium carbonate precipitation

Ca^{2+} is delivered to the oceans as a product of silicate weathering, and when the concentrations of both Ca^{2+} and carbonate are sufficiently high to reach supersaturation, calcium carbonate is formed according to the following reaction:

$$Ca^{2+} + 2\,CO_3^{2-} + 2H^+ \;<->\; CaCo_3 + CO_2 + H_2O \tag{4}$$

Calcium carbonate solubility is mainly controlled by pH and temperature (Morse and Arvidson, 2002). Changes to pH determine the speciation of DIC (***Figure 1.3***) (Zeebe and Wolf-Gladrow, 2001). Once dissolved in seawater, aqueous CO_2 reacts with the water to form the thermodynamically preferred species of inorganic carbon. The inorganic carbon species maintain equilibrium with one another through the following reactions:

$$CO_{2\,(aq)} + H_2O_{(aq)} < -> H_2CO_{3\,(aq)} \tag{5}$$

$$H_2CO_{3\,(aq)} < -> HCO^-_{3\,(aq)} + H^+ \tag{6}$$

$$HCO^-_{3\,(aq)} < -> CO^{2-}_{3\,(aq)} + H^+ \tag{7}$$

Seawater pH has likely remained between ~6 and 9.5 throughout geologic time (Halevy and Bachan, 2017), a range at which bicarbonate (HCO_3^-) is the dominant species. The conversion of carbon dioxide to bicarbonate releases a proton, lowering seawater pH. This relationship explains why large-scale injections of CO_2 into seawater will drive ocean pH down. Acidification of the ocean (i.e. decreasing pH) lowers the concentration of carbonate ions in seawater and increases the concentration of dissolved carbon dioxide, leading to decreased supersaturation, decreased nucleation of calcium carbonate minerals, and, ultimately, the dissolution of calcium carbonate, which is an important buffer of seawater pH.

Higher temperatures result in decrease in the solubility of aqueous CO_2, thereby favouring precipitation of calcium carbonate. As a result, thick carbonate successions tend to be associated with warm, shallow, equatorial waters (Ziegler et al., 1984).

Calcium carbonate typically precipitates in seawater as either magnesian calcite or aragonite. The preferred polymorph, which is believed to have changed several times during the Precambrian, is dominantly controlled by the Mg/Ca ratio of seawater and temperature, with aragonite being preferred under warmer, more Mg-rich conditions (Hardie, 1996; Morse et al.,

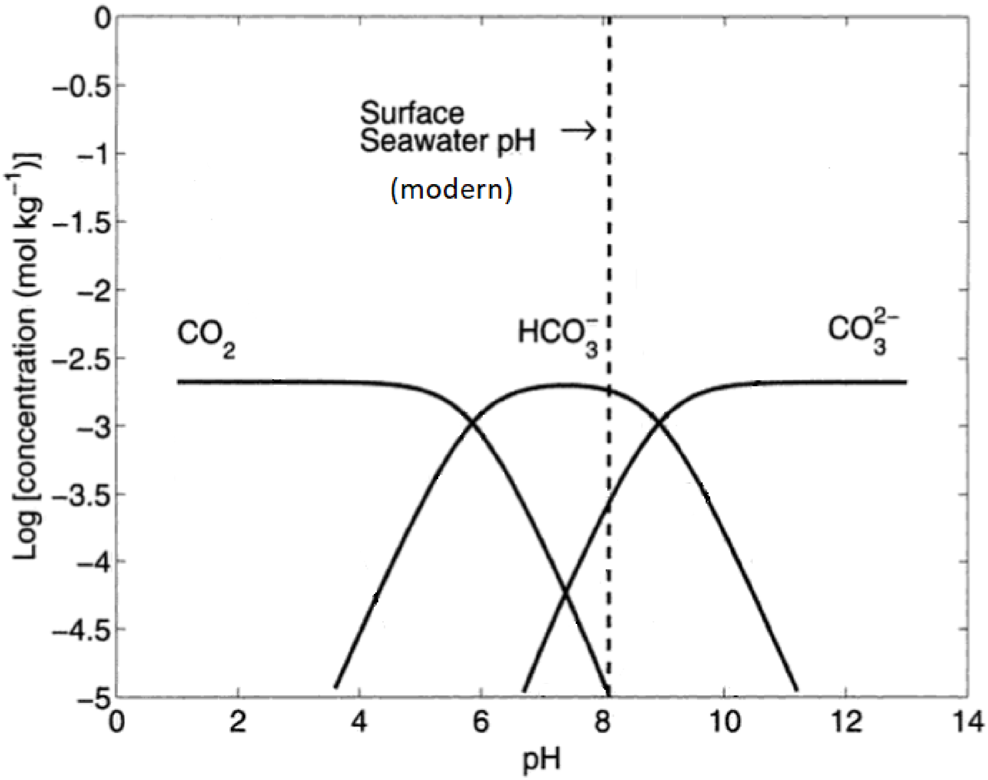

Figure 1.3: *A Bjerrum diagram showing the speciation of inorganic carbon in seawater. Modified from Zeebe and Wolf-Gladrow (2001).*

1997). An aragonite-precipitating ocean is both predicted and observed in the geologic record throughout most of the Neoproterozoic (Hardie, 2003).

Many Precambrian carbonates are preserved today as dolostones (Daly, 1909), which has led some workers to suggest that dolomite ($CaMg(CO_3)_2$) may have been the stable carbonate mineral precipitating in the ocean during some intervals of the Proterozoic (Tucker, 1982). However, laboratory experiments still cannot replicate reasonable conditions under which large volumes of dolomite would precipitate from seawater, despite having reached supersaturation (Land, 1998). Although there is some evidence for primary synsedimentary dolomite precipitation (Hood et al., 2011), it is generally accepted that the abundance of dolostone in the Proterozoic rock record is the result of diagenesis during which precursor magnesian calcite or aragonite is recrystallized to dolomite.

Carbonate minerals precipitated in the water column will accumulate on the seafloor provided it is above the carbonate compensation depth, the depth below which carbonate minerals will dissolve due to thermodynamic instability arising from decreased saturation state (Berger and Winterer, 1974). These carbonate sediments will ultimately lithify into carbonate rocks, where they become a proxy archive for the elemental and isotopic composition of the seawater at the time of formation.

1.3 Interpreting Stable Carbon Isotopes

One of the key and most robust geochemical proxies of sedimentary carbonates is their stable carbon isotope ratio. The carbon isotope record of marine carbonate rocks broadly represents the isotopic composition of the DIC pool at the time the carbonate mineral formed and can be useful both for inferring past environments and as a chemostratigraphic tool. Carbon has two stable isotopes, ^{12}C and ^{13}C, with natural abundances of 98.9% and 1.1% respectively. Secular variations in seawater carbon isotopes result from changes in isotopic fractionation between oxidized (carbonate minerals) and reduced (organic matter) carbon species and the relative importance of these two sinks. These fluctuations in $^{13}C/^{12}C$ in the DIC pool are recorded in both carbonate minerals and buried organic matter and can be used as a tool for correlating sedimentary successions. Large fluctuations in carbon isotope ratios in the Neoproterozoic make them particularly useful for correlations during this time interval (Kaufman and Knoll, 1995; Knoll and Walter, 1992). This correlation tool is particularly valuable for Precambrian successions, where the sparse fossil record precludes biostratigraphy and magnetostratigraphy is of limited use.

Carbon isotope ratios are expressed in per mil units in standard *delta* (δ) notation, which is defined according to the following equation:

$$\delta^{13}\mathrm{C}\ (‰) = \left(\frac{\left(\frac{^{13}\mathrm{C}}{^{12}C}\right)\mathrm{sam}}{\left(\frac{^{13}\mathrm{C}}{^{12}\mathrm{C}}\right)\mathrm{std}} - 1 \right) * 1000 \qquad (8)$$

The international reference standard used for stable carbon isotopes is the Pee Dee Belemnite (PDB) or Vienna Pee Dee Belemnite (VPDB), for which $^{13}C/^{12}C$= 0.0112372 (Coplen, 1988; Craig, 1957). Samples that are 'enriched' have a higher $^{13}C/^{12}C$ ratio than that of the reference standard ($\delta^{13}C$ value > 0‰). Likewise, the term 'depleted' is commonly used for samples with a $^{13}C/^{12}C$ ratio lower than the reference standard.

The isotopic composition of the marine DIC reservoir is dependent on the relative fluxes and isotopic compositions of multiple sources: the atmosphere (diffusive exchange with the atmosphere), the exposed continent (terrestrial weathering products transported to ocean by rivers), the mantle (mid-ocean ridge volcanic activity), and the rates of primary productivity (conversion to organic carbon) and subsequent remineralization or burial of organic carbon. Changes to any of these carbon reservoirs, fluxes, or the isotopic compositions associated with them can cause fluctuations in $\delta^{13}C$ of the ocean DIC reservoir.

Isotopic fractionations are imparted during various steps of the carbon cycle, with the most significant fractionation occurring during photosynthesis, due to a kinetic fractionation effect which favours the incorporation of the lighter isotope in biomass. Fractionations are expressed by ε, which is defined as follows:

$$\varepsilon_{A-B}(‰) = \left(\frac{1000 + \delta_A}{1000 + \delta_B} - 1\right) * 1000 \tag{9}$$

Metabolic pathways used by cyanobacteria during oxygenic photosynthesis produce a fractionation of up to ~ -24 ‰ (Pardue et al., 1976), resulting in the organic carbon pool being very isotopically depleted relative to the DIC pool.

The carbon isotope composition of the atmosphere and surface ocean are linked due to CO_2 freely exchanging at the atmosphere-ocean interface (Lynch-Stieglitz et al., 1995). Dissolution of atmospheric CO_2 into seawater is associated with a small temperature-dependent fractionation of $\varepsilon_{CO2g\text{-}CO2aq}$ = 1.1 ‰ at 20°C (Vogel et al., 1970). For subsequent conversion to bicarbonate, $\varepsilon_{CO2aq\text{-}HCO3\text{-}}$ = -9.5 ‰, and precipitation of calcite and aragonite from bicarbonate are $\varepsilon_{HCO3\text{-}\text{-}cal}$ = 0.9 ‰ and $\varepsilon_{HCO3\text{-}\text{-}arag}$ = 2.7 ‰, respectively (Mook et al., 1974; Rubinson and Clayton, 1969).

The net effect is that at 20°C, atmospheric CO_2 displays an 8.4 ‰ depletion relative to the $\delta^{13}C$ of oceanic DIC, and carbonate sediments are enriched by 0.9 to 2.7 ‰ depending on which polymorph precipitates. Carbon sourced from the mantle has a $\delta^{13}C$ ranging from -5 to -7 ‰ (Des Marais and Moore, 1984). The $\delta^{13}C$ of riverine DIC is variable as it depends on the weathering source, but is generally estimated to be ~ -6.5 ‰ in the modern day (Scholle and Arthur, 1980).

Fluctuations in the carbon isotope record can occur as a result of either a steady-state change to the system or a non-steady-state perturbation. Non-steady state anomalies result from fast influxes of carbon followed by a recovery, the length of which is controlled by the residence time of carbon in the ocean. Steady-state anomalies occur over a longer period of time, caused by a change in the $\delta^{13}C$ of a flux into or out of the reservoir, with the length of time over which the shift occurs controlled by the residence time of carbon in the reservoir. Residence time is calculated from the size of the reservoir and the fluxes in or out at steady state.

The unusually enriched background $\delta^{13}C$ recorded in the Neoproterozoic is commonly interpreted to record an increase in the proportion of organic carbon buried. Long-term fluctuations in the carbon isotope record (on the order of $>10^5$ yrs) are traditionally attributed to changes in the fraction (f_{org}) of organic carbon (C_{org}) burial relative to total carbon (e.g. Bartley and Kah, 2004; Frank et al., 2003). Consequently, protracted intervals of high $\delta^{13}C_{carb}$ are often interpreted as being periods of net increase in atmospheric O_2, as the rate of O_2 being produced during photosynthesis is higher than the rate at which it is being consumed during decay of organic matter due to a higher proportion of the organic matter being buried rather than decaying (Karhu and Holland, 1996; Schidlowski et al., 1975). In general, the higher burial proportion of organic carbon is inferred to be due to higher rate of burial, either through increased primary productivity or increased sedimentation rates (Campbell and Allen, 2008; Des Marais et al., 1992; Galy et al., 2015). Alternatively, recent modeling has shown that changes in erosion rates controlled by tectonics may result in changes in $\delta^{13}C$ independent of the rate of organic carbon burial. These results imply that increased $\delta^{13}C$ and oxygenation may not be as closely linked as previously believed (Shields and Mills, 2017). Additionally, anoxic photosynthesis may have played an important role in Precambrian biogeochemical cycling, with some organisms likely using sulfide as an electron donor in largely anoxic Proterozoic oceans and producing oxidized sulfur compounds instead of O_2 (Johnston et al., 2009).

Another mechanism argued to be equally plausible as a cause for long-lasting $\delta^{13}C$ enrichment of the Neoproterozoic is widespread production of isotopically-depleted diagenetic carbonate cement, resulting from alkalinity generated via oxidation of organic carbon or methane within sediments (Schrag et al., 2013). This would drive the DIC pool to more enriched values without a compensatory increase in atmospheric O_2, and this process is more likely to have occurred under the low O_2 conditions in the Proterozoic compared to modern day (Schrag et al., 2013).

Several hypotheses have been invoked to explain the high-magnitude, short-term perturbations to the carbon cycle that are also characteristic of the Neoproterozoic. A shut-down in organic carbon burial would result in the $\delta^{13}C$ of DIC gradually approaching mantle values (~ -6‰) (Kump, 1991) but cannot alone explain excursions extending below that. Rothman et al. (2003) proposed that these exceptionally negative excursions could be the result of an unusually large organic carbon reservoir in the ocean, whereby intervals of increased remineralization from a large C_{org} pool could cause inflated negative excursions in $\delta^{13}C$ of the DIC pool. Because organic carbon is formed through biological consumption of inorganic carbon, $\delta^{13}C_{carb}$ and $\delta^{13}C_{org}$ have covaried throughout most of Earth's history. An apparent disappearance of this isotopic coupling from the end of the first Snowball event until the end of the Ediacaran Period led to speculation that a sufficiently large oceanic C_{org} reservoir would drown out signals from the DIC pool (Rothman et al., 2003; Swanson-Hysell et al., 2010). However, Johnston et al. (2012) present evidence that this decoupling was not global and posit that local decoupling observed in some parts of the world results from detrital organic carbon mixing with the primary organic carbon thus diluting the signal. Another leading hypothesis is the oxidation of isotopically-depleted, reduced carbon from a large methane clathrate reservoir (Bjerrum and Canfield, 2011; Schrag et al., 2002). Bartley and Kah (2001) inferred that the high magnitude of $\delta^{13}C$ excursions observed in the Neoproterozoic may be a natural consequence of a decline in the size of the marine DIC reservoir which would result in a system less capable of buffering short term perturbations to the carbon cycle.

In order to use carbon isotopes either to make inferences about the global environment or as a correlative tool, the assumption must be made that the signals preserved in the rock are both primary and representative of the global ocean (Frimmel, 2010; Melezhik et al., 2001). The $\delta^{13}C$ record is often affected by secondary alteration from diagenetic and metamorphic processes. Fine-grained carbonate sediments that accumulate at slow rates are especially prone to contribution from authigenic carbonate, which can drive $\delta^{13}C$ towards negative values (Schrag et al., 2013; Sun and Turchyn, 2014). Subaerial exposure surfaces in young sediments often show a decline in $\delta^{13}C$ due to isotopic exchange between carbonates and meteoric water mixed with decaying organic matter (Allan and Matthews, 1982; Kenny and Knauth, 2001). This mechanism can alter both oxygen and carbon isotope ratios simultaneously, therefore covariance of oxygen and carbon isotope ratios can provide evidence for post-depositional alteration of the carbon isotopes (Allan and Matthews, 1982; Fairchild et al., 2000). Even when geochemical tests can rule out meteoric and shallow-burial diagenetic alteration, basin restriction may influence the preserved isotopic signal. However, different processes have much different effects, such that there is no single model for how restriction influences the $\delta^{13}C$ record. In a basin that is episodically isolated from the open ocean, isotopic changes to global seawater may not be recorded, and Rayleigh fractionation during evaporation can create enrichments in the heavier isotopes (Pierre, 1989). These complications reinforce the importance of establishing a detailed sedimentological framework to assess whether isotopic signatures truly represent a primary open marine signal that has experienced limited post-depositional alteration.

Despite difficulties of interpreting carbon isotope signals due to the uncertainties about ocean and atmosphere chemistry in the past, much research on the Precambrian world still relies on the clues carbon isotopes can provide. Available evidence indicates that that many salient $\delta^{13}C$ trends are reproducible globally. Not only can the carbon isotope record facilitate correlations between radiometrically dated strata and their undated equivalents, it can also reveal information about both biological and physical processes at play in the Precambrian world.

1.4 The Snowball Earth Hypothesis

The Snowball Earth hypothesis was first proposed by (Kirschvink, 1992) in an attempt to explain the occurrence of Neoproterozoic glaciogenic deposits and associated iron formations recognized on nearly every major craton, including land masses thought to have been at a low latitude during the late Proterozoic (Harland, 1964). In addition to paleomagnetic data indicating low latitudes (Sohl et al., 1998; Hoffman and Li, 2009), some of the glacial deposits were observed to contain carbonate clasts or to be bracketed by carbonate strata, suggesting paleolatitudes within 33° of the equator (Harland, 1964; Ziegler et al., 1984). Kirschvink (1992) proposed that the unique arrangement of landmasses during the late Proterozoic, specifically their concentration in middle to low latitudes, could have led to global cooling. Unvegetated continents have a higher albedo relative to ocean surfaces, and higher rates of silicate weathering would cause a decrease in atmospheric pCO_2 and global cooling. Additionally, oceans at high latitudes are often covered by a high albedo fog or cloud layer, further reducing the amount of solar energy absorbed compared to the amount absorbed at equatorial oceans (Ramanathan et al., 1989). This cooling could lead to growth of high albedo polar ice caps, lowering the sea level and adding more high albedo landmass as the continental shelves are increasingly exposed. These positive albedo feedbacks are suggested to have eventually caused the entire earth to be covered in ice, evocatively described by Kirschvink (1992) as resembling a snowball. As originally argued, with the oceans covered in pack ice, ocean circulation would have stopped and oxygen from the atmosphere would have no longer diffused into seawater, leading to anoxia. Ferrous iron would have built up in solution in the ocean over time as it was released at mid-ocean ridges and from seafloor sediments.

The possibility of a fully frozen Earth as a stable climatic state was first proposed based on simple, 1D energy balance models (Budyko, 1969; Sellers, 1969), but it was assumed that the Earth had never experienced one because escape from a snowball state would be difficult and no mechanisms were known that could trigger a return to a non-glaciated climatic state. However, Caldeira and Kasting (1992) solved this conundrum, recognizing that CO_2 derived from volcanic outgassing would accumulate in the atmosphere regardless of the frozen surface because plate tectonics is immune to ice cover. With the hydrological cycle halted and the surface of the ocean and much of the landmass covered in ice, both photosynthesis and silicate weathering would have essentially ceased and no longer have been able to act as buffers for the increasing levels of CO_2. Consequently, CO_2 could have accumulated in the atmosphere up to a critical point where the greenhouse effect overcame the ice albedo effect and ice cover began to melt in the tropics. Open ocean, once exposed, would have absorbed solar energy and accelerated the warming of the planet, driving an ice albedo runaway in the opposite direction. Once ocean and atmosphere could interact, O_2 would have diffused from the atmosphere into the seawater and the ocean's built-up reservoir of iron would have precipitated as iron oxides, blanketing the seafloor in iron-rich deposits. Kirschvink (1992) suggested that the switch from an 'icehouse' to a 'greenhouse' state was likely to have been relatively fast, resulting in a very warm post-glacial earth.

Kirschvink (1992) outlined three predictions that could be used to test the Snowball Earth hypothesis: global synchronicity of onset and demise of glaciation, extreme greenhouse conditions following the glaciations, and stagnation and anoxia of the ocean beneath the ice during the glaciations. Geological evidence of all three predictions was introduced by (Hoffman et al., 1998) after extensive fieldwork in Northwestern Namibia studying the Neoproterozoic Otavi Group. Hoffman et al. (1998) recognized deposits from two discrete glaciations: the earlier *Sturtian* and the later *Marinoan*, each capped by a distinctive carbonate unit with negative carbon isotope ($\delta^{13}C_{carb}$) values, consistent with the accumulation of volcanic CO_2 in the atmosphere for millions of years. Hoffman et al (1998) also observed that the second glaciation was preceded by a pronounced drop in $\delta^{13}C_{carb}$, which they attributed at the time to a decline in productivity in the ocean as the earth cooled into a frozen state. Hoffman et al. (1998) suggested that one of the driving forces in triggering the Snowball glaciation was the break-up of Rodinia drawing down CO_2 from the atmosphere. Increased rates of silicate weathering and sedimentation associated with Rodinia's fragmentation may have also caused a rise in the proportion of organic carbon being buried, which is an idea supported by generally high $\delta^{13}C_{carb}$ values through the Neoproterozoic (Knoll et al., 1986).

In the two decades since the 'Neoproterozoic Snowball Earth' hypothesis of Hoffman et al. (1998) was published, the hypothesis has been widely studied, scrutinized, and developed as more geochemical and geological evidence has emerged and increasingly sophisticated models have been applied to understanding both the snowball climate itself (e.g., Benn et al., 2015) and climatic conditions leading into and following snowball glaciation (e.g. Le Hir et al., 2009; Yang et al., 2017). Initial criticism of the snowball hypothesis was rooted in objection to unrealistic reductions in solar forcing required to initiate snowball Earth and the thickness and sedimentological characteristics of the Neoproterozoic glacial deposits, which were thought to be more consistent with an active hydrological cycle (Christie-Blick et al., 1999; Jenkins and Scotese, 1998; Leather et al., 2002). Purportedly syn-glacial oolitic, peloidal, and stromatolitic carbonates record positive $\delta^{13}C_{carb}$ values, contradicting the prediction that carbon isotope compositions would trend towards the low value (~ -6‰) of volcanic input (Kennedy et al., 2001a). Furthermore, glacial deposits are reported to contain sedimentological evidence of being deposited in an open ocean affected by waves (Allen and Etienne, 2008). Others have argued that these glacial deposits can be interpreted as gravitation flow deposits completely unrelated to glaciation (Eyles and Januszczak, 2007; Nascimento et al., 2016), although the overwhelming consensus is that the purported glacial deposits are indeed glacial in origin (Arnaud et al., 2011). Global synchronicity of the onset and termination of each glaciation is strongly supported by agreement between dates for the glaciogenic deposits from locations worldwide including Australia, northern Canada, and south China (see Rooney et al., 2015 for a review of relevant age constraints).

The challenge of finding a plausible trigger for Snowball Earth has been undertaken by many researchers using various approaches. Modeling has demonstrated that a runaway ice albedo feedback will take effect once ice cover has reached a critical latitude of 30° (Budyko, 1969). For ice cover to reach this far, the majority of continental landmass being positioned in the tropics was an important factor (Schrag et al., 2002). Higher sedimentation rates from riverine sources during the fragmentation of Rodinia would increase burial of organic matter, and higher rates of continental weathering would increase the flux of phosphorous into the ocean, resulting in more primary productivity given that phosphorous was likely the limiting nutrient (Tyrell, 1999; Föllmi, 1996). This increased organic carbon burial could both explain the higher background $\delta^{13}C$ ratios observed in the Neoproterozoic and be expected to result in the development of methane hydrate reservoirs. Schrag at al. (2002) argued that the eventual slow release of methane from overfilled reservoirs could have triggered global glaciation by destabilizing the atmosphere. Specifically, a sufficient methane flux over hundreds of thousands of years would have caused a decrease in atmospheric pCO_2 through the silicate weathering feedback, and at the same time, would have driven a large negative $\delta^{13}C$ excursion, similar to that observed to occur prior to the second (Marinoan) snowball Earth in Namibia (Halverson et al., 2002). Interruption of this methane flux, on the other hand, would have resulted in rapid loss of the greenhouse, quickly plunging Earth into a snowball state.

Other workers have proposed that weathering of large volumes of continental flood basalt associated with the break-up of Rodinia could have been the major cause of atmospheric CO_2 drawdown that started the global cooling that drove the Earth into the Sturtian glaciation

(Donnadieu et al., 2004; Goddéris et al., 2003). This 'Fire and Ice' hypothesis is supported by a shift towards more primitive Nd isotope signatures in mudstones and higher ratios of unradiogenic Sr in marine carbonates deposited in the 130 Myrs leading up to the beginning of the first Neoproterozoic global glaciation (Cox et al., 2016). The highly unstable climatic conditions in the aftermath of the first Snowball could have made falling into a second global glaciation much more likely, even without the dramatic trigger required for the first. Tziperman et al. (2011) proposed a biological driver, whereby the increase in the proportion of organic matter sinking into the anoxic lower ocean would have led to more anoxic remineralization by sulfate- and iron-reducing bacteria, increasing carbonate alkalinity in seawater and consequently drawing down atmospheric pCO_2. Macdonald and Wordsworth (2017) hypothesized that magma associated with the Franklin Large Igneous Province that intruded into evaporites would have resulted in large plumes of sulfate aerosols, which, if injected into the stratosphere, would have increased planetary albedo, possibly enough to trigger the Sturtian glaciation. However, this explanation cannot account for the onset of the Marinoan glaciation.

The extent and severity of the Snowball Earth events are topics of debate as well. Kirschvink (1992) and Hoffman et al. (1998) originally postulated a completely frozen over ocean and ice-covered continents, which would have arrested the hydrological cycle. This 'hard snowball' has since been found to be inconsistent with geological observations and climate models, which are unable to simulate realistic conditions under which deglaciation could occur from build-up of CO_2 in the atmosphere (Le Hir et al., 2008; Pierrehumbert, 2004). Hyde et al. (2000) developed a coupled climate/ice-sheet model in which several simulations resulted in a ring of unfrozen seawater along the equator, referring to this state as a 'Slushball' or 'soft snowball'. The problem with a soft snowball state is that it would prevent CO_2 from accumulating in the atmosphere to the levels required to trigger deglaciation (Le Hir et al., 2008). Whereas one appeal of the soft snowball hypothesis among geologists is that it allows for the observed accumulation of Phanerozoic-like glacial deposits, modeling now shows that large, wet-based ice sheets would accumulate under a snowball climate (Donnadieu et al., 2003) and would even be influenced by orbital cycles (Benn et al., 2015). And as demonstrated by Partin and Saddler (2016), the depositional record of the Sturtian and Marinoan glaciations is strongly distinct from Phanerozoic glaciations when scaled for duration of glaciation.

The duration of the snowball events has also been the subject of much discussion, and recently many new age constraints from geological dating have narrowed down estimates to ~57 Ma for the Sturtian glaciation and >4 Ma for the Marinoan glaciation (Macdonald et al., 2010a; Prave et al., 2016; Rooney et al., 2015). Earliest attempts to approximate the longevity of the global glaciations came from modeling CO_2 buildup in the atmosphere, assuming that the rate of subaerial volcanic outgassing during the Neoproterozoic matched modern rates (Caldeira and Kasting, 1992). In this idealized energy balance model, pCO_2 reached the critical threshold in approximately 4 Myrs. Accounting for the lower solar luminosity and gas exchange between the atmosphere and ocean through ice cracks, the maximum duration would be ~30 Myrs (Hoffman et al., 1998). A different model using the difference in $^{87}Sr/^{86}Sr$ between pre- and post-glacial carbonates, assuming a complete shutdown of the hydrological cycle during the glaciations, suggests a maximum duration on the order of 10^6 years (Jacobsen and Kaufman, 1999). However, this model neglected dissolution of marine carbonates during the glaciation which should have strongly buffered the oceans with respect to $^{87}Sr/^{86}Sr$. Bodiselitsch et al. (2005) documented iridium anomalies at the base of cap carbonates in the Democratic Republic of the Congo and Zambia, and used these anomalies to estimate that the Marinoan glaciation likely lasted 12 Myrs, with a minimum constraint of 3 Myrs. However, these results have not been replicated in any other cap carbonate (Peuker-Ehrenbrink et al., 2016).

Although modeling has yielded a wide array of results, dating of samples from exposures of Cryogenian strata worldwide has allowed the onsets and terminations of the glaciations to be narrowed down to relatively small age ranges. A suite of ages from U-Pb ID-TIMS dating of volcanic ash beds below and interbedded with Sturtian glacial deposits in northwestern Canada constrain the onset of the Sturtian glaciation to between 716.9±0.4 Ma and 717.4±0.2 Ma (Macdonald et al., 2010; Macdonald et al., 2017). A U-Pb zircon date of 663.03±0.11 Ma from a tuff within Sturtian deglacial sediments in Australia, combined with a Re-Os age of 659.0±4.5 Ma from shales directly overlying the older glacial deposits in Mongolia, provide the closest constraints for the termination of the Sturtian glaciation (Rooney et al., 2015; Cox et al., in review). The interglacial period persisted for ~20 Myrs, followed by the onset of the Marionoan glaciation some time before ca. 639.29±0.26 Ma (Prave et al., 2016). The termination of the Marinoan glaciation is tightly constrained by U-Pb dating of an ash beds, the lower from within glaciomarine deposits in Namibia giving an age of 635.21±0.59 Ma (Prave et al., 2016), and the upper from immediately above Marinoan diamictite in South China giving an age of 635.23±0.57 Ma (Condon et al., 2005). Re-Os dating of a shale directly overlying the glacial deposit in northwest Canada provides an age of 632.3±5.9 Ma, in agreement with the other constraints (Rooney et al., 2015).

Earth's recovery from a snowball state is generally attributed to millions of years of volcanic degassing building atmospheric CO_2 levels up to the critical threshold (Kirschvink 1992; Hoffman et al., 1998). The initial estimate from an energy balance model for this threshold to trigger deglaciation, assuming a 'hard' snowball scenario, is 0.12 bar (Caldeira and Kasting, 1992). Subsequent work suggests that this estimate is too low, and simulations from a general circulation model place the threshold somewhere above 0.2 bar (Pierrehumbert, 2004). This improbably high threshold led workers to search for a factor missing from their models, which may be volcanic output. Dust ejected into the atmosphere during explosive volcanic eruptions is speculated to have an important impact on deglaciation by lowering albedo when deposited onto the ice surface. When incorporated into general circulation models, the effect of dust accumulation can lower the pCO_2 threshold to a more reasonable ~0.1 bar (Abbot and Halevy, 2010; Abbot and Pierrehumbert, 2010; Le Hir et al., 2010).

Models predict that once the critical pCO_2 threshold is met (with help from dust), equatorial melting would have resulted in a runaway albedo feedback causing ice loss and corresponding sea level rise. Atmospheric CO_2 levels were likely hundreds of times higher than modern levels, creating an ultra greenhouse atmosphere with high temperatures and a strongly active hydrological cycle. Although early modeling suggested that the meltback would have lasted only a few thousand years (Hyde et al., 2000; Peltier et al., 2004), the timescale of the transition from a snowball to non-snowball state has been highly controversial. The duration of deposition of cap carbonates has been used in attempts to constrain the duration of deglaciation, based on the supposition that cap carbonates were deposited during the sea level rise associated with melting of ice-cover on land (Hoffman et al., 2007). However, the time span for sea level rise and deposition of cap carbonates could be longer due to delayed thermal expansion. Using a model of mixing of glacial meltwater with the saline deep ocean, Yang et al. (2017) concluded that cap carbonates were likely deposited over a timespan on the order of 10^4 years. Depositional durations estimated from paleomagnetic reversals recorded in the cap carbonate sequences are on the order of 10^5 years or longer (Font et al., 2010; Kilner, 2005; Trindade et al., 2003), although these estimations are questionable as the reversal frequency during time is uncertain.

The cap carbonate sequences, metres to decametres thick and deposited on continental margins and in epicontinental seas, display anomalously low $\delta^{13}C$ (e.g. Hoffman et al., 1998; Halverson et al., 2005). Various mechanisms have been proposed as the source of alkalinity that would have allowed for widespread carbonate precipitation, including overturning of highly alkaline deep waters in a stratified ocean (Grotzinger and Knoll, 1995; James et al., 2001), enhanced weathering increasing the riverine flux of alkalinity (Hoffman and Schrag, 2002), and anaerobic oxidation of methane from methane clathrate reservoirs destabilized during post-glacial flooding (Jiang et al., 2003; Kennedy et al., 2001b). Sedimentological features recorded in the cap carbonates suggest stormy conditions during deposition. Giant symmetric wave ripples, with heights of 20-40 cm, observed in post-Marinoan successions worldwide indicate a deep wave base, high waves, and wind velocities reaching 20 m/s (Allen and Hoffman, 2005; Higgins and Schrag, 2003).

The question of how life survived through these global glaciations is still unanswered. Some argue for the 'Slushball' model, where microorganisms could have survived in unfrozen ocean in the equatorial region, while others suggest that inland seas or cryoconite holes on the ice surface could have acted as refuges for simple lifeforms (Hoffman, 2016; Campbell et al., 2011; Moczydlowska, 2008; Vincent et al., 2000). No matter the precise survival mechanisms, we know that some life, including eukaryotes and possibly even the earliest metazoans, lasted through the climatic extremes of the Cryogenian, and may have even thrived in the aftermath. The Ediacaran Period (635-541 Ma) marks the first unambiguous appearance of complex multicellular organisms. The relationship between the Cryogenian glacial episodes and the subsequent radiation of animal life remains speculative, despite their enticing temporal proximity, and will likely continue to be the focus of much research in the coming years.

1.5 Defining the Tonian-Cryogenian Boundary

Division of the Precambrian into meaningful and accurate units of geologic time poses an ongoing challenge. Subdivision of the Phanerozoic Eon (541 Ma-present) has largely been accomplished using biostratigraphy, with the lower boundary of each stage defined by a Global Stratotype Section and Point (GSSP). A GSSP is a globally correlative horizon based on an important transition or event recorded in a selected type section, typically the first appearance of a fossil species, and marked by a 'golden spike' (Cowie et al., 1986). This way of subdividing time becomes problematic when working with rocks older than the Cambrian Explosion, due to the limited biostratigraphic record and relative scarcity of well-preserved outcrops. Because of this difficulty, currently all but one of the Precambrian geologic time scale boundaries are defined by Global Standard Stratigraphic Ages (GSSAs), which are fixed chronological reference points. Though this simplified the initial segmentation of Precambrian time, it is widely preferred within the stratigraphic community to use subdivisions based on the sedimentary rock record; researchers are pushing to extend the use of GSSPs further back in the time scale (Knoll, 2000; Shields-Zhou et al., 2016).

The concept of the Cryogenian Period was born when Harland (1964) suggested defining a geological time interval that encompassed the widespread glacial deposits that occurred late in the Proterozoic Eon. His proposed 'Infracambrian' or 'Varangian' period began with the appearance of the first glacial deposits and ended at the first appearance of Cambrian fossil assemblages. Over the next decades, this period underwent a name change to 'Late Precambrian', then to 'Sinian', and subdivision was suggested between the two large glacial episodes (Dunn et al., 1971; Harland et al., 1982; Harland, 1990). Finally, following a 1988 meeting of the Subcommission on Precambrian Stratigraphy of the International Commission on Stratigraphy, Plumb (1991) introduced a division of the Proterozoic Eon into the Paleoproterozoic, Mesoproterozoic, and Neoproterozoic Eras. He subdivided each era into periods with lower boundaries defined by GSSAs. The Neoproterozoic Era (1000-541 Ma) was subdivided into the Tonian Period (1000-850 Ma), the Cryogenian Period (850-650 Ma), and Neoproterozoic III (650 Ma to the base of the Cambrian). The Tonian Period, named from the Greek word for 'stretch', was meant to encompass rifting associated with the break-up of Rodinia. The Cryogenian Period, as the name implies, was intended to span the global glaciations, and Neoproterozoic III was designated to cover the timespan between the end of the last glaciation and the beginning of the Cambrian Period. As more radiometric dates from Neoproterozoic strata emerged, it became clear that the set GSSAs do not adequately bracket the intended intervals, and adjustments to the time scale are necessary.

Knoll et al. (2006) redefined Neoproterozoic III as the Ediacaran Period, with a lower boundary GSSP at the base of the ca. 635.5 Ma Marinoan cap carbonate in the central Flinders Range of

South Australia. This boundary was defined based on lithology (specifically the post-Marinoan cap carbonate, which is distinctive and recognized globally) rather than biostratigraphy, opening a door for more Neoproterozoic GSSPs to be defined in alternative manners.

After a 2014 meeting of a Cryogenian-focused subcommission of the International Commission of Stratigraphy, the Tonian-Cryogenian GSSA was shifted to 720 Ma as a placeholder while the Cryogenian Subcommission considers where to place the GSSP. Following guidelines established by the International Commission on Stratigraphy (Cowie et al., 1986; Remane et al., 1996), a GSSP should not be placed at an unconformity, which creates a challenge due to the nature of the lower Cryogenian boundary. Glacial scouring and subaerial erosion from falling sea level are typical of the Tonian-Cryogenian contact. Other rules include accessibility of the type section, the absence of major changes in facies within the boundary interval, and potential for geochronometry and magnetostratigraphy. There is agreement that the Cryogenian GSSP should be beneath the oldest glaciogenic deposits; defining and correlating with the exact point will require high resolution geochemical data with particular emphasis on the carbon isotope record (Shields-Zhou et al, 2016). As of now, nominations for the type section are being made for the Cryogenian Subcommission to review (eg. Fairchild et al., 2017), and it is possible that a golden spike will be driven into a basal Cryogenian GSSP within the next few years.

1.6 The Islay Anomaly

A pre-Sturtian negative carbon isotope excursion has been observed in late Tonian carbonate successions in multiple locations on many paleocontinents, (see ***Figure 1.4***; summarized in ***Table 1.1***), and in many ways is analogous to the pre-Marinoan *Trezona* anomaly that was documented earlier (McKirdy et al., 2001; Halverson et al,. 2002). This anomaly has been dubbed the Islay anomaly, after the unit of the same name in the Dalradian Supergroup of Scotland where a negative $\delta^{13}C$ anomaly was first well documented and identified as preceding the Sturtian glaciation (Brasier and Shields, 2000; Prave et al., 2009). In some locations, the purported Islay anomaly marks a drop in $\delta^{13}C_{carb}$ of approximately 10‰, and a small coeval decline in $\delta^{13}C_{org}$ (Hoffman et al., 2012; Strauss et al., 2014). Re-Os dates from northwestern Canada bracketing the peak of the anomaly indicate that the Islay carbon isotope excursion took place between 739.9 ±6.1 Ma and 732.2 ±3.9 Ma, followed by a complete recovery to baseline $\delta^{13}C$ values before the onset of the Sturtian glaciation ca. 717 Ma (Rooney et al., 2014; Strauss et al., 2015). However, recent work in Scotland on a conformable transition from pre-glacial carbonates into glacial diamictite shows a negative carbon isotope excursion of similar magnitude immediately before the onset of the Sturtian glaciation, suggesting an age much closer to 717 Ma (Fairchild et al., 2017). This has raised speculation of the existence of two separate 'Islay anomalies', and highlights the need for more detailed end-Tonian $\delta^{13}C$ records (Halverson et al., 2018).

The pre-Sturtian Islay anomaly is commonly viewed as analogous to the better-documented pre-Marinoan Trezona anomaly. It is generally believed that the perturbations to the carbon cycle that caused these anomalies are related to the triggers for the Snowball Earth events (Halverson and Shields, 2011), but there is no consensus on exactly what caused either excursion. Negative carbon isotope excursions preceding global glaciations were initially postulated to be due to global cooling leading into the snowball events that would have led to considerably decreased biological productivity in the oceans (Hoffman et al., 1998). However, subsidence modeling produced an estimate of ~0.6 Myrs for the duration of the pre-Marinoan Trezona anomaly (Halverson et al., 2002), and biological productivity should not have been deeply affected by cooling this long in advance of the glaciation reaching the equator (Schrag et al., 2002). Methane release from clathrate reservoirs was also suggested, and for the Trezona anomaly this hypothesis is supported by sulfur isotope data consistent with increased rates of sulfate reduction associated with microbial remineralization of a reduced carbon reservoir (Bjerrum and Canfield, 2011; Halverson et al., 2009; Schrag et al., 2002). Hypotheses for a diagenetic origin have also been suggested, ranging from early meteoric alteration during exposure associated with the falling sea level leading into the glaciation (Knauth and Kennedy, 2009; Swart and Kennedy, 2012) to burial diagenesis associated with CO_2-rich brines (Derry, 2010a, 2010b), but a study of the stratigraphic relationships and geochemical constraints of the Trezona anomaly have indicated that a secondary origin is unlikely (Rose et al., 2012).

The causal linkage between the mechanism that generated the Islay anomaly and initiated the Cryogenian glacial was effectively invalidated by age constraints for the pre-Sturtian anomaly in northwestern Canada, which took place millions of years prior to the onset of the glaciation. Strauss et al. (2015) proposed instead that the Islay Anomaly may have been caused by the uplift and weathering of evaporite basins and shallow epicontinental seafloors during the breakup of Rodinia. These epicontinental seas, which likely covered vast amounts of area between

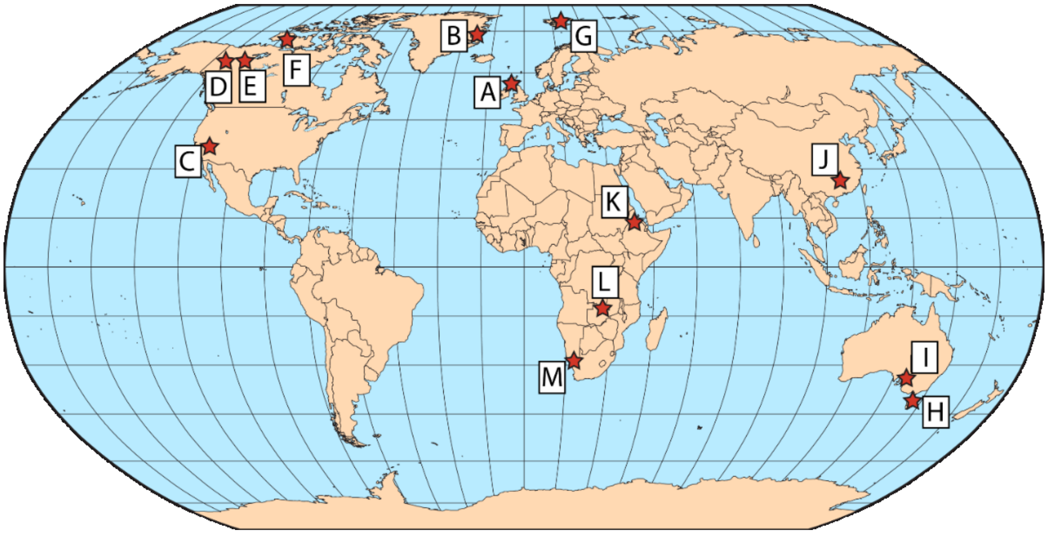

Figure 1.4: *World map showing locations of sections where Islay anomaly was documented. See Table 1.1 for corresponding information and references.*

Summary of Documented Occurences of Pre-Sturtian Negative Carbon Isotope Anomalies

	Paleocontinent	Stratigraphic host	Modern-day Location	Nadir (approx.)	Magnitude (approximate)	Main References
(A)	Laurentia (E)	Garbh Eileach Fm., Appin Subgroup	Inner Hebrides, Scotland	-6 ‰ -7 ‰	-10 ‰ -11 ‰	Brasier and Shields, 2000 Prave et al., 2009 Fairchild et al., 2017
(B)	Laurentia (E)	Bed Group 19, Andree Land Group	NE Greenland	-10 ‰	-16 ‰	Fairchild et al., 2000 Klaebe et al., 2018
(C)	Laurentia (W)	Beck Spring Dolomite, Pahrump Group	Death Valley, California, USA	-3 ‰ -4 ‰	-8 ‰ -9 ‰	Corsetti and Kaufman, 2003 Smith et al., 2015
(D)	Laurentia (NW)	Callison Lake Fm., Mount Harper Group	Ogilvie Mountains, Yukon, Canada	-3 ‰	-7 ‰	Strauss et al., 2015
(E)	Laurentia (NW)	Coppercap Fm, Coates Lake Group	Mackenzie Mountains, NWT, Canada	-7 ‰	- 13 ‰	Rooney et al., 2014 Jefferson and Parrish, 1989
(F)	Laurentia (NW)	Kilian Formation, Shaler Spgp	Minto Inlier, Nunavut, Canada	-7 ‰	-11 ‰	Jones et al., 2010 Thomson et al., 2015
(G)	Laurentia (E)	Russoya Mb., Polarisbreen Group	Eastern Province, Svalbard, Norway	-7 ‰	- 13 ‰	Halverson et al., 2006 Hoffman et al., 2012
(H)	Tasmania	Black River Fm., Togari Group	Smithton synclinorium, NW Tasmania	-2.5 ‰	-6.5 ‰	Calver, 1998
(I)	Australia	Burra Group	Adelaide Rift Complex, Australia	-3 ‰	-7 ‰	Hill and Walter, 2000
(J)	Cathaysia Block, South China (W)	Dajiangbian Fm.	Hunan Province, South China	-5.5 ‰	?	Feng and Zhang, 2016
(K)	Arabia (S)	Marian Bohkahko Fm. and Didikama Fm., Tambien Group	Negash Syncline, Tigre, Ethiopia	-3 ‰ -10 ‰ -2.5 ‰	-8 ‰ -15 ‰ -7.5 ‰	Swanson-Hysell et al., 2015
(L)	Congo/ Kalahari	Mwashia Sbgp. and Lower Roan Sbgp., Roan Group	Copperbelt, Zambia	-5 ‰ -2.5 ‰	-10 ‰ -7.5 ‰	Bull et al., 2011
(M)	Kalahari (W)	Hilda Subgroup, Port Nolloth Group	Gariep Belt South Africa	-5 ‰ 1 ‰	-12 ‰ -6‰	Macdonald et al., 2010b

Table 1.1: *Summary of documented pre-Sturtian anomalies.*

amalgamated landmasses during the existence of Rodinia (Li et al., 2013), are believed to have been evaporitic environments containing large amounts of buried organic carbon as well as authigenic carbonates. Their weathering would have resulted in large fluxes of isotopically-depleted carbon into the ocean. A positive $\delta^{34}S$ anomaly in sulfates on Victoria Island in northern Canada that coincides temporally with the Islay anomaly is consistent with evaporite weathering triggering increased pyrite formation and burial (Kaufman et al., 2006). However, the relationship between $\delta^{13}C$ and $\delta^{34}S$ is consistent with other mechanisms as well, such as methane release.

With the recent findings that have suggested the presence of at least two pre-Sturtian negative carbon isotope excursions, an older one ca. 739 Ma and a younger one ca. 720 Ma, and the importance of using negative carbon isotope anomalies in defining the base of the Cryogenian period, it is essential to revisit published records of the purported Islay anomaly to investigate relative and absolute age constraints on the pre-Cryogenian anomalies and compare them to new data from northern Namibia, which will be presented in Chapter 2.

1.6.1 (A) Scotland

The Islay Anomaly was first documented by Brasier and Shields (2000) within exposures of the Dalradian Supergroup in the Inner Hebrides of Scotland. The Dalradian Supergroup was deposited on the Eastern margin of Laurentia during the Neoproterozoic, possibly in a series of rift basins that formed as early precursors to the opening of the Iapetus Ocean (Anderton, 1982). It is now exposed in the Caledonian orogenic belt, outcropping between the Great Glen Fault and the Highland Boundary Fault across the Scottish mainland and stretching into northwestern Ireland (Spencer, 1971). A recent investigation of contact between pre-glacial and glacial strata, best exposed in the Garvellach Islands near Oban, suggests that the transition between the pre-glacial carbonates and the Sturtian glacial diamictite at this location is continuous, with no evidence of sub-glacial scour or karst associated with a drop in base level (Ali et al., 2017; Fairchild et al., 2017). Here, the newly named Garbh Eileach Formation of the Appin Group lies transitionally below Port Askaig Tillite Formation glacial deposits. The Garbh Eileach Formation is made up shallow-water carbonates followed by silty and sandy dolostones, interpreted as a peritidal environment in a semi-arid climate (Fairchild et al., 2017).

Carbon isotope data from this area shows a negative anomaly reaching -6 ‰ fewer than 50 metres beneath the base of the glacial deposits (see ***Figure 1.5 A***), implying a younger age than previously believed based on syn-anomaly dates from northwestern Canada (Fairchild et al., 2017; Rooney et al., 2014; Strauss et al., 2015). This new information suggests that there may be two separate anomalies that have previously been conflated into a single (i.e., the Islay) anomaly. Additionally, work done further west, on the island of Islay shows the pre-Sturtian anomaly reaching a nadir of ~ -6 ‰ and recovers back to positive $\delta^{13}C$ values beneath the erosional contact with the Port Askaig Formation glacial deposits, and also reveals a second negative anomaly lower in the stratigraphy, within the Ballachilish Formation, that has been tentatively correlated with the Bitter Springs Stage (Prave et al., 2009; Sawaki et al., 2010). However, Halverson et al. (2018) have suggested that the older anomaly could be correlative with the pre-Sturtian negative anomaly observed in northern Canada, which will be discussed below.

1.6.2 (B) Northeastern Greenland

A similar negative excursion occurs in the uppermost Andrée Land Group of East Greenland. The Andrée Land Group is primarily composed of carbonates and fine-grained siliciclastics and lies beneath Sturtian glacial deposits (Ulvesø Formation) of the Tillite Group. The Andrée Land Group is subdivided into twenty bed groups (Sønderholm and Tirsgaard, 1993), with the uppermost three recording shallow platform deposition (Bed Group 18) followed by an abrupt transition to deeper water slope deposits (Bed Group 19), then a return to shallow platform facies (Bed Group 20). The negative anomaly is only recorded within the deep-water deposits of Bed Group 19 (Fairchild et al., 2000; Klaebe et al., 2018) (See ***Figure 1.5B***). Fairchild et al. (2000) suggested that $\delta^{13}C$ stratification within the water column, where the deeper waters were isotopically depleted relative to surface waters, could produce the observed relationship between deep-water facies and negative $\delta^{13}C$ values and proposed that basin geometry may have limited circulation and generated stratification. In this case, even a primary $\delta^{13}C$ anomaly would not be representative of an isotopic change in global ocean DIC. In contrast, Klaebe et al. (2018) recognized the presence of diagenetic carbonate cements within the facies exhibiting the negative $\delta^{13}C$ excursion and argued that the anomaly is a local secondary signal. However, this anomaly appears to correlate both in magnitude and in sequence stratigraphic context with a coeval anomaly preserved in shallow-water carbonates in Svalbard, as discussed further below (Halverson et al., 2018).

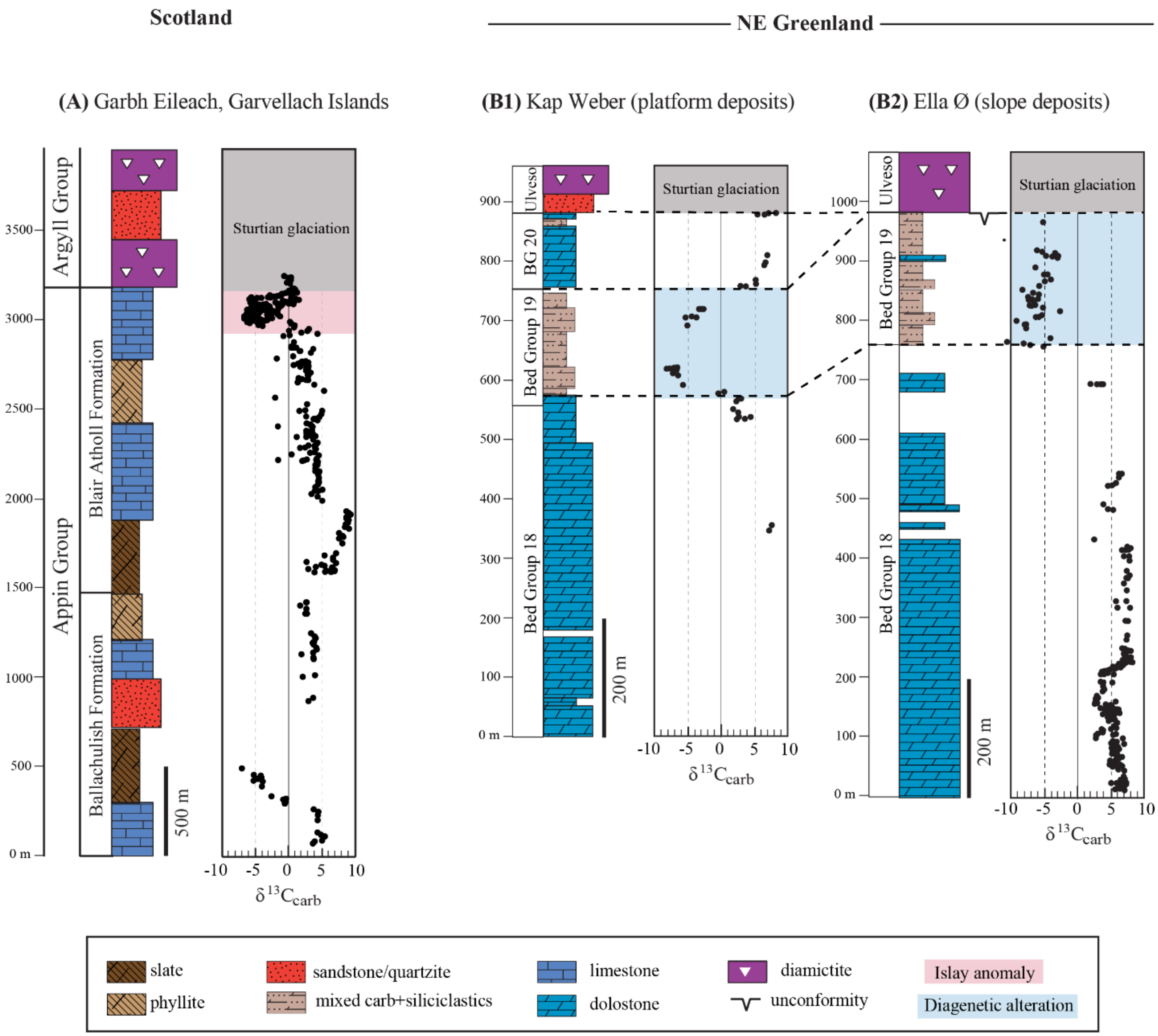

Figure 1.5: *The Islay anomaly in Scotland and Greenland. Garbh Eilaech section (A) modified from Fairchild et al. (2017). Data from Brasier and Shields (2000), Prave et al. (2009), Sawaki et al. (2010), and Fairchild et al. (2017). B1: Section from Kap Weber, NE Greenland. Modified from Klaebe et al., 2018. B2: Section from Ella O, NE Greenland. Modified from Klaebe et al., 2018.*

1.6.3 (C) Southwestern USA

The Basin and Range Province of southwest USA features exposures of kilometres of Neoproterozoic strata from the western margin of Laurentia, including the Pahrump Group in Death Valley which encompasses the late Tonian lead-up to the Cryogenian as well as the Cryogenian glacial deposits (Prave, 1999). The pre-Sturtian Beck Spring Dolomite of the Pahrump Group consists of interbedded dolostone and siliciclastics ranging from siltstone to pebble conglomerates, arranged in cyclic, metre-scale parasequences.

This formation hosts two separate negative $\delta^{13}C_{carb}$ excursions, one at its base and one at the top of the formation, directly beneath the erosional contact with the Kingston Peak diamictite (Corsetti and Kaufman, 2003; Smith et al., 2016) (see ***Figure 1.6 C***). This upper anomaly is interpreted as the Islay anomaly (Hoffman et al., 2012; Smith et al., 2016), and reaches a nadir close to -3 ‰. The basal carbon isotope anomaly of the Beck Spring Dolomite, which has a much wider scatter of $\delta^{13}C$ values, continues into siliciclastic Horse Thief Spring Formation, interpreted to represent deposition within a sahbka environment (Mahon et al., 2014). This type of depositional environment is more prone to early stage diagenesis that could impart a negative $\delta^{13}C$ signature. Combined with the mixed positive and negative values, the most parsimonious explanation is that this lower anomaly does not represent a global seawater signal (Strauss et al., 2015).

1.6.4 (D,E,F) Northern Canada

Neoproterozoic successions deposited in extensional basins along the northwestern margin of Laurentia are exposed in a series of inliers stretching across Northern Canada, including the Ogilvie Mountains and the Mackenzie Mountains in the northern Cordillera of the Yukon and Northwest Territories, and the Minto Inlier in Nunavut. Many important dates for constraining the timing of the Cryogenian glaciations and carbon isotope anomalies come from these successions, both from U-Pb zircon dating of ash beds and detrital zircons, and Re-Os dating of organic-rich shales (eg. Macdonald et al., 2010; Rooney et al., 2014, 2015). Recently, updated correlations based on carbon isotope chemostratigraphy and sequence stratigraphy, combined with new radiometric ages, have provided more robust temporal and geological constraints on the late Tonian negative $\delta^{13}C$ anomaly in this region (Thomson et al., 2015; Strauss et al., 2015).

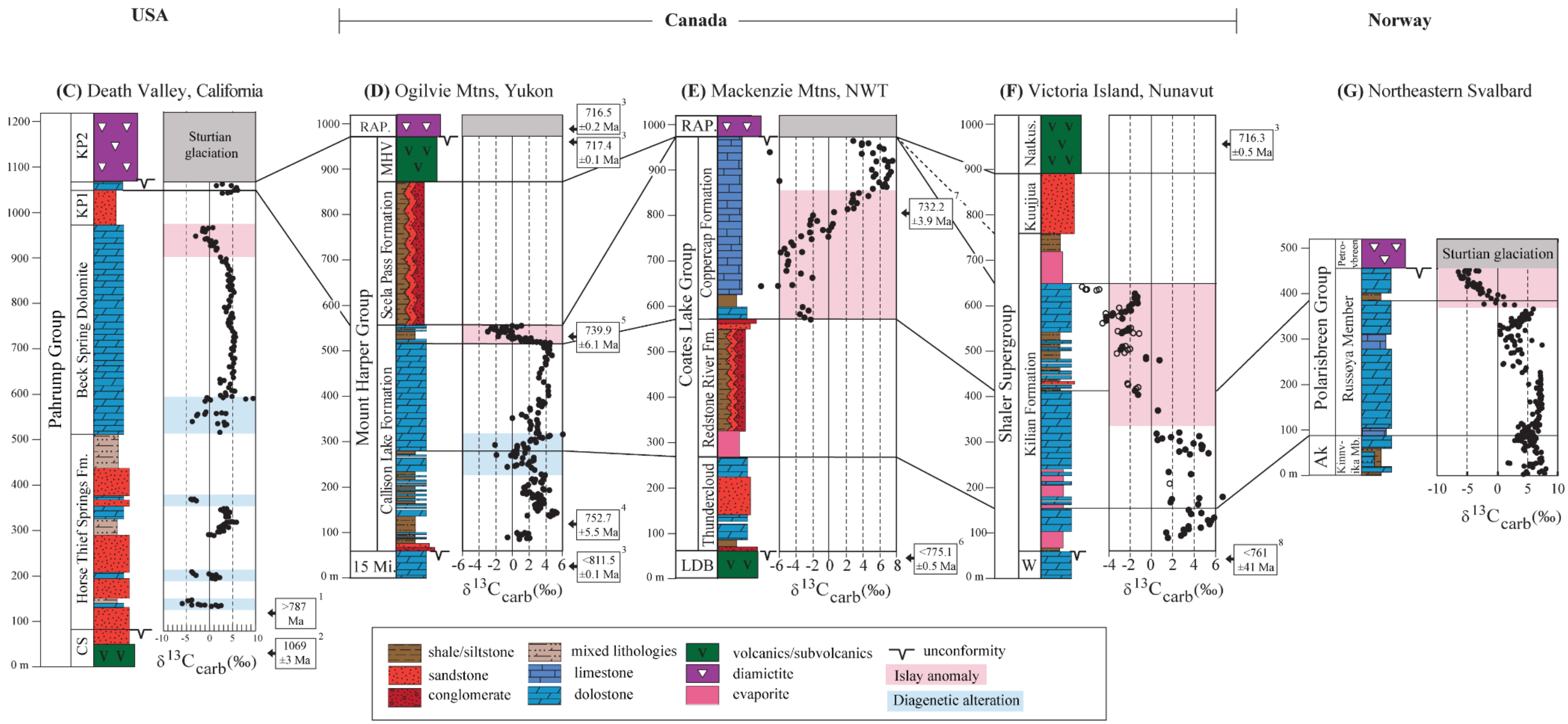
USA
Canada
Norway
(C) Death Valley, California
(D) Ogilvie Mtns, Yukon
(E) Mackenzie Mtns, NWT
(F) Victoria Island, Nunavut
(G) Northeastern Svalbard
Pahrump Group
KP2
KP1
Beck Spring Dolomite
Horse Thief Springs Fm.
CS
Sturtian glaciation
Mount Harper Group
RAP.
MHV
Seela Pass Formation
Callison Lake Formation
15 Mi.
Coates Lake Group
Coppercap Formation
Redstone River Fm.
Thundercloud
LDB
Shaler Supergroup
Natkus.
Kuujjua
Kilian Formation
W
Polarisbreen Group
Petro-vbreen
Russøya Member
Kinnv-ika Mb.
Ak
716.5 ±0.2 Ma
717.4 ±0.1 Ma
739.9 ±6.1 Ma
752.7 ±5.5 Ma
<811.5 ±0.1 Ma
732.2 ±3.9 Ma
<775.1 ±0.5 Ma
716.3 ±0.5 Ma
<761 ±41 Ma
>787 Ma
1069 ±3 Ma
$\delta^{13}C_{carb}$(‰)
shale/siltstone
sandstone
conglomerate
mixed lithologies
limestone
dolostone
volcanics/subvolcanics
diamictite
evaporite
unconformity
Islay anomaly
Diagenetic alteration

Figure 1.6: *The Islay anomaly in the USA, Canada, and Svalbard. Death Valley section (C) modified from Smith et al. (2015). CS= Crystal Spring Formation, KP= Kingston Peak Formation. Ogilvie Mountains, Mackenzie Mountains, and Victoria Island sections (D,E,F) modified from Strauss et al. (2015). 15 Mi= Fifteen Mile Group, MHV= Mount Harper Volcanics, RAP= Rapitan Group, LDB= Little Dal Basalt, Natkus.= Natkusiak Formation, W= Wynniatt Formation. Svalbard section (G) modified from Halverson et al. (2018). Correlations between C and D from Smith et al. (2015). Correlations between D,E,F from Strauss et al (2015). Correlations between F and G are from Halverson et al. (2018). Ages are from the following: 1: Mahon et al (2014). 2: Heaman and Grotzinger (1992). 3: Macdonald et al. (2010). 4: Rooney et al. (2015). 5: Strauss et al. (2014). 6: Milton et al. (2017). 7: Rooney et al. (2014). 8: van Acken et al. (2013).*

(D) Ogilvie Mountains, Yukon

The Callison Lake Formation of the Mount Harper Group is exposed in the Coal Creek and Hart River Inliers in the Ogilvie Mountains (Abbott, 1997; Mustard and Roots, 1997). This late-Tonian unit comprising mixed carbonate-siliciclastics is divided into four informal members, from oldest to youngest: the Heterolithic, Talc, Ramp, and Transitional members (Strauss et al., 2015). The lower boundary of the Mount Harper Group is defined by an unconformity characterized by brecciation and silicification of the underlying Fifteenmile Group. The Heterolithic member, ~25-150 metres thick, is made up of siliciclastics varying in grain size from siltstone to pebble conglomerate, overlain by shale with laterally discontinuous biohermal stromatolite. It is sharply overlain by the Talc member, which ranges in thickness from approximately 45 to 110 metres and is made up primarily of shales rich in authigenic talc, in some intervals interbedded with various carbonate facies. This member also shows evaporite pseudomorphs and likely represents deposition in an episodically restricted marginal marine environment (Strauss et al., 2015). Overlying the Talc member is the Ramp member, consisting of hundreds of metres of gray bedded dolostone, followed by the Transitional member, dominantly made up of interbedded stromatolitic dolostone and black shale, grading upwards into the coarser siliciclastic sediments of the overlying Seela Pass Formation. A negative δ^{13}C anomaly is recorded within the Transitional member (Macdonald et al., 2010a; Strauss et al., 2014)(see ***Figure 1.6 D***). This pronounced negative excursion is ascribed to the Islay anomaly, reaching a nadir as low as -5.8 ‰ in sections where it is most pronounced, with partial recovery to positive values either truncated by an unconformity or masked by a transition to siliciclastics. A Re-Os date from the declining arm of the anomaly gives an age of 739.9 ±6.1 Ma (Strauss et al., 2014). Additionally, within the upper Talc member, $\delta^{13}C_{carb}$ declines, sometimes below -5

‰, which is interpreted as likely being related to diagenetic alteration in the episodically evaporative depositional environment (Strauss et al., 2015).

(E) Mackenzie Mountains, Northwest Territories

In the Mackenzie Mountains, located northwest of the Ogilvie Mountains, the Coppercap Formation of the Coates Lake Group has been correlated with the Callison Lake Formation. The Coppercap Formation, which overlies siliciclastics of the Redstone River Formation, is unconformably overlain by Sturtian diamictite. Siltstones and microbialites form the base of the Coppercap Formation, succeeded by 100 metres of limestone marl, separated by a flooding surface, collectively comprising the lower half of the formation. The upper half marks a transition to limestone micrites and grainstones as the dominant facies (Rooney et al., 2014).

The carbon isotope profile shows negative $\delta^{13}C$ values in the marl-dominated lower half of the formation, recovering to approximately 6‰ in the upper half of the formation beneath the erosional truncation (see ***Figure 1.6 E***). Approximately 40 metres below the unconformity, $\delta^{13}C$ values appear to begin to downturn. A Re-Os depositional age of 732.2±3.9 Ma is determined near where the ascending arm of the $\delta^{13}C$ anomaly crosses 0‰ (Rooney et al., 2014).

(F) Minto Inlier, Nunavut

The late Precambrian Shaler Supergroup is exposed on the northern end of Victoria Island in the Minto Inlier. In this outcrop belt, pre-Cryogenian strata are capped by basalltic flows of the Natkusiak volcanics rather than glaciogenic deposits. The Natkusiak Formation, dated at 718±2 Ma, is part of the Franklin Large Igneous Province (Heaman et al., 1992). Lying uncomformably beneath these mafic volcanics is the siliciclastic-dominated Kuujjua Formation, which unconformably overlies the carbonate-dominated Kilian Formation, both containing minor evaporite deposits that suggest an arid paleoclimate (Rainbird, 1991). The Killian Formation reaches a maximum thickness of approximately 550 metres and is informally divided into eight members consisting dominantly of either evaporites or dolostones which often show coarsening upward cycles. The overlying Kuujjua Formation marks a shift to siliciclastic deposition (Rainbird, 1991).

The carbon isotope profile of the lower half of the Kilian Formation shows a wide scatter of $\delta^{13}C$ values ranging between 1 and 6 ‰, shifting into a gradual decline in the upper half of the formation and reaching a $\delta^{13}C$ low of nearly -7 ‰ at the top of the last carbonate unit (Prince, 2014; Thomson et al., 2015). This negative isotopic excursion is succeeded by evaporites and fine-grained siliciclastics, followed by the sandstones of the Kuujjua Formation (see ***Figure 1.6 F***). The observed $\delta^{13}C$ decline is tentatively correlated with the negative excursion in the Callison Lake and Coppercap formations, with the recovery presumably absent due to the transition to siliciclastic deposition in the uppermost Kilian Formation.

1.6.5 (G) Northeastern Svalbard

Well-preserved Neoproterozoic strata from the Akademikerbreen carbonate platform of eastern Laurentia are exposed on the eastern terrane of Svalbard (Fairchild and Hambrey, 1995). The Polarisbreen Group comprises latest Tonian to middle Ediacaran strata, including glaciogenic diamictites and associated facies associated with both Cryogenian glaciations. The mixed carbonate-siliciclastic Russøya Member of the Polarisbreen Group constitutes the pre-Sturtian strata in Svalbard. It is unconformably overlain by the Petrovbreen Member Sturtian glacial deposits (Hoffman et al., 2012). The upper Russøya Member shows $\delta^{13}C$ values above 5 ‰ descending as low as -7 ‰, followed by a slight recovery. This anomaly, which in many areas is erosionally truncated, has been correlated with the pre-Sturtian negative excursion observed in northern Canada (Halverson et al., 2017; Hoffman et al., 2012; ***Figure 1.6 G***).

1.6.6 (H&I) Tasmania and Australia

The Black River Dolomite of the Togari Group is thought to represent the pre-Sturtian strata of Tasmania, exposed in the Smithton synclinorium in northwestern Tasmania (Calver, 1998). The Black River Dolomite consists primarily of peritidal carbonates, often stromatolitic, diagenetic black chert, and black shale. Tasmania's geographic position during the Neoproterozoic is uncertain, but many reconstructions of Rodinia place Tasmania adjacent to the eastern margin of Australia (Li et al., 2008).

The carbon isotope profile of the Black River Dolomite, though sparse, shows $\delta^{13}C_{carb}$ values close to 4 ‰ for the lower half of the formation, followed by a fall to -2.5 ‰ beneath the Julius River Member glacial diamictites (***Figure 1.7 H***). This decline has been attributed to the Islay anomaly, and has also been tentatively correlated with a similar negative anomaly (reaching approximately -4 ‰) observed in the Burra Group of the Adelaide Rift Complex in Australia (Hill and Walter, 2000) **(*Figure 1.7 I*)**.

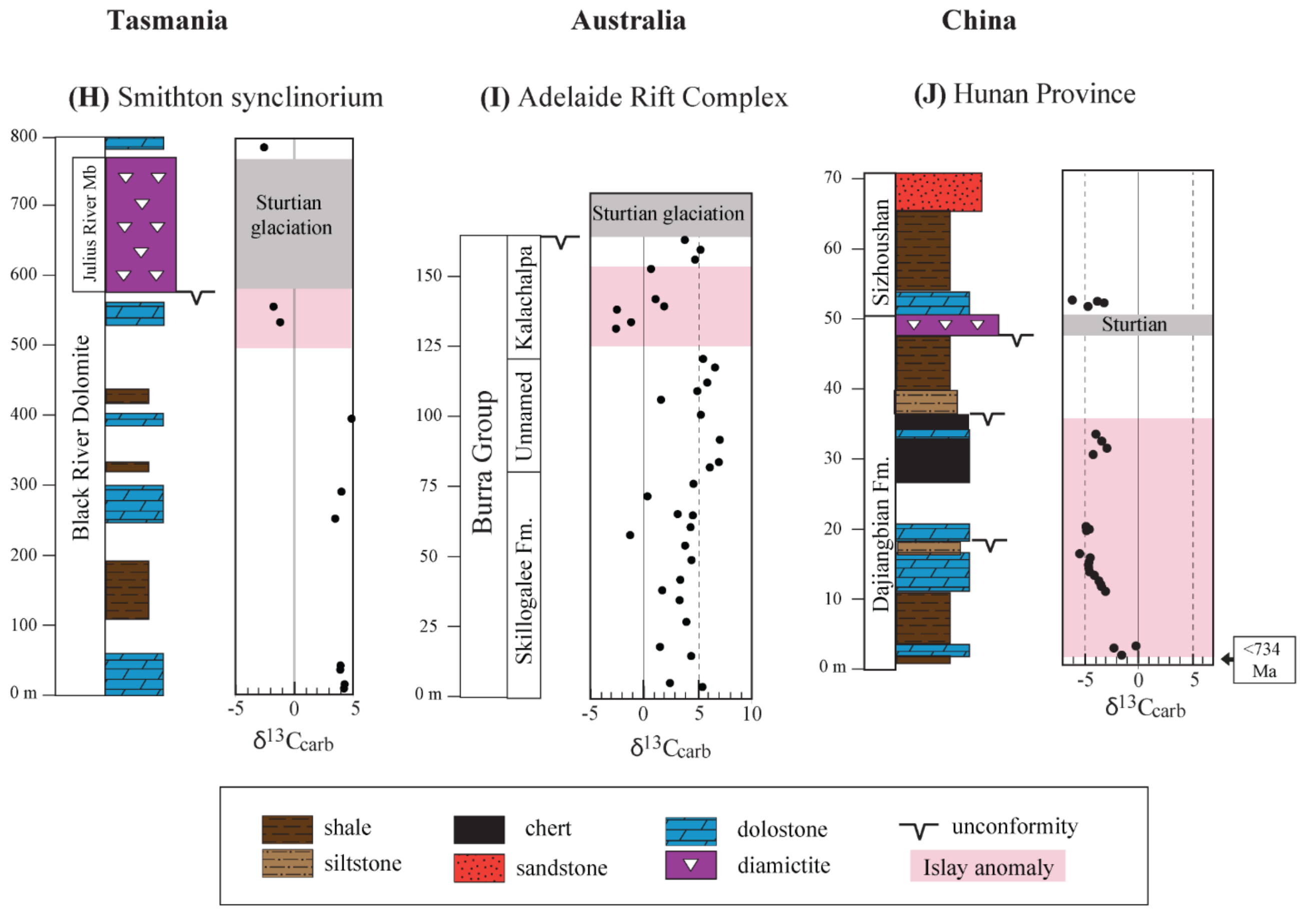

Figure 1.7: *The Islay anomaly in South China, Australia, and Tasmania. South China section (I) modified from Feng and Zhang (2016), Adelaide Rift Complex section (J) modified from Hill and Walter (2000). Tasmania section (K) modified from Calver et al. (1998). Date from South China from Wu et al. (2013).*

1.6.7 (J) South China

The Dajiangbian Formation in southern China records pre-Sturtian sedimentation on the western margin of the Cathaysia block of South China, deposited within a subsiding rift basin that formed during the breakup of Rodinia. The upper part of this succession, along with the overlying Sturtian Sizhoushan Formation, is exposed in the Sizhoushan syncline in the southern region of the Hunan Province (Feng and Zhang, 2016). Dating of detrital zircons gives a maximum age constraint of 734 Ma for the Dajiangbian Formation (Wu et al., 2013). The upper Dajiangbian Fm consists of shales and chert with intebedded dolostone that suggest deposition that shifted between shallow and deep marine.

The carbon isotope profile through the Dajiangbian Formation shows $\delta^{13}C$ values dropping from 0 ‰ to a nadir of -5.4 ‰, followed by a partial recovery to -2.5 ‰ (***Figure 1.7 J***). Carbonates are absent in the uppermost 10 metres of the section beneath the subglacial erosional unconformity.

1.6.8 (K) Ethiopia

In the Tigray region of northern Ethiopia, the Neoproterozoic Tambien Group is exposed in a series of synclines uplifted during the East African Orogeny (Stern, 1994). This succession, up to 5 km thick, comprises Tonian and Cryogenian strata from the south of the Arabian-Nubian shield (Beyth et al., 2003; Miller et al., 2003; Stern et al., 2006). The easternmost exposure of the Tambien Group, hosted within the Negash syncline, is cored by a late Tonian mixed cabonate and siliciclastic succession and overlying Sturtian glaciogenic deposits. The latest Tonian formations, from oldest to youngest, are the Didikama Formation, Mattheos Formation, and Marian Bohkakho Formation. The Didikama Formation consists mostly of parasequences of fine-grained siliciclastics, sandstones, and deep-water carbonates. The Mattheos Formation is carbonate-dominated, showing a transition from deep to shallow carbonate facies. The Marian Bohkakho Formation marks a return to intercalated deep-water carbonates and fine-grained siliciclastics.

The carbon isotope profile of these formations in the Negash syncline show three separate negative excursions ***(Figure 1.8 K)*** (Swanson-Hysell et al., 2015). The lowermost negative excursion is situated approximately 400 metres above the base of the Didikama Formation and is relatively low magnitude, reaching a nadir of close to -2 ‰. The middle anomaly, only documented on the eastern arm of the syncline, documents a gradual decline from approximately 4 ‰ to -1 ‰ over 150 metres, followed by a sharp drop to as low as -10 ‰ within the 10 metres beneath an inferred disconformity separating the Didikama Formation and the overlying Matheos Formation, which marks an abrupt return to a ca. 5 ‰ background. Swanson-Hysell et al. (2015) interpret this middle anomaly to be the Islay anomaly. The $\delta^{13}C$ values begin to decline once again in the Marian Bohkahko Formation, falling to nearly -3 ‰ beneath the unconformity with the Sturtian diamictite. This decline coincides with a shift to deeper-water facies in which secondary authigenic carbonate cements are more likely to occur, and therefore may not be a true

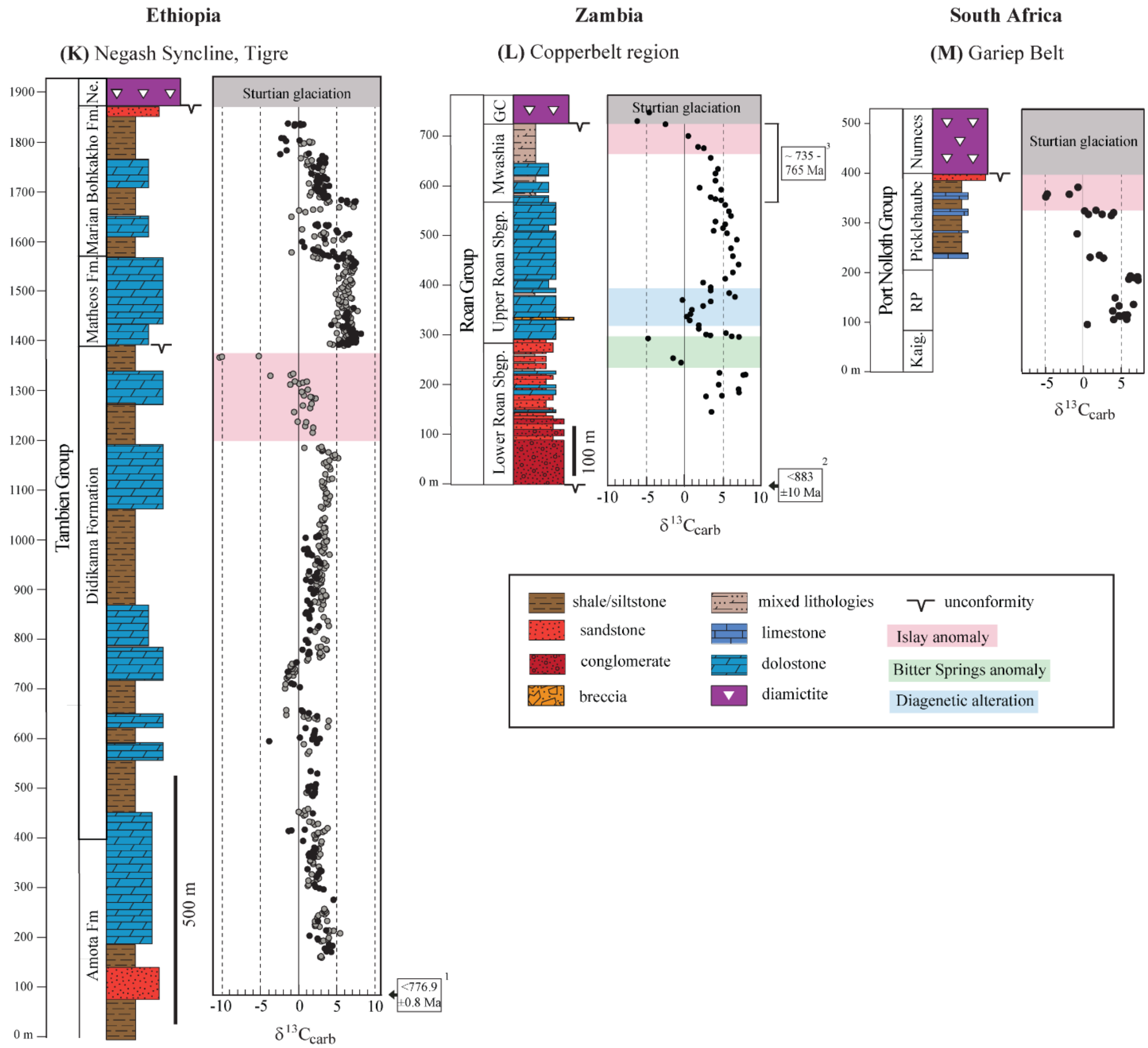

Figure 1.8: *The Islay anomaly in Ethiopia, Zambia, and South Africa. Negash syncline section (K) from Swanson-Hysell et al. (2015). Ne= Negash diamictite. Copperbelt section (L) modified from Bull et al. (2011), GC= Grand Conglomerat. Gariep Belt section (M) modified from Macdonald et al. (2010b). Kaig. = Kaigas Formation; RP = Rosh Pinah Formation. Ages from the following references: 1: Swanson-Hysell et al. (2015); 2: Armstrong et al. (2005); 3: Key et al. (2001).*

record of global seawater. However, the authors tentatively suggest that it could correlate with a similar downturn observed at the top of the Coppercap Formation in northern Canada.

1.6.9 (L) Zambia

The Neoproterozoic Roan Group was deposited off a rifted continental margin into the Katanga basin between the Congo and Kalahari cratons. It is now exposed around the Kafue Anticline in the Zambian Copperbelt, where it hosts several copper deposits (Bull et al., 2011). It unconformably overlies granites that provide a maximum depositional age of 883±10 Ma for the base of the Roan Group (Armstrong et al., 2005). It is subdivided into a siliciclastic-dominated Lower Roan Subgroup, a carbonate-dominated Upper Roan Subgroup, and the uppermost Mwashia Subgroup, which consists primarily of carbonate and carbonaceous siltstones (Bull et al., 2011). Dating of mafic lavas within the Mwashia Subgroup suggests that it was likely deposited between 765-735 Ma (Key et al., 2001). The Mwashia Subgroup is unconformably overlain by Sturtian-aged glacial deposits forming the Grand Conglomerat.

The carbon isotope trend of the Roan Group shows two negative excursions, the younger of which is recorded in the Mwashia Subgroup and reaches ~ -5 ‰ below a subglacial erosion surface at the base of the Grand Conglomerat ***(Figure 1.8 L).*** The older anomaly in the uppermost Lower Roan Subgroup is of a comparable magnitude. The younger anomaly is ascribed to the Islay anomaly, and the older to the Bitter Springs Stage (Bull et al., 2011), although both are only defined by three data points making the inferred correlations ambiguous at best.

1.6.10 (M) Northern South Africa (and southern Namibia)

The Gariep Belt in northern South Africa and southern Namibia contains exposures of the Neoproterozoic Port Nolloth Group, deposited off the rifted western margin of the Kalahari Craton in the Adamaster Ocean (Jasper et al., 2000; Stowe et al., 1984). The Hilda Subgroup lies beneath diamictite of the Numees Formation ascribed to the Sturtian glaciation (Macdonald et al., 2010b). The Hilda Subgroup is divided into three formations, the oldest being the Kaigas Formation consisting of up to 100 metres of diamictite, which has caused much confusion and miscorrelation with the Numees diamictite, as well as speculation about a third, pre-Sturtian Snowball event (Frimmel et al., 1996; Frimmel and Fölling, 2004). It is now accepted that the purported Kaigas glaciation was not global and its deposits are probably not even of glacial origin (Rooney et al., 2015; Zhang et al., 2009). The overlying Rosh Pinah Formation consists of up to 850 metres of siliciclastics and carbonates deposited into an actively rifting graben (Alchin et al., 2005). A depositional age of 741±6 Ma is reported from Pb-Pb zircon dating of felsic volcanic rocks hosted within the Rosh Pinah Formation (Frimmel et al., 1996). The Picklehaube Formation comprises ~200 metres of shallowing upward carbonate sequences. Unconformably overlying the Hilda Subgroup is the Sturtian Numees Formation, composed of massive and stratified diamictite. Much of the pre-Sturtian $\delta^{13}C$ data reported from this area in the past (Fölling and Frimmel, 2002) may be unreliable due to miscorrelations, therefore only the $\delta^{13}C$ data reported by Macdonald et al. (2010b) are considered here (***Figure 1.8 M***). The carbon isotope profile of the Hilda Subgroup shows $\delta^{13}C$ values near 0 ‰ immediately above the Kaigas Formation, followed by a recovery to nearly 8 ‰ over the following 100 metres, then a gradual decline down to nearly -5 ‰ within the 200 metres beneath the Numees diamictite.

1.7 Conclusion

Despite the many documented occurrences globally of pre-Sturtian $\delta^{13}C$ excursions, the 'Islay' anomaly has not been conclusively reported in the Otavi Group of northwestern Namibia, a succession which played a key role in the development of the Snowball Earth Hypothesis (e.g. Hoffman et al., 1998). In the next chapter, I will discuss a depositional framework and regional correlations for the pre-Cryogenian Ugab Subgroup of the Otavi Group and use these to integrate the existing carbon isotope data with our new results to present an updated carbon isotope profile for the Ugab Subgroup, which is consistent with the recent proposal of the existence of two discrete pre-Sturtian negative $\delta^{13}C$ anomalies.

CHAPTER 2

2.1 Introduction

The Neoproterozoic Otavi Group of northwestern Namibia plays an important role in the exposition of the Snowball Earth Hypothesis. It was within this carbonate-dominated succession that Hoffman et al. (1998) found the initial geologic evidence supporting the hypothesis and used sedimentological features and geochemical and isotopic signatures preserved in the Otavi Group to further develop the hypothesis (e.g. Hoffman et al 1998a,b; Hoffman and Schrag, 2002). These findings sparked an interest that later led to widespread acceptance of the Snowball Earth Hypothesis by the geological community.

Located along what is now the southern margin of the Congo craton, the Otavi Group, reaching a thickness of up to 4 km, is the sedimentary succession from a ca. 770-590 Ma carbonate platform (Hoffmann and Prave, 1996; Miller, 2008). During the late Tonian, rifting between the Congo craton and a craton to the south (in present day coordinates) resulted in the opening of the deep-water basin with a broad carbonate platform to the north, divided by a well-developed platform-margin to slope transition. The Otavi Group of northwestern Namibia hosts two distinct glaciogenic deposits (Hoffmann and Prave, 1996) and provides a carbon isotope profile with several well-defined negative anomalies including two post-glacial recoveries and the pre-Marinoan Trezona anomaly, which is remarkably well-preserved (Halverson et al., 2002). The pre-Sturtian Islay anomaly, however, is notably not well documented.

The Ugab Subgroup of the Otavi Group comprises the most immediately pre-Cryogenian strata of northwestern Namibia and is only present south of the shelf-break of the Otavi Platform where it was deposited in the Outjo basin adjacent to the Huab Ridge. Negative $\delta^{13}C$ values have been documented in the Ugab Subgroup where it outcrops in the Summas Mountains region (Hoffman and Halverson, 2008; Hoffman, unpublished data), but their affinity with the Islay anomaly is uncertain, and the stratigraphic relationships between the Ugab Subgroup strata in the Summas Mountains and other exposures of the subgroup are not well-defined.

This chapter will provide an overview of the Otavi Group and present new carbon isotope data from sections of the Ugab Subgroup measured in the Summas Mountains Inlier and a separate inlier ~ 120 km to the west, the Vrede Domes. The chemostratigraphic data and lithological variations in the measured sections will be used to investigate the depositional history of the Ugab Subgroup and the transition into the Sturtian glaciation.

2.2 Paleogeographic and tectonic context

The Neoproterozoic Damara Supergroup in northwestern Namibia comprises the sedimentary successions deposited on the southern margin of the Congo craton during the fragmentation of Rodinia and subsequent early stages of Gondwana assembly. The earliest episode of rifting is archived by the clastic-dominated Nosib Group, but rifting continued through deposition of the lower Otavi Group. The rift-drift transition occurred ca. 650 Ma (Halverson et al., 2002), just prior to the onset of the Marinoan glaciation, and passive margin sedimentation continued into the upper Otavi Group. Pan-African convergence, specifically collision between the Rio de la Plata craton and the Congo craton ca. 590 Ma, is recorded by the foreland basin molasse Mulden Group (e.g. Martin and Porada 1977a,b; Miller, 1997, 2008).

The location of the Congo- São Francisco craton during Rodinia time is not well constrained. Most paleogeographic reconstructions place the Congo- São Francisco craton as a smaller continent separate from Rodinia (Kröner and Cordani, 2003; Tohver, 2006; Li et al., 2008). It is unknown what craton was adjacent to the (present-day) south margin of the Congo craton at the beginning of the Neoproterozoic. Though early work presumed it to be the Kalahari craton (e.g. Martin and Porada, 1977; Miller 1983), this hypothesis has been challenged (Prave 1996; Gray et al., 2008; Foster et al., 2015). Regardless of these uncertainties, paleomagnetic data suggest that the Congo- São Francisco craton remained at low latitude for the duration of the Cryogenian Period, drifting from 12° to 39° between approximately 740 Ma to 550 Ma (Hoffman et al., 1998; Hoffman and Li, 2009; Meert et al., 1995; Trindade and Macouin, 2007).

Early during the fragmentation of Rodinia, north-south crustal stretching opened a rift basin between the Congo craton and its conjugate margin to the south. Initial rifting, ca. 900-760 Ma, resulted in the deposition of the Nosib Group as siliciclastic sediments were shed southward off the Congo craton into the emerging rift basin (Miller, 2008). As extension continued episodically for ~140 Ma, the Huab and Makalani Ridges developed in the basin from uplift and back-rotation along large-scale normal faults. The Makalani Ridge was active earlier than the Huab Ridge, with uplift during deposition of the Ombombo Subgroup resulting in northward shedding

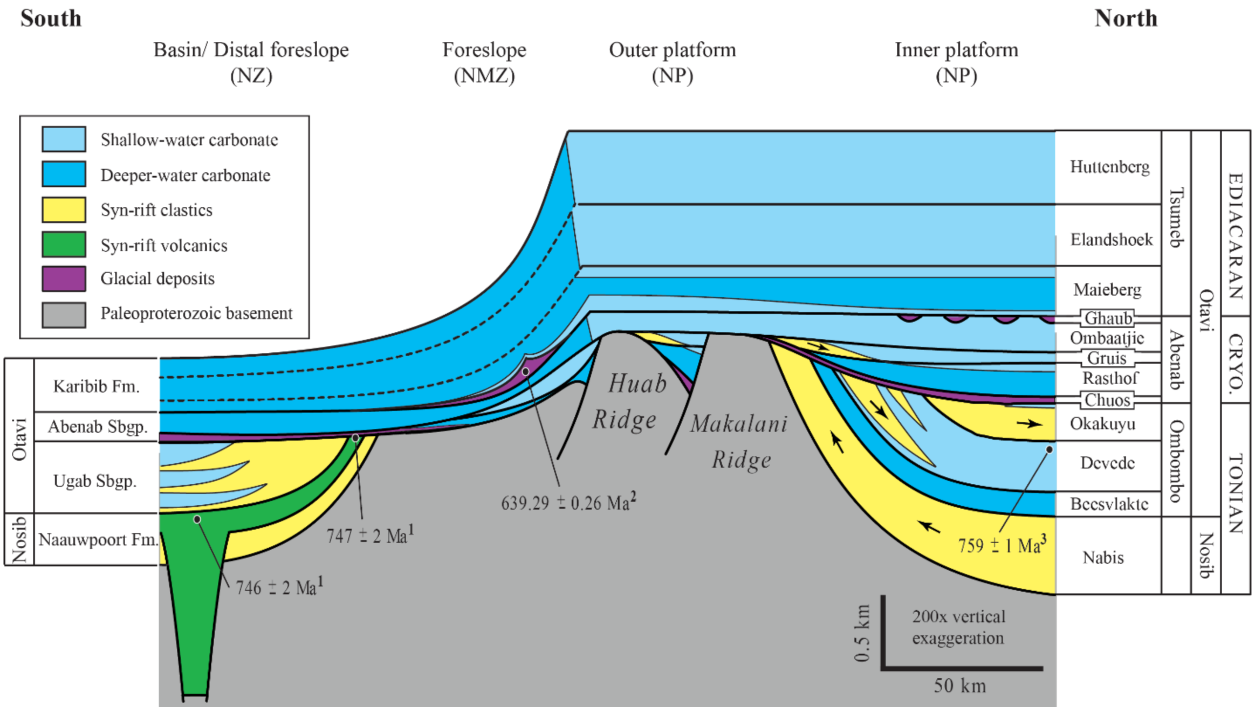

Figure 2.1*: A generalized cross-section of the Otavi Platform at the end of the Ediacaran Period. Modified from Hoffman et al., 2017. Arrows indicate paleoflow direction. Radiometric dates are from the following references: 1: Hoffman et al., 1996; 2: Prave et al., 2016; 3: Halverson et al., 2005.*

of siliciclastic sediments down the Makalani dipslope towards the Congo craton, into the Makalani sub-basin. South of the Makalani Ridge, in the Outjo sub-basin, the 746±2 Ma (Hoffman et al., 1996) Naauwpoort Formation was erupted as the result of extensional volcanism, followed by deposition of intercalated siliciclastic sediments and peritidal carbonates of the Ugab Subgroup. Intensity of the crustal stretching increased southwards, causing differentiation between the Makalani sub-basin and the deeper Outjo sub-basin to the south (Henry et al., 1990). Uplift and rotation of the Huab Ridge likely began sometime during the Sturtian glaciation, resulting in the development of the small ridge-bounded Huab sub-basin on the dip-slope within the half-graben (Hoffman and Halverson, 2008). Rifting continued throughout the Sturtian glaciation and ended during the interglacial interval, roughly mid-way through deposition of the Abenab Subgroup. As crustal stretching ceased ca. 650 Ma and thermal subsidence took over as the dominant control on the basin (Halverson et al., 2002), a stable shallow-water carbonate platform developed with a shelf-break at the scarp of the Huab ridge. South of this break was a foreslope leading into the deep-water Outjo sub-basin, and to the north was the shallow Hoanib Lagoon. Ensuing thermal subsidence on the passive margin

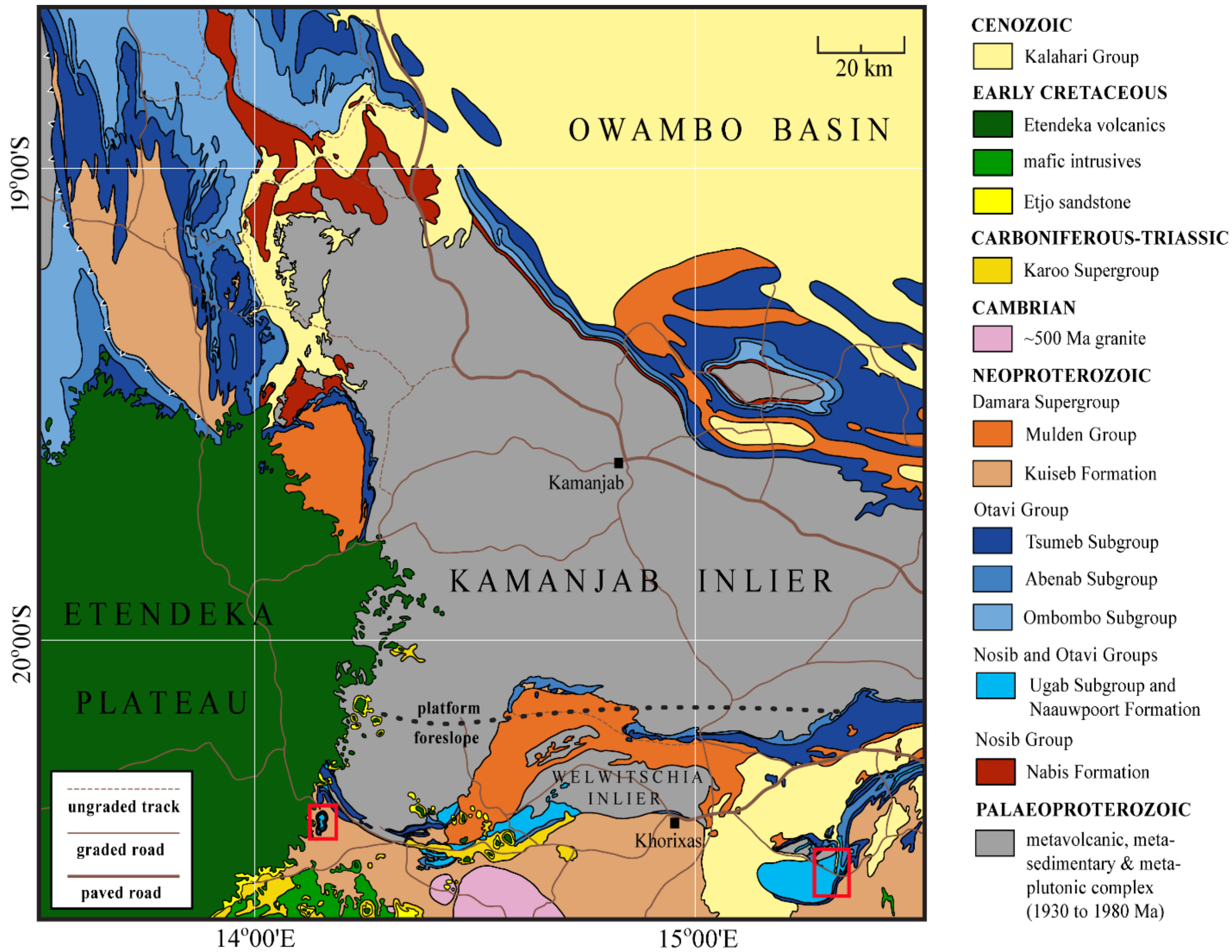

Figure 2.2*: Geologic map of the area Otavi Fold Belt area, surrounding the Kamanjab Inlier, modified from Hoffman and Halverson (2008). Field areas outlined in red boxes; Vrede Domes to the left and the Summas Mountains to the right.*

accommodated nearly two kilometres of almost entirely carbonate deposition comprising the upper Abenab Subgroup and the Tsumeb Subgroup (**Figure 2.1**).

The late Neoproterozoic amalgamation of the Congo-São Francisco, Rio de la Plata, and Kalahari cratons represents an important part in the assembly of Western Gondwana. Though the relative timing of collisions has been contested (eg., Stanistreet et al, 1991; Prave 1996; Frimmel and Frank 1998; Gray et al., 2008; Oriolo et al., 2017), most recent work indicates that the Damara Orogen began with the closure of the Adamaster Ocean to the (modern-day coordinates) west of the Congo craton through oblique convergence with the Rio De La Plata craton. The cratons collided between 650-580 Ma (Goscombe and Gray, 2007) and the resulting transpressional Kaoko orogen became a source of sediment influx to the Otavi Platform, causing the deposition of a foreland basin molasse, the Mulden Group. These deposits were subsequently folded and deformed as the Congo and Kalahari cratons converged, closing the Khomas Sea (and Outjo basin) ca. 550 Ma (Schmitt et al., 2012). It has been suggested that prior to the Congo-Kalahari collision, a separate microcontinent, the Swakop terrane, collided with and became sutured to the southern margin of the Congo craton (Hoffmann, 1987).

The three-branched Damara orogenic system consists of the roughly NNW-trending Kaoko and Gariep belts along the western coast of Namibia, from collision of the Rio de la Plata craton with the Congo craton and the Kalahari craton respectively, and the ENE- trending Inland Branch, also referred to as the Damara Belt, from the collision of the Congo and Kalahari cratons (Miller, 1983). The Otavi Group is exposed in a curved fold-and-thrust belt adjacent to the intersection of the Kaoko and Damara orogenic belts (**Figure 2.2**). This region is sometimes referred to as the Otavi fold belt, and it is centered on the Kamanjab Inlier, a large area of uplifted Paleoproterozoic basement rock (Miller, 2008). The Makalani dipslope is exposed along the western flank of the Kamanjab Inlier, and the Huab ridge paleokarst and corresponding platform-foreslope transition are exposed on the southern flank of the Kamanjab Inlier in the Fransfontein Ridge (Hoffman and Halverson, 2008).

Miller (1983, 2008) divided Namibia into tectonostratigraphic zones associated with the Damara Orogen, (see **Figure 2.3**), with alternate names for the zones offered by Hoffmann et al. (1989). The Otavi Group lies within three of these tectonostratigraphic zones: the Northern Platform, the Northern Margin Zone, and the northernmost Northern Zone, where there is a gradational transition into the basinal correlatives of the Swakop Group (Miller, 2008).

The Northern Platform (NP) or Otavi Platform contains the platform facies rocks of the Otavi Group. Damara Supergroup successions are exposed along the western and southern rim of the NP and extend beneath Phanerozoic cover in the Owambo Basin to the east. The western border of the NP is defined by the east-vergent Sesfontein Thrust, which juxtaposes metamorphosed Otavi Group from the internal zone of the Kaoko Belt against the less deformed fold and thrust belt. The southern border is the platform-to-slope transition; it is well-exposed along the southern flank of the Kamajab Inlier. The Northern Margin Zone (NMZ) is a thin strip of foreslope deposits rimming the southern edge of the NP. The NMZ is separated from the Northern Zone to the south by the Khorixas-Gaseneirob Thrust (KGT). The Northern Zone (NZ) or Outjo Zone

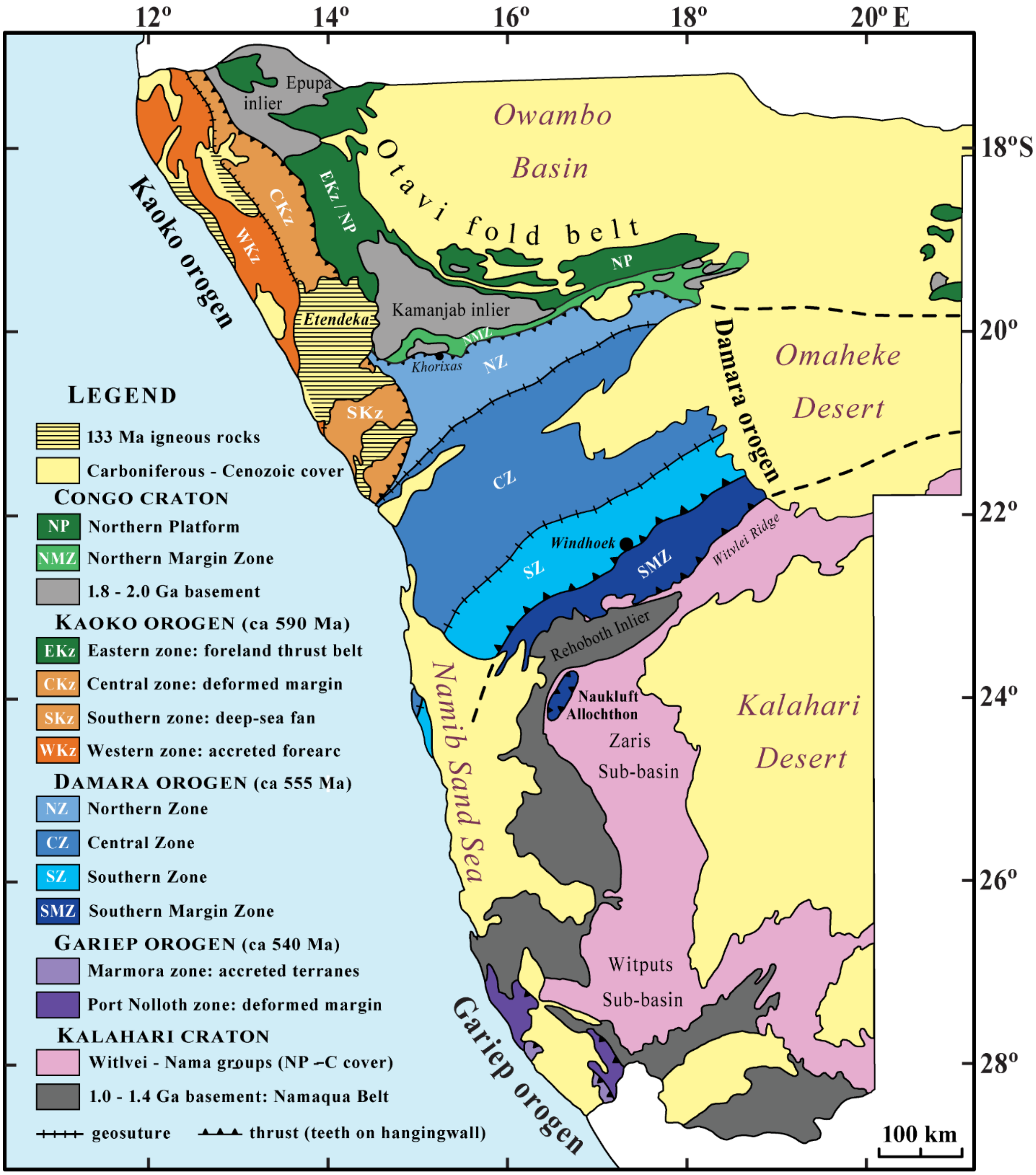

Figure 2.3: *Tectonostratigraphic map of Namibia, modified from Hoffman and Halverson (2008) to add NMZ from Miller (2008).*

made up part of the seafloor of the Outjo basin during rifting and spreading. When the Kalahari and Congo cratons collided ca. 550 Ma, the NZ was thrust northward along the KGT onto the NMZ. It is mostly within the NZ that the Ugab Subgroup outcrops. The southern boundary of the NZ is the Otjihorongo Thrust. South of the NZ, tectonostratigraphic interpretations differ as some workers believe that the Central Zone represents a separate (Swakop) microcontinent (Hoffmann 1987). Nevertheless, the stratigraphy of the Central Zone closely resembles that of the NMZ (Hoffmann 1987; Hoffmann et al., 2004) indicating at least a similar if not contiguous basin development.

2.3 Otavi Group Stratigraphy

This section will provide an overview of the Otavi Platform stratigraphy, followed by an overview of the equivalent successions on the foreslope and the basin proximal to the foreslope (**Figure 2.4**). Carbonate facies are classified using a scheme defined by Hoffman and Halverson (2008), described in **Table 2.1**. As both field sites fall within the NZ, the basinal stratigraphy is the most relevant to this thesis, but the platform and foreslope stratigraphy have been more extensively studied in the context of Snowball Earth and are relevant to the interpretation of the downslope correlatives in the basin.

The Ugab Subgroup in the northernmost NZ is often assigned to the Swakop Group (e.g., Clifford, 2008; Hoffmann et al., 2004; Miller et al., 1980). However, for this study, it is assigned ito the Otavi Group, the equivalents of which unambiguously extend into the northernmost NZ. The exact location where the Otavi Group laterally transitions into the Swakop Group is difficult to identify due to the gradational nature of the transition. Furthermore, the basinal Otavi Group includes stratigraphic nomenclature from the Swakop Group (e.g. Karibib Formation and Ugab Subgroup) (Hoffman and Halverson, 2008).

2.3.1 Platform Stratigraphy

Otavi Group successions on the platform are exposed north of the Kamanjab Inlier in the foreland belt stretching up to the Epupa Inlier, and east extending to the Otavi Mountainlands. It is worth noting that the interglacial formation names in the Otavi Mountainlands area of the eastern NP (SACS 1980) differ from those assigned to equivalent strata to the west (Hoffmann and Prave 1996); the nomenclature introduced by Hoffmann and Prave (1996) is used here. The Otavi Platform can be separated into the outer platform, containing the elevated rift shoulders of

	Facies	Description	Depositional environment
Shallowest	Microbialaminite	Thinly laminated carbonate sediments with crinkly lamination. May have sedimentary structures that suggest a shallow depositional environment such as teepee structures and breccias.	Intertidal to supratidal zones
	Grainstone	Carbonate sands. Often display dark-coloured silicification, likely due to the high primary permeability, which occasionally preserves giant ooids and crossbedding	Sub- to lower intertidal zone, under continual influence of wave break action
Shoaling →	Stromatolite	Mounded microbial growth structures, often Tungussia-type - columnar stromatolites with divergent branching patterns, and pinkish in colour. Conophyton-type stromatolites may also be present.	Sub-tidal zone, maximum depth limited by photic zone
	Ribbonite	Finely laminated silt-to-fine-sand -sized carbonate sediments showing low-angle cross-stratification. May be mixed with siliciclastic muds (marly ribbonite).	Low-energy zone well below breaking waves but above the storm wave base
Deepest	Rhythmite	Parallel-laminated carbonate muds, may also contain turbidites.	Below storm wave base

Table 2.1: *Carbonate lithofacies classification scheme as described by Hoffman and Halverson (2008).*

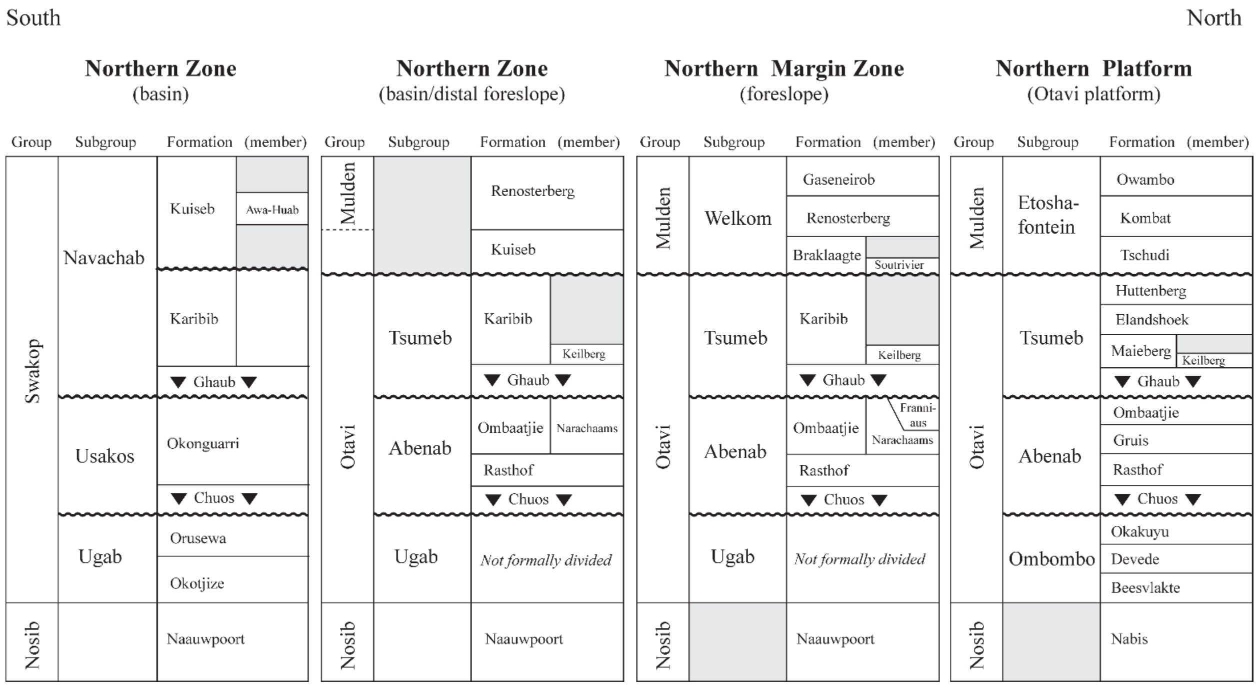

Figure 2.4: *Generalized stratigraphic nomenclature of the Damara Supergroup in the NP, NMZ, and northern NZ. Corrugated lines represent surfaces of significant erosion. The relationship between the Kuiseb Formation and the Mulden Group is uncertain. NZ nomenclature from Miller (2008); Northernmost NZ nomenclature as described by Hoffman (2016;2017); NMZ nomenclature from Frets (1969) and Hoffman and Halverson (2008); NP nomenclature from Hedberg (1979), Hoffmann and Prave (1996), and Hoffman and Halverson (2008).*

the Huab and Makalani Ridges, and the inner platform, north of the Makalani Ridge, encompassing the Hoanib Lagoon (Halverson et al., 2002).

The Otavi Group variably lies directly on Paleoproterozoic basement rock of the Congo craton or the ca. 900-760 Ma Nosib Group, which is made up primarily of coarse clastic sediments derived during early rifting, and local volcanic rocks related to extension (Miller, 2008). On the platform, the Nabis Formation makes up the Nosib Group (SACS, 1980), consisting dominantly of fluvial sandstones, sometimes underlain by a basal conglomeratic alluvial fan wedge. The sandstones are feldspathic and sometimes exhibit crossbedding, with paleocurrent measurements indicating a southward flow direction (Miller, 2008). The Nabis Formation ends abruptly beneath a sharp flooding surface marking the base of the Ombombo Subgroup, the basal subgroup of the Otavi Group within the NP.

The Otavi Group

Ombombo Subgroup

The Ombombo Subgroup is made up of the Beesvlakte, Devede, and Okakuyu formations, encompassing lower siliciclastics, middle carbonates, and upper shallow-water siliciclastics respectively (Hoffmann and Prave, 1996; Hoffman and Halverson, 2008). Northward paleocurrent measurements indicate that the clastic sediments were derived from the uplifted Makalani Ridge to the south (Hoffman and Halverson, 2008).

The Beesvlakte Formation is composed dominantly of argillite. It is commonly tectonized and recessive, but where exposed, it reaches a maximum thickness of just over 200 m. Though mostly made up of fine-grained siliciclastics, the Beesvlakte Formation contains a middle carbonate unit topped by a subaerial exposure surface, followed by an abrupt return to fine grained siliciclastics, which slowly grade upwards into carbonates of the Devede Formation.

The Devede Formation is up to approximately 400 m thick. It comprises a series of carbonate parasequences bounded by subaerial exposure surfaces and flooding surfaces. It is dominantly dolostone but contains siliciclastics, often at the base of parasequences in the lower half of the formation, and the upper half of the formation contains abundant Tungussia-type stromatolites (Hoffman and Halverson, 2008). An ash bed from near the top of the Devede Formation gives a U-Pb zircon age of 759.3±1.3 Ma (Halverson et al., 2005).

The Devede Formation is separated from the overlying Okakuyu Formation by a scoured surface. The Okakuyu Formation is made up of stacks of progradational siliciclastic parasequences bounded by subaerial exposure surfaces, interpreted to record deltaic deposition. The parasequences consist of siltstone that grades upward into quartz-rich sandstone and conglomerate. In the upper parasequences some conglomerates contain undeformed basalt clasts. The youngest parasequence ends with a thick, cliff-forming stromatolite unit that is capped by a brecciated unconformity (Hoffman and Halverson, 2008).

Abenab Subgroup

The Ombombo Subgroup is unconformably overlain by the glaciogenic Chuos Formation of the basal Abenab Subgroup, marking the beginning of the Cryogenian Period. Its thickness is extremely variable, ranging from absent in some locales to up to a kilometre thick in depositional centres such as paleovalleys and moraines (Hoffman et al., 2017). The Chuos Formation is dominantly diamictite, both stratified and massive, with clasts made up of Paleoproterozoic metamorphic basement rock, sandstones from the Nosib Group, carbonates and siliciclastics from the underlying Ombombo Subgroup, and locally, volcanics. Associated with the diamictites in the Chuos Formation, there are also conglomerates and pebbly sandstones deposited by flowing water possibly in subglacial meltwater channels, laminated siltstones containing ice rafted debris, and iron formation (Hoffman and Halverson, 2008).

Chuos glaciogenic deposits are abruptly but conformably overlain by the Rasthof Formation cap carbonate sequence (Hoffmann and Prave, 1996), deposited during a sea-level highstand following extensive melting of continental glaciers during the collapse of the Sturtian Snowball earth (Hoffman et al., 1998a,b). This formation is informally divided into three members (Hoffman and Halverson, 2008), beginning with the abiotic member at the base, consisting of dark grey, parallel-laminated dolostone and dolomitic limestone. The abiotic member ranges in thickness from 3-15 m in the Hoanib Lagoon to over 70 m thick on the outer platform, where it contains thin dolostone turbidites. The abiotic member transitions to the microbial member, which consists of over 100 m of microbialaminites, and contains distinctive roll-up structures near the middle of the member. The unusual microbialaminite contains abundant, chaotic mounds but is interpreted as having formed below storm wave base (Pruss et al., 2010). It transitions upwards into the epiclastic member, which is made up of decametres of light grey, coarsening-upwards dolomite grainstone. The top of the Rasthof Formation on the platform is a subaerial exposure surface (Hoffman and Halverson, 2008).

The Gruis Formation overlies the Rasthof Formation on the NP where it grades laterally from m-scale cycles of shallow marine carbonate facies in the inner platform, through cycles of terrigenous clastics capped by microbialaminites closer to the outer platform, to alluvial fan conglomerates and sandstones adjacent to the Huab and Makalani Ridges. The upper boundary of the formation is a subaerial exposure surface of regional extent (Hoffman and Halverson, 2008).

The Ombaatjie Formation lies on top of the Gruis Formation, and its base is believed to mark the transition from rifting to passive margin subsidence (Halverson et al., 2002). The Ombaatjie Formation varies in thickness from ~200 m on the inner platform to half that on the outer platform. It consists of seven or eight retrogradational carbonate parasequences which are made up dominantly of limestone in the lower half of the formation and become more dolomitic upsection (Hoffman and Halverson, 2008; Halverson et al., 2002). The pre-Marinoan Trezona negative carbon isotope anomaly is recorded in the uppermost parasequence (Hoffman et al., 1998; Halverson et al., 2002). The Ombaatjie Formation ends beneath an erosional surface associated with the Marinoan glaciation.

Tsumeb Subgroup

The Ghaub Formation, made up of Marinoan glaciogenic deposits, is the basal formation of the Tsumeb Subgroup (Hoffmann and Prave, 1996). The bulk of the Ghaub Formation was deposited on the foreslope, as will be discussed below. Marinoan glacial deposits are absent on the outer platform and limited to pockets and lenses of diamictite generally only a couple metres thick in the inner platform. Clasts of the Ghaub Formation diamictite are generally carbonate, derived from scouring of the underlying Abenab and Ombombo Subgroups, with rare granitoid basement clasts. In the Otavi Mountainlands, there are also abundant quartz arenite clasts (Hoffman and Halverson, 2008; Hoffman, 2011). The Ghaub Formation is overlain by the Maieberg Formation cap carbonate sequence, followed by two thick carbonate successions, the Elandshoek and Hüttenberg Formations, separated by sequence boundaries (Hedberg, 1979; Hoffman and Halverson, 2008).

The Keilberg Member of the Maieberg Formation is the transgressive cap dolostone at the base of the cap carbonate sequence (Hoffman and Halverson, 2008). The Keilberg Member conformably overlies the Ghaub Formation, and where the Ghaub Formation is absent on much of the platform, it lies directly on the Ombaatjie Formation. The Keilberg Member is thickest on the outer platform and records the sequence of sedimentary features distinctive of the Marinoan cap carbonate, which are described in detail by Hoffman et al. (2007) and Hoffman (2011). This sequence begins with marly dolostone turbidites coarsening upwards into peloidal dolostone with sheet crack cements, followed by tubestone stromatolites (absent on distal foreslope), swaley cross-stratified peloidal dolostone, giant wave ripples (only on lower slope and inner platform), and finally, fining upward into marly turbidites. The marly dolostone turbidites at the top of the Keilberg Member grade upwards into the pink-coloured marly limestone rhythmites of the middle Maieberg Formation. This middle member contains the maximum flooding interval, and grades into the upper member, consisting of dolostone grainstones and terminating with a subaerial unconformity.

The Elandshoek Formation is made up of stacks of metres-thick predominantly grainstone cycles, bounded by exposure or flooding surfaces. Stromatolites appear in the upper half of the formation. A major flooding surface marks the transition to the Hüttenberg Formation.

The lower Hüttenberg Formation is composed of hundreds of metres of dolostone ribbonite followed by approximately 200 metres of ooid-rich dolomite grainstone (Hoffman and Halverson, 2008). The Hüttenberg Formation ends with a significant unconformity onto which the Mulden Group was deposited.

2.3.2 Foreslope and Basin Stratigraphy

In the NMZ and NZ, syn-rift clastics of the Nosib Group are capped by volcanic rocks produced by extensional tectonics (Miller, 2008). The Naauwpoort Formation of the Nosib Group consists of a lower unit of coarse clastics overlain by these volcanic rocks, which were erupted mainly from two centres, one in the Summas Mountains located approximately 30 km ESE of the town of Khorixas, and the other located to the west (Frets, 1969; Miller, 1980). The Naauwpoort Formation volcanics are dominantly alkaline to peralkaline rhyolites, but minor mafic rocks occur as well (Miller, 2008).

Otavi Group

Ugab Subgroup

In the northernmost NZ, the Ugab Subgroup forms the base of the Otavi Group and sits stratigraphically between the Nosib Group and the Chuos Formation. The Ugab Subgroup consists mainly of peritidal carbonates intercalated with siliciclastics. Its relationship to the Ombombo Subgroup is still not fully understood, but an age 746 ±2 Ma from the Naauwpoort Formation suggests that the Ugab must be at least 15 m.y. younger than the upper Devede Formation (Hoffman et al., 1996). If the basalt clasts in the Okakuyu Formation are equivalent to Nauuwport Formation, then the entirety of the Ombombo Subgroup predates Ugab Subgroup deposition (Halverson et al., 2005).

The youngest possible age for the top of the Ugab Subgroup can be inferred from a maximum age constraint of 717.4±0.2 Ma for the onset of the Sturtian glaciation in northwestern Canada (MacDonald et al., 2010; Macdonald et al., 2017).

Miller (1980; 2008) divided the Ugab Subgroup of the NZ into the Okitjize and Orusewa Formations, with the former being a carbonate-dominated and the latter being siliclastic-dominated. The Okitjize Formation is described as a succession of dolostone interbedded with schist and marly schist that is locally hundreds of metres thick but laterally pinches out. The Okitjize Formation is conformably overlain by the Orusewa Formation, which generally consists of schist overlain by a quartzite unit that is highly variable in degree of sorting and composition, suggested to represent deposition of eroded material associated with the pre-Sturtian fall in sea-level (Miller, 2008).

Abenab Subgroup

The Chuos Formation on the foreslope and in the basin largely consists of massive diamictite containing clasts of basement rock, quartzite, dolostone in variable proportions, and sometimes clasts of Naauwpoort volcanics. The Chuos Formation also contains minor units of stratified diamictite and intervals of laminated siltstone with ice-rafted debris. It is sharply overlain by the Rasthof Formation.

Rasthof Formation on the foreslope generally contains a lower unit of rhythmite or ribbonite that grades into an upper unit of dark-grey to black deep-water microbialaminite. Unlike on the NP, there is usually no upper epiclastic member, and the formation does not end with a subaerial exposure surface. On the foreslope, the Rasthof Formation is often disconformably overlain by an interval of uniform grainstone interpreted to represent submarine channel deposits. Further basinward, the Rasthof Formation is conformably overlain by argillites of the Narachaams Member (Hoffman and Halverson, 2008) of the Ombaatjie Formation, interpreted as being the basinal equivalent of the upper Rasthof, Gruis, and Ombaatjie Formations of the NP (Hoffman and Halverson, 2008). It is composed dominantly of greenish to reddish argillite, often laminated and sometimes silty, with minor deep-water carbonate. The Narachaams Member is capped by the erosion surface associated with the base of the Marinoan glaciation, except on the lower foreslope where it is disconformably overlain by the Franni-aus Member, a coarsening-upwards wedge of carbonate turbidites and debris flows often containing silicified ooids and oolitic grainstone clasts. Its upper boundary is the sub-Ghaub erosion surface, and it is interpreted to record the low-stand wedge deposited during the drop in base level associated with the initial expansion of high latitude ice sheets (Hoffman and Halverson, 2008).

Tsumeb Subgroup

The Ghaub Formation does not appear on the upper foreslope and is predominantly concentrated on the lower foreslope as an ice grounding-line wedge approximately 5 to 10 km basinward of the platform margin (Hoffman et al., 2007; Domack and Hoffman, 2011). The wedge reaches a thickness of over 600 m in depressions and tapers basinward. It consists almost entirely of carbonate diamictite, with clasts of both dolostone and limestone, and laminated intervals of sediment density flows and plume fallout hosting ice-rafted debris. The grounding-line wedge is topped by a relatively thin, well-stratified, fining-upward unit called the Bethanis Member, made up of medium-to-dark brown turbidites and debrites with abundant ice-rafted debris. The Bethanis Member is interpreted to represent the terminal collapse of the ice sheet (Domack and Hoffman, 2011). South of where the grounding line wedge tapers out, Ghaub diamictite occurs only sporadically and clasts include quartzite.

The Ghaub Formation is sharply but conformably overlain by a cap carbonate sequence which makes up the base of the Karibib Formation. The Karibib Formation is the basinal equivalent to the Maieberg, Elandshoek, and Hüttenberg formations of the NP (Hoffman and Halverson, 2008). South of the platform to foreslope transition, the sequence boundaries separating the formations of the Tsumeb Subgroup are not well developed, and consequently the formations can no longer be distinguished and grade laterally into the deeper-water Karibib Formation. This correlation is confirmed by carbon isotope data (Hoffman and Halverson, 2008).

The Karibib Formation is divided into three members: the Keilberg Member, which is the cap carbonate transgressive sequence, a middle member reflecting the maximum flooding interval, and an upper member deposited during a time of sea level highstand. The Keilberg Member of the foreslope and basin maintains similarities to its platform equivalent, including sheet crack cements near the base of the member, but it generally lacks the tubestone stromatolite unit south of the upper foreslope. The middle member generally consists of marly dolostone or limestone rhythmite, which transitions into an upper member of non-marly dolostone rhythmite containing debrites (Hoffman et al., 2016; Hoffman and Halverson, 2008). The Karibib Formation ends with a significant erosional unconformity, often associated with heavy silicification, overlain by the Kuiseb Formation, which is considered by some as equivalent to the Braklaagte Formation at the base of the Mulden Group, representing progradational marine deposition associated with the foreland basin molasse (Hoffman and Halverson, 2008; Hoffman et al., 2016).

2.4 Ugab Subgroup Stratigraphy

In order to better understand the depositional history of the Ugab Subgroup, more measured sections were required, particularly in the Summas Mountains region. Additionally, sampling of a complete section in the Vrede Domes was necessary in order to chemostratigraphically correlate strata from the Summas Mountains to those from the Vrede Domes.

2.4.1 Methods: Field Work

Field work was primarily executed in the two outcrop belts with the best exposures of the Ugab Subgroup: the Summas Mountains and the Vrede Domes. In the Summas Mountains, a single full section and two partial sections were measured on Rondehoek Farm with carbonate samples collected at ~3 m intervals where possible. At the Vrede Domes, multiple closely spaced sections were measured in both the South Dome and North Dome, and carbonates from a section in the South Dome were sampled every ~4 m where possible for carbon isotope analysis. Sections were measured using 2 m collapsible measuring sticks.

Siliciclastics were described based on grain size as argillite, siltstone, sandstone, or conglomerate. Lithological composition of grains or clasts, as well as sedimentary structures such as crossbedding and grading, were noted. Carbonate units were classified based on the carbonate lithofacies scheme described in **Table 2.1** (Hoffman and Halverson, 2008). Non-gradational transitions between facies were noted and described as flooding surfaces, erosional scour surfaces, or subaerial exposure surfaces.

We synthesized these new stratigraphic logs and data with previously published and unpublished results of many past field seasons of work done in the Vrede Domes and Summas Mountains regions, including detailed measured sections and $\delta^{13}C_{carb}$ profiles.

2.4.2 The Summas Mountains Inlier

The Summas Mountains Inlier (**Figure 2.5**) is located in the NZ approximately 30 km ESE of the town of Khorixas. It is a former volcanic center and one of the two sources of the Naauwpoort

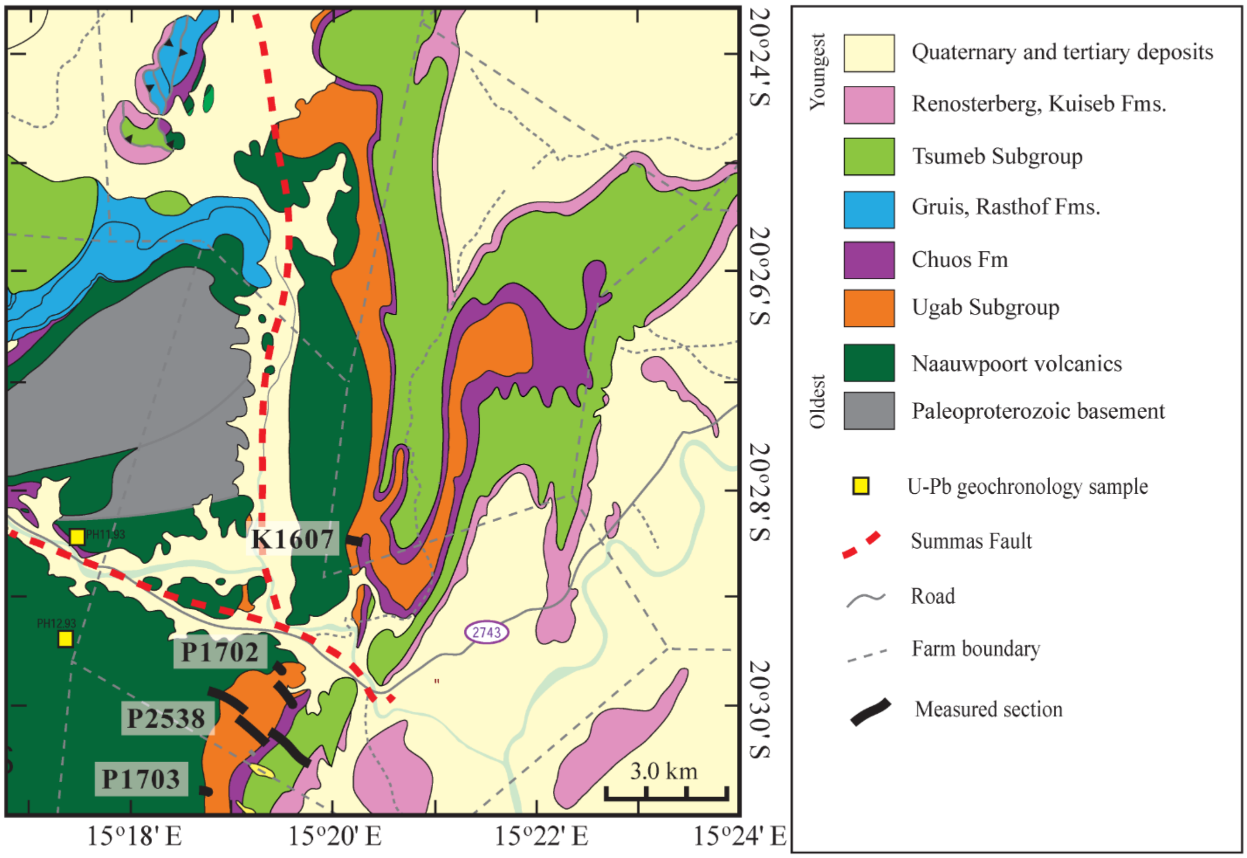

Figure 2.5*: Geologic map of the eastern flank of the Summas Mountains, modified from Hoffman and Halverson (2008). Radiometric dates from geochronology samples published in Hoffman et al. (1996).*

Formation rift-related volcanics (Miller, 1980). The Naauwpoort Formation in the Summas Mountains consists mainly of per-alkaline to alkaline rhyolitic tuffs, with minor mafic volcanics (Miller, 1980). At the core of the inlier, proposed to be a cauldron-subsidence structure (Guj, 1974), the cumulative thickness of the rhyolitic ash-flow tuffs exceeds 6km and the base is not visible (Miller, 1974; 1980). The Ugab Subgroup outcrops on the eastern edge of the Summas Mountains, where it paraconformably overlies Naauwpoort Formation volcanic rocks and lies beneath the Chuos Formation, separated by a low-angle unconformity. The Chuos Formation here is continuous and ranges in thickness from at least 25 metres to over 300 metres. Mapping suggests that the Chuos Formation on the eastern flank of the Summas Mountains is directly overlain by the Karibib Formation of the Tsumeb Subgroup, with the entire remainder of the Abenab Subgroup absent (Hoffman and Halverson, 2008).

2.4.2.1 Ugab Subgroup Lithostratigraphy

Previous workers measured sections of the Ugab Subgroup south of the Huab Riverbed, on Loewenfontein Farm, and created the composite section P2538 (**Figures 2.5, 2.6**; Hoffman and Halverson, 2008). Twenty shallowing-upward depositional cycles separated by flooding surfaces or, less commonly, by subaerial erosive surfaces were documented in this section.

Our section, K1607, measured on Rondehoek Farm ~5 km NNE of P2538, records fewer cycles, and the carbonate units seen in the uppermost 50 m of the Loewenfontein section are absent in the Rondehoek section. Both sections have decametres of coarse-grained siliciclastic sediments at the base, generally consisting of quartz-rich conglomerate and quartz arenite. Sections P1702 and P1703, measured on Loewenfontein Farm 1.5 km NE and 2 km S of P2538 respectively, and only spanning the lowermost 150-200 metres of exposure, show that this basal unit of coarse siliciclastics is highly variable in thickness. It is absent in P1703, which instead has nearly 150 km of tuffaceous siltstone at the base. In P1702, it consists of three siliciclastic parasequences, the lower two capped by thick conglomerate units. Directly overlying this coarse siliciclastic unit in P2538 are four small-scale deep-water carbonate parasequences that are absent in the Rondehoek section but could possibly coincide with the gap in exposure. Another possible explanation for this could be onlap onto an uneven surface of the underlying coarse siliciclastic unit, or the fine carbonate unit could have been squeezed out during deformation, as it is rheologically weaker than the bracketing units of sandstone and grainstone.

The next ~200 metres of section are dominated by carbonate cycles, sometimes interbedded with argillite or siltstone. Above this, the parasequences become more siliciclastic-rich, with argillite at the base and often culminating with sandstone. K1607 ends with a sandstone-capped parasequence unconformably overlain by glacial diamictite. P2538, however, continues, and parasequences transition into fine-grained siliciclastics capped by carbonates.

Assuming our correlations between P2538 and K1607 are correct, subglacial scouring cut nearly 200 metres deeper into the Ugab Subgroup on the Rondehoek Farm, 5 km to the north, compared to the Loewenfontein Farm.

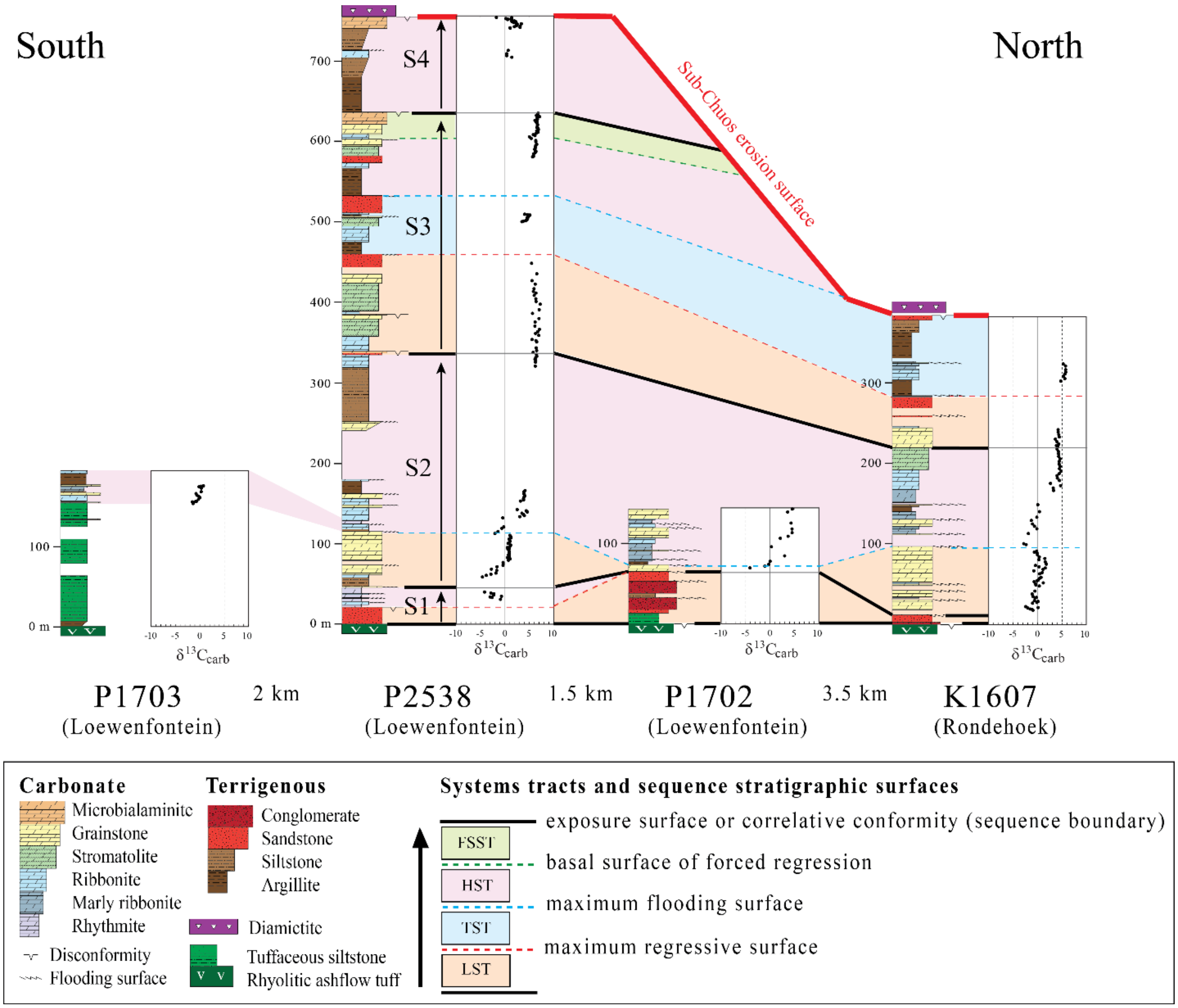

Figure 2.6: *Sequence stratigraphic architecture of the Ugab Subgroup in the Summas Mountains. Coordinates at base of each section in Table 2.2. Section locations marked on geological map in Figure 2.5. HST= highstand systems tract, TST= transgressive systems tract, LST= lowstand systems tract, FSST= falling stage systems tract.*

2.4.2.2 Sequence Stratigraphic Architecture

Due to a paucity of measured sections in the Summas Mountains Inlier, sequence stratigraphic interpretations here are only tentative. Four fourth-order depositional sequences have been identified, denoted as S1-S4 in **Figure 2.6**. We interpret the basal coarse siliciclastic unit as a lowstand systems tract (LST), overlain in P2538 by a short highstand systems tract represented by several fine carbonate parasequences. The end of this deep-water unit marks the transition to

Section	Latitude	Longitude	Location
K1607*	S 20°28.557'	E 015°19.950'	Summas Mts, Rondehoek Farm
P2538*	S 20°29.966'	E 015°19.550'	Summas Mts, Loewenfontein Farm
P1702*	S 20°29.604'	E 015°19.330'	Summas Mts, Loewenfontein Farm
P1703*	S 20°30.230'	E 015°18.709'	Summas Mts, Loewenfontein Farm

Table 2.2: *Coordinates at the bases of sections measured in the Summas Mountains. Asterisks denote sections with carbon isotope data.*

sequence 2, which begins with two to four parasequences consisting mostly of grainstone, interpreted as an LST. A maximum flooding surface above a thick carbonate unit is viewed as the beginning of a thick HST, made up of at least six parasequences of ribbonite or marly ribbonite, or less commonly argillite, grading into grainstone. The first exposure surface recorded in P2538 is interpreted as a sequence boundary, overlain by an LST at the base of sequence 3. The top of the LST is a flooding surface above a thick sandstone unit. This flooding surface marks the beginning of a TST consisting of two parasequences, the first capped by stromatolite and the second by sandstone. The maximum flooding surface is within the thick argillite unit that overlies the sandstone. The HST is relatively short-lived, and overlain by an FSST that culminates in microbialaminites and an exposure surface, which is the sequence boundary at the base of sequence 4, and is associated with a major flooding surface.

More closely spaced sections of the Ugab Subgroup should be measured in the Summas Mountains to verify the correlations and sequence stratigraphic interpretations.

2.4.3 The Vrede Domes

The Vrede Domes (**Figure 2.7**) are a pair of domal structures located in the Northern Zone, approximately 80 km west of the town of Khorixas (**Figure 2.6**). They have been interpreted as doubly-plunging anticlines formed from interference folding during E-W shortening associated with the Kaoko orogen, followed by N-S shortening associated with the Damara orogen (Maloof, 2000). These domes, stretching approximately 5 km from the northernmost point of the North Dome to the southernmost point of the South Dome, expose Otavi Group strata in concentric rings with the Ugab Subgroup making up the center rings. The Ugab Subgroup here shows a rapid lateral transition from coarse siliciclastic deposition in the north to carbonate-dominated strata in the south. The South Dome exposes the Ugab strata up to a greater depth than the North

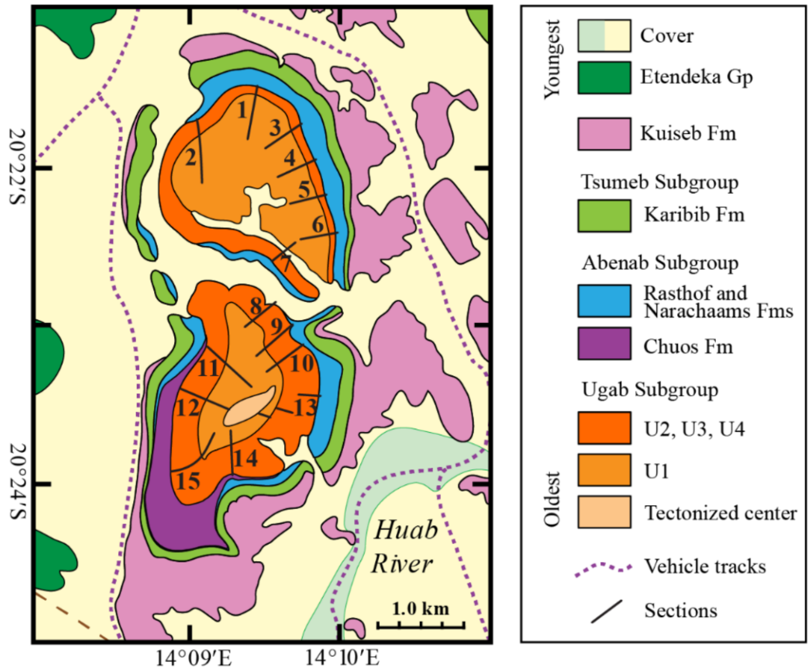

***Figure 2.7**: Geologic map of the Vrede Domes region, modified from Hoffman et al. (2016).*

Dome; however the base of the Ugab Subgroup cannot be seen. The core of the South Dome is a highly tectonized carbonate unit. It is unknown if the Naauwpoort Formation lies beneath, or if the Ugab Subgroup lies directly on Paleoproterozoic basement.

The Chuos Formation is not laterally continuous in the Vrede Domes, and only overlies the Ugab Subgroup in the southern end of the South Dome, where it appears as a thick wedge interpreted as a moraine-like deposit due to the stratigraphic onlap of overlying strata and absence of significant incision into the underlying Ugab Subgroup (Hoffman et al., 2016; Hoffman et al., 2017). Where the Chuos Formation is absent, the Rasthof Formation unconformably overlies the Ugab Subgroup.

2.4.3.1 Ugab Subgroup Lithostratigraphy

Prior detailed stratigraphic logging and mapping in the Vrede Domes resulted in division of the Ugab Subgroup into four unnamed units, referred to from lowermost to uppermost as U1, U2, U3, and U4. These units were originally defined and described by Maloof (2000) and assigned to the Ombombo Subgroup, but later workers reassigned the strata to the Ugab Subgroup while keeping the same divisions of units (Hoffman and Halverson, 2008; Hoffman et al., 2016). The stratigraphically deepest unit exposed in the domes is a highly tectonized limestone that forms the core of the South Dome. Surrounding this marble is U1, consisting mainly of black to maroon limestones which are dolomitized on the eastern side, and sandstones. Near the top of the unit, there is often a transition to coarse-grained polymictic conglomerate. U1 appears only in the South Dome and is capped by a flooding surface. Unit U2 is made up of polymictic conglomerate, sandstone, and dolostone ribbonite, generally in fining-upwards cycles. However, the unit as whole coarsens upwards. In the North Dome, U2 is dominated by coarse-grained conglomerate, with beds of the other lithologies being infrequent. A maximum age constraint of 743±10 Ma exists for the upper U2 from U-Pb dating of detrital zircons (Nascimento et al., 2017; Hoffman and Halverson, 2018), presumably derived from the Nauuwpoort volcanics. The top of U2 is defined by a flooding surface and U3 marks a transition to carbonate-dominated deposition. This unit is characterized by shoaling upward cycles of dolostone ribbonites, *Tungussia*-type stromatolites, and grainstones with silicified ooid beds containing invidual ooids up to 0.5 cm in diameter. A major flooding surface marks the top of U3. U4 comprises almost entirely dolostone ribbonite, usually decametres thick. In some sections, there are subordinate thin beds of grainstone or stromatolite. The Ugab Subgroup ends beneath the Sturtian subglacial erosive surface, in some places brecciated beneath the unconformity. Correlation of U4 across the domes indicates variable erosional truncation on this boundary (**Figure 2.8**).

	Section	Latitude	Longitude	Location
1	S1602	S 20°21.731'	E 014°09.427'	Vrede, N of North Dome
2	P1708	S 20°21.991'	E 014°09.310'	Vrede, NW of North Dome
3	K1606	S 20°21.832'	E 014°09.477'	Vrede, NE of North Dome
4	P1609	S 20°21.938'	E 014°09.544'	Vrede, NE of North Dome
5	P1610	S 20°22.163'	E 014°09.866'	Vrede, E of North Dome
6	P1602	S 20°22.490'	E 014°09.716'	Vrede, SE of North Dome
7	P1704	S 20°22.433'	E 014°09.690'	Vrede, S of North Dome
8	B1701	S 20°23.207'	E 014°09.443'	Vrede, N of South Dome
9	J1705	S 20°23.278'	E 014°09.469'	Vrede, NE of South Dome
10	P1603	S 20°23.356'	E 014°09.596'	Vrede, NE of South Dome
11	K1605	S 20°23.516'	E 014°09.372'	Vrede, NW of South Dome
12	P1604	S 20°23.708'	E 014°09.211'	Vrede, W of South Dome
13	G1532*	S 20°23.590'	E 014°09.503'	Vrede, E of South Dome
14	P1606	S 20°24.012'	E 014°09.443'	Vrede, S of South Dome
15	P1605	S 20°23.947'	E 014°09.107'	Vrede, S of South Dome

Table 2.3: *Coordinates at the bases of sections measured in the Vrede Domes. Asterisk denotes section with carbon isotope data.*

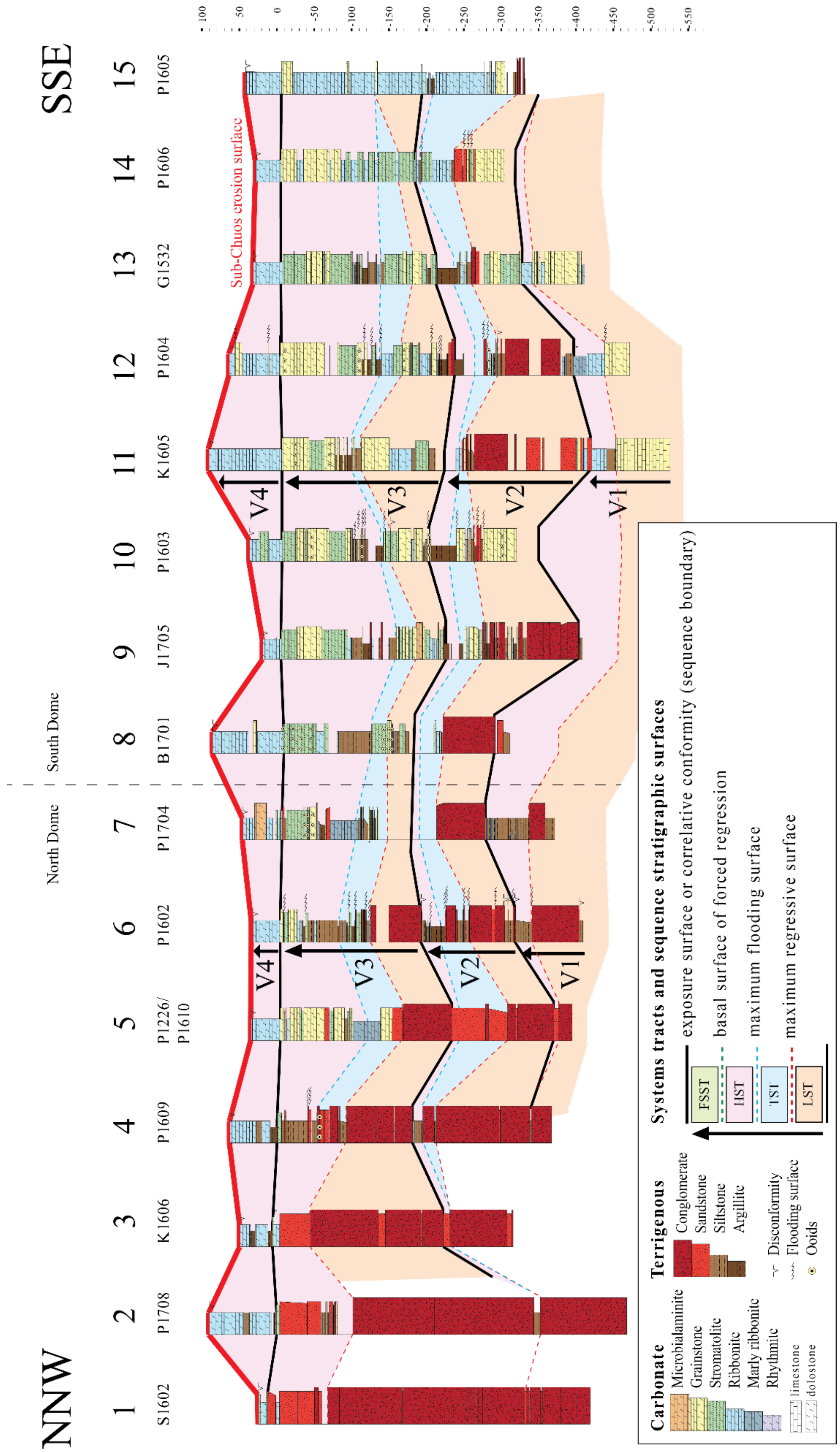
NNW
SSE
North Dome
South Dome
1
2
3
4
5
6
7
8
9
10
11
12
13
14
15
S1602
P1708
K1606
P1609
P1226/
P1610
P1602
P1704
B1701
J1705
P1603
K1605
P1604
G1532
P1606
P1605
Sub-Chuos erosion surface
V1
V2
V3
V4
100
50
0
-50
-100
-150
-200
-250
-300
-350
-400
-450
-500
-550
Carbonate
Microbialaminite
Grainstone
Stromatolite
Ribbonite
Marly ribbonite
Rhythmite
limestone
dolostone
Terrigenous
Conglomerate
Sandstone
Siltstone
Argillite
Disconformity
Flooding surface
Ooids
Systems tracts and sequence stratigraphic surfaces
FSST
HST
TST
LST
exposure surface or correlative conformity (sequence boundary)
basal surface of forced regression
maximum flooding surface
maximum regressive surface

Figure 2.8: *Sequence stratigraphic architecture of the Ugab Subgroup in the Vrede Domes. Coordinates at base of each section in Table 2.3. Section locations marked on geological map in Figure 2.7. HST= highstand systems tract, TST= transgressive systems tract, LST= lowstand systems tract, FSST= falling stage systems tract.*

2.4.3.2 Sequence Stratigraphic Architecture

Four fourth-order depositional sequences have been identified and divided into systems tracts in the Vrede Domes (**Figure 2.8**). It is important to note that these depositional sequences (denoted in **Figure 2.8** as V1-V4) are different from the units U1-U4 defined by Maloof (2000), and also distinct from the depositional sequences recognized in the Summas Mountains (S1-S4). The sequences show repeated rises in base level, likely tectonically controlled, caused by slip on the extensional fault to the north of the Outjo basin.

The base of sequence 1 cannot be seen. In the North Dome, the lowest visible systems tract is an LST, represented by a thick polymictic conglomerate unit, which grades laterally to a thick interval of grainstone in the South Dome. No TST is preserved, and instead, a sharp flooding surface marks the base of the overlying HST. The HST in the North Dome is represented by sandstone or siltstone, sometimes containing carbonate concretions; ribbonite or marly ribbonite make up the HST in the South Dome.

An exposure surface marks the base of Sequence 2, followed by an LST generally consisting of over 50 metres of conglomerate in the North Dome. This thick conglomerate unit continues into the South Dome, where it is variably interbedded with carbonates or finer-grained siliclastics. A TST begins at the top of the conglomeratic unit, ending with a maximum flooding surface near the base of an argillite unit. This is followed by a thin HST represented by the argillite or fine siltstone unit, which can be traced across nearly all the sections.

Sequence 3 begins, once again, with a thick conglomerate unit in the North Dome representing an LST. In the South Dome, the LST consists of a few parasequences capped by stromatolite or grainstone. The maximum regressive surface is generally found at the top of a thick grainstone unit, followed by a well-developed TST recording fining upward. The base of the HST is another significant argillaceous unit, containing several small-scale parasequences, that can be seen in nearly every section. Parasequences coarsen upwards and become dominated by stromatolite and ooid grainstone.

The base of sequence 4 is a significant flooding surface, marked by an abrupt transition to a ribbonite unit, interpreted as an HST. It is erosionally truncated by the sub-Chuos glacial unconformity.

2.5 Carbon and oxygen isotope geochemistry

During the course of our field work, a total of 223 carbonate samples were collected from the Ugab Subgroup; 115 from the Summas Mountains region and 108 from the Vrede Domes. Samples were analyzed in the stable isotope geochemistry lab at McGill University.

2.5.1 Methods: Carbon and oxygen isotope analysis

Carbonate samples were cut using a diamond lapidary blade to expose unweathered surfaces, then rinsed and dried. A table drill was used to collect small amounts of fine powder, along lamination where visible, from cut surfaces of the samples for $\delta^{13}C_{carb}$ and $\delta^{18}O_{carb}$ analyses. Veins and fractures were avoided. Approximately 120 µg of powder from each sample was weighed out for analysis on a Nu Instruments Perspective mass spectrometer coupled to a NuCarb automated carbonate preparation device. Carbon and oxygen isotope ratios were measured simultaneously in dual inlet mode. Batches contained 40 samples with 10 in-house geostandards (NCM and UQ6) regularly interspersed. The samples were heated to 70°C and sequentially reacted with phosphoric acid (H_3PO_4) to produce CO_2, which was then cryogenically isolated. Following that, the isotopic ratios of the CO_2 were measured against reference gas, and $\delta^{13}C_{carb}$ and $\delta^{18}O_{carb}$ were calculated and calibrated to VPDB, with a 1- σ precision <0.05‰.

Crossplots of carbon and oxygen isotope data from each section were used to assess for alteration, with R^2 values calculated to quantify the degree of covariation (**Figure 2.9**). Meteoric diagenesis drives $\delta^{18}O$ to more depleted values because the $\delta^{18}O$ of meteoric water is lower than that of seawater. However, this effect competes with the effect of early dolomitization, which tends to increase $\delta^{18}O$ by 2–4‰ (Halverson et al., 2007).

2.5.2 Carbon Isotope Results: Summas Mountains

It is important to note that both sections from the Summas Mountains have R^2 values suggesting moderate to high levels of diagenetic overprinting (**Figure 2.9; Figure 2.10**), and consequently, trends observed in these sections should be regarded with caution. The carbon isotope data from

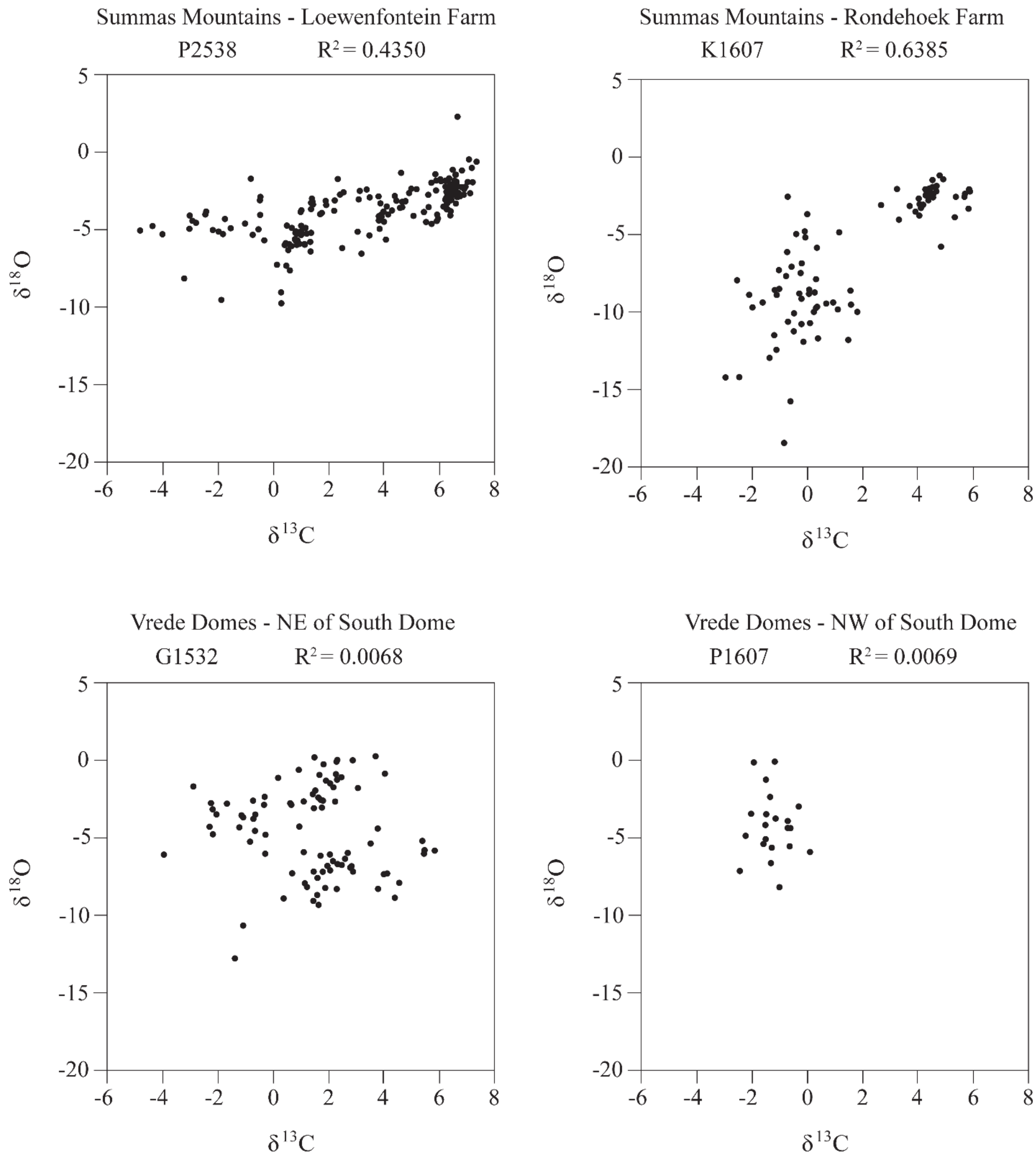

Figure 2.9*: Crossplots of d13C and d18O data from Ugab Subgroup sections P2538, K1607, G1532, and P1607.*

the section at Rondehoek Farm from this study (K1607) closely matches the composite section (P2538) measured previously on Loewenfontein Farm several kilometres to the south (Hoffman and Halverson, 2008) (**Figure 2.6**). Both sections show a double-peaked negative anomaly and a recovery to ~5 ‰ in the basal 150 metres of section, followed by $\delta^{13}C$ remaining relatively stable

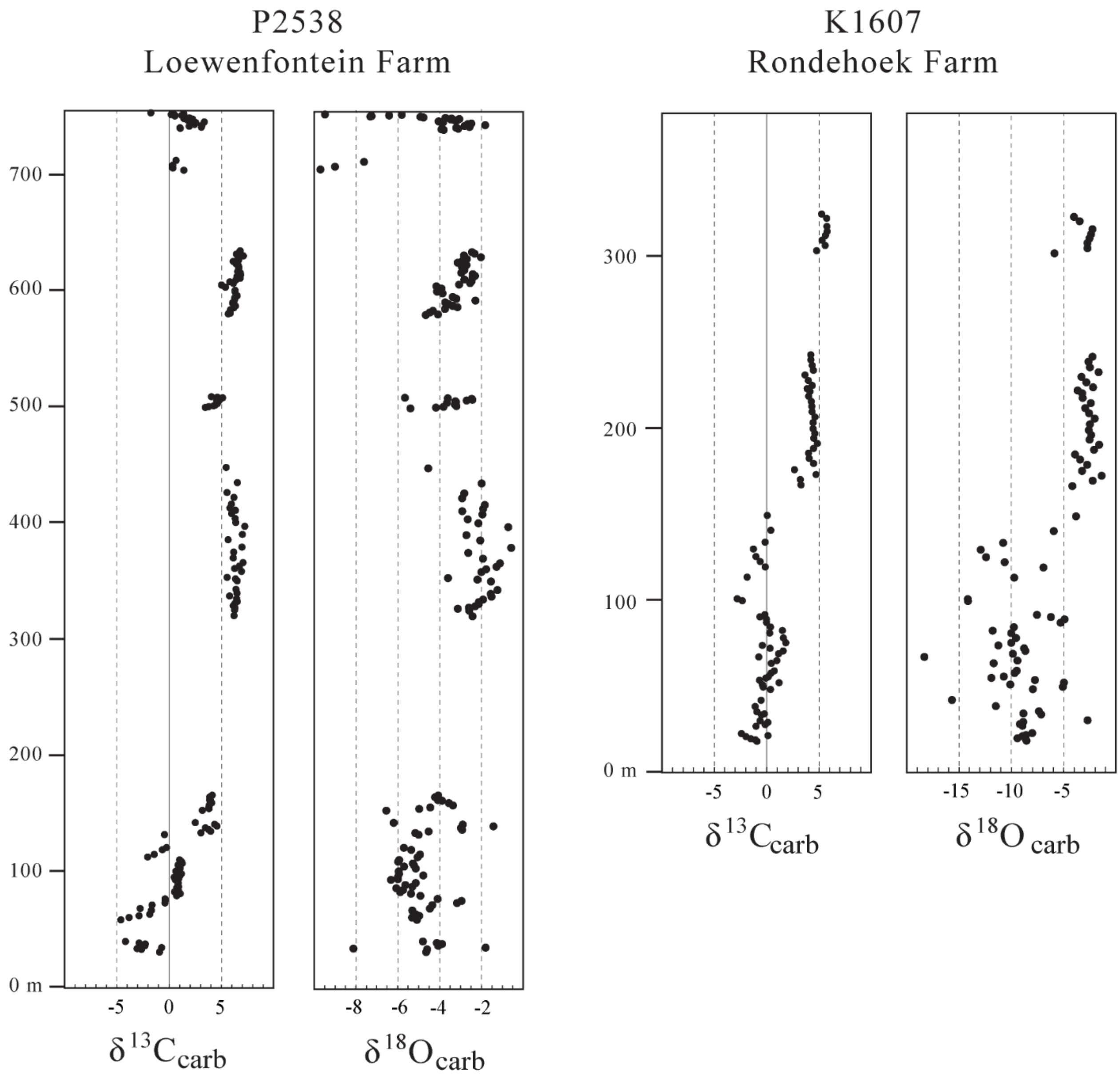

***Figure 2.10**: Carbon and oxygen isotope data from the Summas Mountains sections plotted against stratigraphic height.*

around 5 ‰ for several hundreds of metres. The nadir of the first peak of the anomaly reaches nearly -5 ‰ in the Loewenfontein section, and is not recorded in Rondehoek section, but the ascending arm of the lower peak can be seen from -3 ‰. In both sections, $\delta^{13}C$ rises to approximately 1 ‰ before abruptly dropping back to -3 ‰ directly above a flooding surface. Carbon isotope values then rise to a plateau around 5 ‰, with the Rondehoek section remaining just below 5 ‰ and the Loewenfontein section just above. This ~ 2 ‰ difference may be due to the Rondehoek section having undergone more meteoric alteration than the Loewenfontein section. Additionally, in K1607, the rise to baseline seems to be delayed compared to the correlative strata in P2538. This can also be attributed to alteration. Carbonates from the top of the Loewenfontein section, absent in the Rondehoek section, record $\delta^{13}C$ descending back towards 0 ‰, and drop into the negatives in the metres directly beneath the subglacial erosion surface. This descent coincides with a considerable decrease in $\delta^{18}O$, signifying that alteration is likely.

2.5.3 Carbon Isotope Results: Vrede Domes

Carbon isotope results from the Vrede Domes sections can be seen in **Figure 2.11,** and show negligible correlation between $\delta^{13}C$ and $\delta^{18}O$ (**Figure 2.9**). The full section sampled on the east side of the South Dome (G1532) records a very gradual decline, taking place over nearly 450 metres of strata, from ~5 ‰ at the base of the section to a low around -3 ‰ at the top of the section. The decline plateaus between 1 and 3 ‰ through the middle of the section. The uppermost ribbonite unit of a section measured on the opposite side of the South Dome (P1607; equivalent to K1605) shows a gradual decline in $\delta^{13}C$ similar to that observed in G1532.

2.6 Discussion

2.6.1 Regional Correlations and a composite section

The $\delta^{13}C$ trends at the Vrede Domes and Summas Mountains are starkly different, suggesting that if the trends are primary, the correlatable overlap between the two exposures of the Ugab Subgroup is relatively small. Because the dominant control on base level fluctuation during the deposition of the Ugab Subgroup in both the Summas Mountains and the Vrede Domes was local tectonics, which differed in each area, the identified depositional sequences of little to no use for correlation. Consequently, correlation between the section sampled at the Vrede Domes and the sections from the Summas Mountains was made based on the carbon isotope data. To construct the composite section (**Figure 2.10**), sections P2538, G1532, P1607, and K1607 were each divided into correlatable segments, which were then scaled relative to the segments of P2538, as it is the most complete section. The lower half of the Vrede Domes section records a descent from approximately 5 ‰ to 0 ‰ that can be connected with a similar negative trend in the upper portion of the Summas Mountains section P2538. The decline in $\delta^{13}C$ at the top of P2538 corresponds with scattered $\delta^{18}O$ declining to -10 ‰, which suggests meteoric diagenesis may

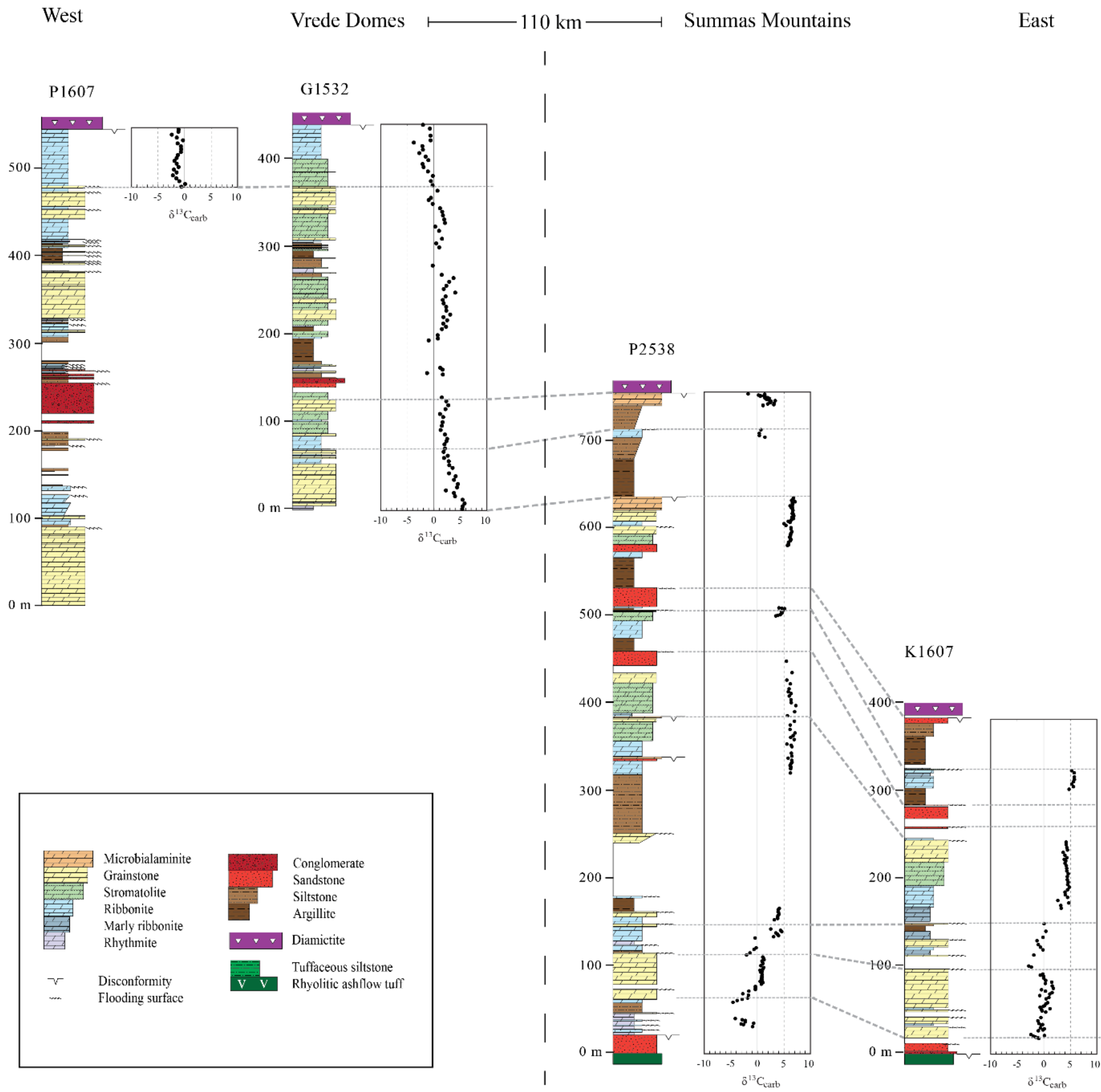

***Figure 2.11**: Correlation between Ugab Subgroup exposure at the Vrede Domes and in the Summas Mountains.*

play a role. However, the bulk of the $\delta^{18}O$ data lie between -4 and -2 ‰, consistent with $\delta^{18}O$ values throughout most of the section, whereas all of the $\delta^{13}C$ data points drop nearly 4 ‰ relative to the baseline. Though some of the samples were likely diagenetically driven towards more depleted values, the decline in $\delta^{13}C$ at the top of P2538 cannot be explained by diagenesis alone. Data from sections P1702 and P1703 were left out of the composite, due to uncertainty with correlations.

The composite section covers a relatively complete record of the pre-Cryogenian in northwestern Namibia, spanning nearly 1 km of strata unconformably lying between radiometrically dated volcanic rocks giving a maximum age constraint for the base of 746±2 Ma (Hoffman et al., 1996), and the sub-glacial erosion surface of the Sturtian glaciation, giving a maximum age constraint for the top of 717±0.2 Ma (Macdonald et al., 2010). This age-constrained profile will prove useful for global correlations.

2.6.2 Late Tonian carbon isotope anomalies and global correlation

Based on the proposed correlations between the two inliers, the Ugab Subgroup preserves two separate negative $\delta^{13}C$ excursions: an older one that is recorded at the base of the Summas Mountains sections, and a younger one in the Vrede Domes where only the declining arm is recorded and the anomaly is truncated by sub-Chuos erosion. The excursion near the base of the Summas Mountains sections is much sharper and reaches more negative values (ca. -3.5 ‰) than the Vrede Domes excursion. However, it has a double-minima, which is not observed in pre-Sturtian anomalies in other parts of the world. The association of the second minimum with a flooding surface and subsequent deep-water facies suggests that this could be a secondary feature resulting from authigenic carbonate contribution.

In the context of the recently updated $\delta^{13}C$ record from Scotland (Fairchild et al., 2017), our data set is consistent with the existence of at least two separate global negative carbon isotope anomalies recorded in marine carbonates deposited between the ca. 802 Ma end of the Bitter Springs anomaly and the onset of the Sturtian glaciation (Fairchild et al., 2017; Halverson et al., 2017). To avoid confusion, in this discussion we will use the convention of Halverson et al. (2017) of referring to the older of the two anomalies (ca. 739 Ma) as the Russøya anomaly following Halverson et al. (2004), and the younger (ca. 720 Ma) as the Garvellach anomaly following Fairchild et al. (2017). We interpret the negative excursion at the base of the Summas Mountains sections as the Russøya anomaly, and the decline in $\delta^{13}C$ observed in the Vrede Domes as the Garvellach anomaly, with the nadir and recovery erosionally severed. The maximum age constraint of ~746 Ma for the base of the Ugab Subgroup in the Summas Mountains (Hoffman et al., 1996) is consistent with a ca. 739 Ma age for the Russøya anomaly, and effectively rules out the possibility of correlation with the Bitter Springs anomaly. Future work that should be done includes re-dating the Naauwpoort Formation volcanics in the Summas

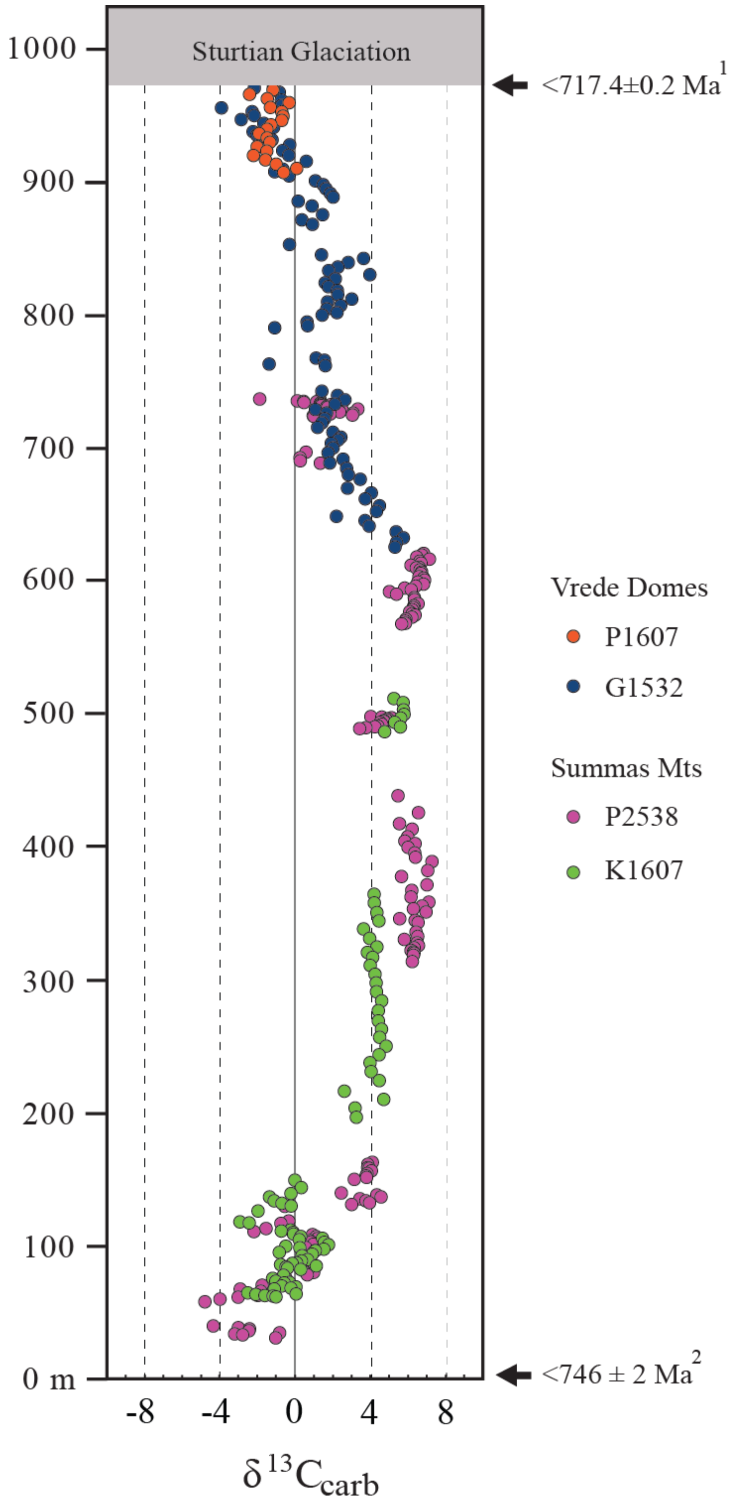

Figure 2.12*: Composite carbon isotope profile of the Ugab Subgroup. Age constraints from following sources: 1 – Macdonald et al., 2010; 2 – Hoffman et al., 1996 .*

Mountains using modern techniques and samples from closer to the base of the Ugab Subgroup, to produce a more precise maximum age constraint.

The carbon isotope record of the uppermost ~700 metres of the Tambien Group in Ethiopia is notably similar to that of the Ugab Subgroup, with a sharper anomaly and return to baseline several hundreds of metres beneath glaciogenic deposits, followed by a gradual decline in the hundreds of metres immediately below the sub-glacial unconformity (Swanson-Hysell et al., 2015). The onset of this upper decline coincides with a shift to deposition of dominantly deeper-water facies, which could suggest this trend may be related to authigenic carbonate contribution. However, our data shows a similar upper decline with seemingly no facies dependence. Therefore, we tentatively suggest that the Ugab Subgroup strata exposed in the Vrede Domes correlates with the Marian Bohkakho Formation of the Tambien Group of Ethiopia.

It is very likely that strata recording the immediately pre-glacial Garvellach anomaly have been removed in many regions by erosive scour beneath the glacial surface. In areas where the Garvellach anomaly has not been removed, the older Russøya anomaly could be mistaken for the ca. 810-802 Ma Bitter Springs anomaly in successions with few or no age constraints. This complicates using the Islay anomaly as a correlative marker, because in sections preserving only one pre-Sturtian negative anomaly, it may difficult to ascertain which of the two excursions is preserved.

2.7. Conclusions

The principal result of this project is that it demonstrates that there are two pre-Sturtian carbon isotope excursions recorded in the Neoproterozoic strata of northwestern Namibia. This is valuable contribution to Neoproterozoic carbon isotope record because it helps to substantiate the recent suggestion that there are two separate global $\delta^{13}C$ excursions, ca. 739 and 720 Ma. This result has important implications for correlating between Tonian successions and for formally defining the base of the Cryogenian period, which will likely be linked to chemostratigraphic records (Shields-Zhou et al., 2016).

The data presented here will aid with the construction of a robust pre-Cryogenian carbon isotope record, which is essential to understanding the factors that led to the first Cryogenian Snowball earth. If there are two pre-Sturtian $\delta^{13}C$ anomalies, the younger of the two may be mechanistically linked to the Sturtian glaciation, representing the pre-Sturtian equivalent to the pre-Marinoan Trezona anomaly, whereas the older may represent an unrelated perturbation to the carbon cycle, likely linked to the protracted fragmentation of Rodinia.

References List

Abbot, D.S., Halevy, I., 2010. Dust aerosol important for Snowball Earth deglaciation. J. Clim. 23, 4121–4132.

Abbot, D.S., Pierrehumbert, R.T., 2010. Mudball: surface dust and Snowball Earth deglaciation. J. Geophys. Res. Atmospheres 115.

Abbott, G., 1997. Geology of the upper Hart River area, eastern Ogilvie Mountains, Yukon Territory. Explor. Geol. Serv. Div. Yukon Reg. Bull. 9, 1–72.

Aguilar, C., Alkmim, F.F., Lana, C., Farina, F., 2017. Palaeoproterozoic assembly of the São Francisco craton, SE Brazil: New insights from U–Pb titanite and monazite dating. Precambrian Res. 289, 95–115.

Alchin, D.J., Frimmel, H.E., Jacobs, L.E., 2005. Stratigraphic setting of the metalliferous Rosh Pinah Formation and the Spitzkop and Koivib suites in the Pan-African Gariep Belt, southwestern Namibia. South Afr. J. Geol. 108, 19–34.

Ali, D.O., Spencer, A.M., Fairchild, I.J., Chew, K.J., Anderton, R., Levell, B.K., Hambrey, M.J., Dove, D., Le Heron, D.P., 2017. Indicators of relative completeness of the glacial record of the Port Askaig Formation, Garvellach Islands, Scotland. Precambrian Res. https://doi.org/10.1016/j.precamres.2017.12.005

Allan, J.R., Matthews, R.K., 1982. Isotope signatures associated with early meteoric diagenesis. Sedimentology 29, 797–817.

Allen, P.A., Etienne, J.L., 2008. Sedimentary challenge to snowball Earth. Nat. Geosci. 1, 817–825.

Allen, P.A., Hoffman, P.F., 2005. Extreme winds and waves in the aftermath of a Neoproterozoic glaciation. Nature 433, 123–127.

Allwood, A.C., Grotzinger, J.P., Knoll, A.H., Burch, I.W., Anderson, M.S., Coleman, M.L. and Kanik, I., 2009. Controls on development and diversity of Early Archean stromatolites. Proc. Natl. Acad. Sci., 106(24), pp.9548-9555.

Anderton, R., 1982. Dalradian deposition and the late Precambrian–Cambrian history of the N Atlantic region: a review of the early evolution of the Iapetus Ocean. J. Geol. Soc. 139, 421–431.

Armstrong, R.A., Master, S., Robb, L.J., 2005. Geochronology of the Nchanga Granite, and constraints on the maximum age of the Katanga Supergroup, Zambian Copperbelt. J. Afr. Earth Sci. 42, 32–40.

Arnaud, E., Halverson, G.P., Shields-Zhou, G., 2011. The geological record of Neoproterozoic glaciations. Geological Society of London. Memoir 36 (752 pp).

Bartley, J.K., Kah, L.C., 2004. Marine carbon reservoir, Corg-Ccarb coupling, and the evolution of the Proterozoic carbon cycle. Geology 32, 129–132.

Benn, D.I., Le Hir, G., Bao, H., Donnadieu, Y., Dumas, C., Fleming, E.J., Hambrey, M.J., McMillan, E.A., Petronis, M.S., Ramstein, G., 2015. Orbitally forced ice sheet fluctuations during the Marinoan Snowball Earth glaciation. Nat. Geosci. 8, 704–707.

Berger, W. and Winterer, E.L., 1974. Plate stratigraphy and the fluctuating carbonate line. Pelagic sediments: on land and under the sea. Special Publication Int. Assoc. Sedimentol. Pp.11-48.

Beyth, M., Avigad, D., Wetzel, H.-U., Matthews, A., Berhe, S.M., 2003. Crustal exhumation and indications for Snowball Earth in the East African Orogen: north Ethiopia and east Eritrea. Precambrian Res. 123, 187–201.

Bjerrum, C.J., Canfield, D.E., 2011. Towards a quantitative understanding of the late Neoproterozoic carbon cycle. Proc. Natl. Acad. Sci. 108, 5542–5547.
Bodiselitsch, B., Koeberl, C., Master, S., Reimold, W.U., 2005. Estimating duration and intensity of Neoproterozoic snowball glaciations from Ir anomalies. Science 308, 239–242.
Bowring, S., Myrow, P., Landing, E., Ramezani, J. and Grotzinger, J., 2003, April. Geochronological constraints on terminal Neoproterozoic events and the rise of Metazoan. In EGS-AGU-EUG Joint Assembly.
Brasier, M.D., Shields, G., 2000. Neoproterozoic chemostratigraphy and correlation of the Port Askaig glaciation, Dalradian Supergroup of Scotland. J. Geol. Soc. 157, 909–914.
Brocks, J.J., Jarrett, A.J., Sirantoine, E., Hallmann, C., Hoshino, Y. and Liyanage, T., 2017. The rise of algae in Cryogenian oceans and the emergence of animals. Nature, 548(7669), p.578.
Budyko, M.I., 1969. The effect of solar radiation variations on the climate of the earth. Tellus 21, 611–619.
Bull, S., Selley, D., Broughton, D., Hitzman, M., Cailteux, J., Large, R., McGoldrick, P., 2011. Sequence and carbon isotopic stratigraphy of the Neoproterozoic Roan Group strata of the Zambian Copperbelt. Precambrian Res. 190, 70–89.
Caldeira, K., Kasting, J.F., 1992. Susceptibility of the early Earth to irreversible glaciation caused by carbon dioxide clouds. Nature 359, 17.
Calver, C.R., 1998. Isotope stratigraphy of the Neoproterozoic Togari Group, Tasmania. Aust. J. Earth Sci. 45, 865–874.
Campbell, A.J., Waddington, E.D., Warren, S.G., 2011. Refugium for surface life on Snowball Earth in a nearly-enclosed sea? A first simple model for sea-glacier invasion. Geophys. Res. Lett. 38.
Campbell, I.H., Allen, C.M., 2008. Formation of supercontinents linked to increases in atmospheric oxygen. Nat. Geosci. 1, 554–558.
Canfield, D.E., Poulton, S.W., Narbonne, G.M., 2007. Late-Neoproterozoic deep-ocean oxygenation and the rise of animal life. Science 315, 92–95.
Cawood, P.A., Kroner, A., Pisarevsky, S., 2006. Precambrian plate tectonics: criteria and evidence. GSA Today 16, 4.
Chen, J.-Y., Oliveri, P., Gao, F., Dornbos, S.Q., Li, C.-W., Bottjer, D.J., Davidson, E.H., 2002. Precambrian animal life: probable developmental and adult cnidarian forms from Southwest China. Dev. Biol. 248, 182–196.
Christie-Blick, N., Sohl, L.E., Kennedy, M.J., 1999. Considering a Neoproterozoic snowball earth. Science 284, 1087–1087.
Clifford, T.N., 2008. The geology of the Neoproterozoic Swakop-Otavi transition zone in the Outjo District, northern Damara Orogen, Namibia. South African Journal of Geology, 111(1), pp.117-140.
Condon, D., Zhu, M., Bowring, S., Wang, W., Yang, A., Jin, Y., 2005. U-Pb ages from the Neoproterozoic Doushantuo Formation, China. Science 308, 95–98.
Coplen, T.B., 1988. Normalization of oxygen and hydrogen isotope data. Chem. Geol. Isot. Geosci. Sect. 72, 293–297.
Corsetti, F.A., Kaufman, A.J., 2003. Stratigraphic investigations of carbon isotope anomalies and Neoproterozoic ice ages in Death Valley, California. Geol. Soc. Am. Bull. 115, 916–932.

Cortijo, I., Mus, M.M., Jensen, S. and Palacios, T., 2015. Late Ediacaran skeletal body fossil assemblage from the Navalpino anticline, central Spain. Precambrian Research, 267, pp.186-195.
Cortijo, I., Cai, Y., Hua, H., Schiffbauer, J.D. and Xiao, S., 2015. Life history and autecology of an Ediacaran index fossil: development and dispersal of Cloudina. Gondwana Research, 28(1), pp.419-424.
Cowie, J.W., Ziegler, W., Boucot, A.J., Bassett, M.G., and Remané, J., 1986. Guidelines and Statutes of the International Commission on Stratigraphy (ICS). Courier Forschungsinstitut Senckenberg , v. 83, pp. 1-14.Cox, G.M., Halverson, G.P., Stevenson, R.K., Vokaty, M., Poirier, A., Kunzmann, M., Li, Z.-X., Denyszyn, S.W., Strauss, J.V., Macdonald, F.A., 2016. Continental flood basalt weathering as a trigger for Neoproterozoic Snowball Earth. Earth Planet. Sci. Lett. 446, 89–99.
Cox, G.M., Isakson, V., Hoffman, P.F., Gernon, T.M., Schmitz, M.F., Shahin, S., Collins, A.S., Preiss, W., Blades, M.L., Mitchell, R.N., Nordsvan, A. (in review). U-Pb zircon (CA-ID-TIMS) age supports globally synchronous Sturtian deglaciation.
Craig, H., 1957. Isotopic standards for carbon and oxygen and correction factors for mass-spectrometric analysis of carbon dioxide. Geochim. Cosmochim. Acta 12, 133–149.
Daly, R.A., 1909. First calcareous fossils and the evolution of the limestones. Geol. Soc. Am. Bull. 20, 153–170.
Derry, L.A., 2010a. On the significance of δ 13 C correlations in ancient sediments. Earth Planet. Sci. Lett. 296, 497–501.
Derry, L.A., 2010b. A burial diagenesis origin for the Ediacaran Shuram–Wonoka carbon isotope anomaly. Earth Planet. Sci. Lett. 294, 152–162.
Des Marais, D.J., Moore, J.G., 1984. Carbon and its isotopes in mid-oceanic basaltic glasses. Earth Planet. Sci. Lett. 69, 43–57.
Des Marais, D.J., Strauss, H., Summons, R.E., Hayes, J.M., 1992. Carbon isotope evidence for the stepwise oxidation of the Proterozoic environment. Nature 359, 605.
Donnadieu, Y., Fluteau, F., Ramstein, G., Ritz, C., Besse, J., 2003. Is there a conflict between the Neoproterozoic glacial deposits and the snowball Earth interpretation: an improved understanding with numerical modeling. Earth Planet. Sci. Lett. 208, 101–112.
Donnadieu, Y., Goddéris, Y., Ramstein, G., Nédélec, A., Meert, J., 2004. A 'snowball Earth'climate triggered by continental break-up through changes in runoff. Nature 428, 303–306.
Dunn, P.R., Thomson, B.P., Rankama, K., 1971. Late Pre-Cambrian glaciation in Australia as a stratigraphic boundary. Nature 231, 498–502.
Erwin, D.H., Laflamme, M., Tweedt, S.M., Sperling, E.A., Pisani, D. and Peterson, K.J., 2011. The Cambrian conundrum: early divergence and later ecological success in the early history of animals. Science, 334(6059), pp.1091-1097.
Eyles, N., Januszczak, N., 2007. Syntectonic subaqueous mass flows of the Neoproterozoic Otavi Group, Namibia: where is the evidence of global glaciation? Basin Res. 19, 179–198.
Fairchild, I.J., Hambrey, M.J., 1995. Vendian basin evolution in East Greenland and NE Svalbard. Precambrian Res. 73, 217–233.
Fairchild, I.J., Spencer, A.M., Ali, D.O., Anderson, R.P., Anderton, R., Boomer, I., Dove, D., Evans, J.D., Hambrey, M.J., Howe, J., 2017. Tonian-Cryogenian boundary sections of

Argyll, Scotland. Precambrian Research, http://dx.doi.org/10.1016/j.precamres.2017.09.020

Fairchild, I.J., Spiro, B., Herrington, P.M., and Song, T. 2000. Controls on Sr and C isotope compositions of Neoproterozoic Sr-rich limestones of east Greenland and north China. In Carbonate sedimentation and diagenesis in the evolving Precambrian world. Edited by J.P Grotzinger and N.P. James. SEPM, Special Publication 67, Tulsa, Okla., pp. 297–314.

Feng, L., Zhang, Q., 2016. The Pre-Sturtian negative d13C excursion of the Dajiangbian formation deposited on the western margin of Cathaysia Block in South China. J. Earth Sci. 27, 225.

Feybesse, J.L., Johan, V., Triboulet, C., Guerrot, C., Mayaga-Mikolo, F., Bouchot, V., N'dong, J.E., 1998. The West Central African belt: a model of 2.5–2.0 Ga accretion and two-phase orogenic evolution. Precambrian Res. 87, 161–216.

Fölling, P.G., Frimmel, H.E., 2002. Chemostratigraphic correlation of carbonate successions in the Gariep and Saldania Belts, Namibia and South Africa. Basin Res. 14, 69–88.

Föllmi, K.B., 1996. The phosphorus cycle, phosphogenesis and marine phosphate-rich deposits. Earth-Science Reviews, 40(1-2), pp.55-124.

Font, E., Nédélec, A., Trindade, R.I.F., Moreau, C., 2010. Fast or slow melting of the Marinoan snowball Earth? The cap dolostone record. Palaeogeogr. Palaeoclimatol. Palaeoecol. 295, 215–225.

Frank, T.D., Kah, L.C., Lyons, T.W., 2003. Changes in organic matter production and accumulation as a mechanism for isotopic evolution in the Mesoproterozoic ocean. Geol. Mag. 140, 397–420.

Frets, D.C., 1969. Geology and structure of the Huab-Welwitschia area, South West Africa : Bulletin of the Precambrian Research Unit, University of Cape Town, v. 5, 235 pFrimmel, H.E., 2010. On the reliability of stable carbon isotopes for Neoproterozoic chemostratigraphic correlation. Precambrian Res. 182, 239–253.

Frimmel, H.E., Fölling, P.G., 2004. Late Vendian closure of the Adamastor Ocean: timing of tectonic inversion and syn-orogenic sedimentation in the Gariep Basin. Gondwana Res. 7, 685–699.

Frimmel, H.E. and Frank, W., 1998. Neoproterozoic tectono-thermal evolution of the Gariep Belt and its basement, Namibia and South Africa. Precambrian Res. 90(1-2), pp.1-28.

Frimmel, H.E., Klötzli, U.S., Siegfried, P.R., 1996. New Pb-Pb single zircon age constraints on the timing of Neoproterozoic glaciation and continental break-up in Namibia. J. Geol. 104, 459–469.

Galy, V., Peucker-Ehrenbrink, B., Eglinton, T., 2015. Global carbon export from the terrestrial biosphere controlled by erosion. Nature 521, 204–207.

Gaucher, C., Sprechmann, P., 2009. Neoproterozoic acritarch evolution. Neoproterozoic–Cambrian biota. In: Gaucher, C., Sial, A.N., Halverson, G.P., Frimmel, H.E. (Eds.), Neoproterozoic–Cambrian Tectonics, Global Change and Evolution: A Focus on Southwestern Gondwana. Developments in Precambrian Geology, vol. 16. Elsevier, pp. 319–326.Gehling, J.G., Runnegar, B.N. and Droser, M.L., 2014. Scratch Traces of Large Ediacara Bilaterian Animals. Journal of Paleontology, 88(2), pp.284-298.

Gibson, T.M., Shih, P.M., Cumming, V.M., Fischer, W.W., Crockford, P.W., Hodgskiss, M.S., Wörndle, S., Creaser, R.A., Rainbird, R.H., Skulski, T.M. and Halverson, G.P., 2017. Precise age of Bangiomorpha pubescens dates the origin of eukaryotic photosynthesis. Geology , v. 46; no. 2; p. 135–138.

Goddéris, Y., Donnadieu, Y., Nédélec, A., Dupré, B., Dessert, C., Grard, A., Ramstein, G., Francois, L.M., 2003. The Sturtian 'snowball'glaciation: fire and ice. Earth Planet. Sci. Lett. 211, 1–12.
Goscombe, B. and Gray, D.R., 2007. The Coastal Terrane of the Kaoko Belt, Namibia: outboard arc-terrane and tectonic significance. Precambrian Res. 155(1-2), pp.139-158.
Gray, D.R., Foster, D.A., Meert, J.G., Goscombe, B.D., Armstrong, R., Trouw, R.A.J. and Passchier, C.W., 2008. A Damara orogen perspective on the assembly of southwestern Gondwana. Geological Society, London, Special Publications, 294(1), pp.257-278.
Grotzinger, J.P., Bowring, S.A., Saylor, B.Z., Kaufman, A.J., 1995. Biostratigraphic and geochronologic constraints on early animal evolution. Science 598–604.
Grotzinger, J.P., James, N.P., 2000. Precambrian carbonates: evolution of understanding. In: Carbonate Sedimentology and Diagenesis in the Evolving Precambrian World, SEPM Spec. Publ. 67, pp. 3-20.
Grotzinger, J.P., Kasting, J.F., 1993. New constraints on Precambrian ocean composition. J. Geol. 101, 235–243.
Grotzinger, J.P., Knoll, A.H., 1995. Anomalous carbonate precipitates: is the Precambrian the key to the Permian? Palaios 578–596.
Grotzinger, J.P., Watters, W.A. and Knoll, A.H., 2000. Calcified metazoans in thrombolite-stromatolite reefs of the terminal Proterozoic Nama Group, Namibia. Paleobiology, 26(3), pp.334-359.
Halevy, I., Bachan, A., 2017. The geologic history of seawater pH. Science 355, 1069–1071.
Halverson, G.P., Hoffman, P.F., Schrag, D.P., Kaufman, A.J., 2002. A major perturbation of the carbon cycle before the Ghaub glaciation (Neoproterozoic) in Namibia: Prelude to snowball Earth? Geochem. Geophys. Geosystems 3, 1–24.
Halverson, G.P., Hoffman, P.F., Schrag, D.P., Maloof, A.C., Rice, A.H.N., 2005. Toward a Neoproterozoic composite carbon-isotope record. Geol. Soc. Am. Bull. 117, 1181–1207.
Halverson, G.P., Hurtgen, M.T., Porter, S.M., Collins, A.S., 2009. Neoproterozoic-Cambrian biogeochemical evolution. Dev. Precambrian Geol. 16, 351–365.
Halverson, G.P., Kunzmann, M., Strauss, J.V., Maloof, A.C., 2017. The Tonian-Cryogenian transition in Northeastern Svalbard. Precambrian Res. https://doi.org/10.1016/j.precamres.2017.12.010
Halverson, G.P. and Shields-Zhou, G., 2011. Chemostratigraphy and the Neoproterozoic glaciations. Geological Society, London, Memoirs, 36(1), pp.51-66.
Hardie, L.A., 2003. Secular variations in Precambrian seawater chemistry and the timing of Precambrian aragonite seas and calcite seas. Geology 31, 785–788.
Hardie, L.A., 1996. Secular variation in seawater chemistry: An explanation for the coupled secular variation in the mineralogies of marine limestones and potash evaporites over the past 600 my. Geology 24, 279–283.
Harlan, S.S., Heaman, L., LeCheminant, A.N. and Premo, W.R., 2003. Gunbarrel mafic magmatic event: A key 780 Ma time marker for Rodinia plate reconstructions. Geology, 31(12), pp.1053-1056.
Harland, W.B., 1990. A geologic time scale 1989. Cambridge University Press.
Harland, W.B., 1964. Critical evidence for a great infra-Cambrian glaciation. Geol. Rundsch. 54, 45–61.
Harland, W.B., Cox, A.V., Llewellyn, P.G., Pickton, C.A.G., Smith, A.G., Walters, R., 1982. A geologic time scale, 131 pp. Camb. Univ. Press N. Y.

Heaman, L.M. and Grotzinger, J.P., 1992. 1.08 Ga diabase sills in the Pahrump Group, California: Implications for development of the Cordilleran miogeocline. Geology, 20(7), pp.637-640.
Heaman, L.M., LeCheminant, A.N. and Rainbird, R.H., 1992. Nature and timing of Franklin igneous events, Canada: implications for a Late Proterozoic mantle plume and the break-up of Laurentia. Earth Planet. Sci. Lett., 109(1-2), pp.117-131.
Hedberg, R.M., 1979, Stratigraphy of the Ovamboland Basin, South West Africa: Precambrian Research Unit Bulletin 24, University of Cape Town, 325 p.Henry, G., Clendenin, C.W., Stanistreet, I.G. and Maiden, K.J., 1990. Multiple detachment model for the early rifting stage of the Late Proterozoic Damara orogen in Namibia. Geology, 18(1), pp.67-71.
Higgins, J.A., Fischer, W.W., Schrag, D.P., 2009. Oxygenation of the ocean and sediments: consequences for the seafloor carbonate factory. Earth Planet. Sci. Lett. 284, 25–33.
Higgins, J. A., and D. P. Schrag, Aftermath of a snowball Earth, Geochem. Geophys. Geosyst., 4(3), 1028, doi:10.1029/2002GC000403, 2003.Hill, A.C., Cotter, K.L., Grey, K., 2000. Mid-Neoproterozoic biostratigraphy and isotope stratigraphy in Australia. Precambrian Res. 100, 281–298.
Hill, A.C., Walter, M.R., 2000. Mid-Neoproterozoic (830–750 Ma) isotope stratigraphy of Australia and global correlation. Precambrian Res. 100, 181–211.
Hoffman, P.F., 1991. Did the breakout of Laurentia turn Gondwanaland inside-out. Science 252, 1409–1412.
Hoffman, P.F., Hawkins, D.P., Isachsen, C.E. and Bowring, S.A., 1996. Precise U–Pb zircon ages for early Damaran magmatism in the Summas Mountains and Welwitschia Inlier, northern Damara belt, Namibia. Comm. Geol. Surv. Namibia, 11, pp.47-52.
Hoffman, P.F., Kaufman, A.J., Halverson, G.P., Schrag, D.P., 1998a. A Neoproterozoic snowball earth. Science 281, 1342–1346.
Hoffman, P.F., Kaufman, A.J., Halverson, G.P. and Schrag, D.P., 1998. Comings and goings of global glaciations on a Neoproterozoic tropical platform in Namibia. GSA today, 8(5), pp.1-9.
Hoffman, P.F., 1999. The break-up of Rodinia, birth of Gondwana, true polar wander and the snowball Earth. J. Afr. Earth Sci. 28, 17–33.
Hoffman, P.F., Schrag, D.P., 2002. The snowball Earth hypothesis: testing the limits of global change. Terra Nova 14, 129–155.
Hoffman, P.F., 2005. 28th DeBeers Alex. Du Toit Memorial Lecture, 2004. On Cryogenian (Neoproterozoic) ice-sheet dynamics and the limitations of the glacial sedimentary record. South African Journal of Geology, 108(4), pp.557-577.
Hoffman, P.F., Halverson, G.P., Domack, E.W., Husson, J.M., Higgins, J.A. and Schrag, D.P., 2007. Are basal Ediacaran (635 Ma) post-glacial "cap dolostones" diachronous?. Earth Planet. Sci. Lett. 258(1-2), pp.114-131.
Hoffman, P.F. and Li, Z.X., 2009. A palaeogeographic context for Neoproterozoic glaciation. Palaeogeogr., Palaeoclimatol., Palaeoecol., 277(3-4), pp.158-172.
Hoffman, P.F., 2011. Strange bedfellows: glacial diamictite and cap carbonate from the Marinoan (635 Ma) glaciation in Namibia. Sedimentology, 58(1), pp.57-119.
Hoffman, P.F., Halverson, G.P., Domack, E.W., Maloof, A.C., Swanson-Hysell, N.L., Cox, G.M., 2012. Cryogenian glaciations on the southern tropical paleomargin of Laurentia (NE Svalbard and East Greenland), and a primary origin for the upper Russøya (Islay) carbon isotope excursion. Precambrian Res. 206, 137–158.

Hoffman, P.F., Bellefroid, E., Hodgin, E.B., Johnson, B.W., Kunzmann, M., Sansjofre, P., Strauss, J., Schrag, D.P., 2014. A Cryogenian–early Ediacaran carbonate shelf break dominated by glacial paleotopography, Fransfontein ridge, Kunene region, Namibia. GSA Annual Meeting, Vancouver 2014, Abstracts, Paper 130-2.
Hoffman, P.F., Bellefroid, E.J., Crockford, P.W., de Moor, A., Halverson, G.P., Hodgin, E.B., Hodgskiss, M.S.W., Holtzman, B.K., Jasechko, G.R., Johnson, B.W. and Lamothe, K.G., 2016. A misfit Cryogenian diamictite in the Vrede domes, Northern Damara Zone, Namibia: Chuos (Sturtian) or Ghaub (Marinoan) Formation? Moraine or paleovalley. Commun. Geol. Surv. Namibia, 17, pp.1-16.
Hoffman, P.F., 2016. Cryoconite pans on Snowball Earth: supraglacial oases for Cryogenian eukaryotes? Geobiology, 14(6), pp.531-542.
Hoffman, P.F., Lamothe, K.G., LoBianco, S.J., Hodgskiss, M.S., Bellefroid, E.J., Johnson, B.W., Hodgin, E.B. and Halverson, G.P., 2017. Sedimentary depocenters on Snowball Earth: Case studies from the Sturtian Chuos Formation in northern Namibia. Geosphere, 13(3), pp.811-837.
Hoffman, P.F. and Halverson, G.P., 2018. Discussion of "Depositional ages and provenance of the Neoproterozoic Damara Supergroup (northwest Namibia): Implications for the Angola–Congo and Kalahari cratons connection" by Débora B. Nascimento, Renata S. Schmitt, André Ribeiro, Rudolph AJ Trouw, Cees W. Passchier, and Miguel AS Basei. Gondwana Research.
Hoffmann, K.H., 1987. Application of tectonostratigraphic terrane analysis in the Damara Province of central and northern Namibia. In Abstract Volume, AL Du Toit Golden Jubilee Conference on Tectonostratigraphic Terrane Analysis. Royal Society and Geological Society of South Africa, Cape Town (pp. 25-27).
Hoffmann, K.H., 1989. New aspects of lithostratigraphic subdivision and correlation of late Proterozoic to early Cambrian rocks of the southern Damara Belt and their correlation with the central and northern Damara Belt and the Gariep Belt. Commun. Geol. Surv. Namib., 5, 61-70.
Hoffmann, K.H., Prave, A.R., 1996. A preliminary note on a revised subdivision and regional correlation of the Otavi Group based on glaciogenic diamictites and associated cap dolostones. Commun. Geol. Surv. Namib. 11, 77–82.
Hoffmann, K.H., Condon, D.J., Bowring, S.A. and Crowley, J.L., 2004. U-Pb zircon date from the Neoproterozoic Ghaub Formation, Namibia: constraints on Marinoan glaciation. Geology, 32(9), pp.817-820.
Hofmann, H.J., 2000. Archean stromatolites as microbial archives. In Microbial sediments (pp. 315-327). Springer, Berlin, Heidelberg.
Hood, A.v.S., Wallace, M.W., Drysdale, R.N., 2011. Neoproterozoic aragonite-dolomite seas? Widespread marine dolomite precipitation in Cryogenian reef complexes. Geology 39, 871–874.
Hyde, W.T., Crowley, T.J., Baum, S.K., Peltier, W.R., 2000. Neoproterozoic 'snowball Earth' simulations with a coupled climate/ice-sheet model. Nature 405, 425–429.
Ivantsov, A.Y. and Fedonkin, M.A., 2002. Conulariid–like fossil from the Vendian of Russia: a metazoan clade across the Proterozoic/Palaeozoic boundary. Palaeontology, 45(6), pp.1219-1229.
Jacobsen, S.B., Kaufman, A.J., 1999. The Sr, C and O isotopic evolution of Neoproterozoic seawater. Chem. Geol. 161, 37–57.

James, N.P., Narbonne, G.M., Kyser, T.K., 2001. Late Neoproterozoic cap carbonates: Mackenzie Mountains, northwestern Canada: precipitation and global glacial meltdown. Can. J. Earth Sci. 38, 1229–1262.
Jasper, M.J.U., Stanistreet, I.G., Charlesworth, E.G., 2000. Neoproterozoic inversion tectonics, half-graben depositories and glacial controversies, Gariep fold-thrust belt, southern Namibia. Commun. Geol. Surv. Namib. Henno Martin Commem. Vol. Windhoek Namib. Geol. Surv. Namib. 1887–1896.
Jenkins, G.S., Scotese, C.R., 1998. An early snowball earth? Science 282, 1643–1643.
Jiang, G., Kennedy, M.J., Christie-Blick, N., 2003. Stable isotopic evidence for methane seeps in Neoproterozoic postglacial cap carbonates. Nature 426, 822–826.
Johnston, D.T., Macdonald, F.A., Gill, B.C., Hoffman, P.F., Schrag, D.P., 2012. Uncovering the Neoproterozoic carbon cycle. Nature 483, 320–323.
Karhu, J.A., Holland, H.D., 1996. Carbon isotopes and the rise of atmospheric oxygen. Geology 24, 867–870.
Kaufman, A.J., Knoll, A.H., 1995. Neoproterozoic variations in the C-isotopic composition of seawater: stratigraphic and biogeochemical implications. Precambrian Res. 73, 27–49.
Kaufman, A.J., Williams, B.P., Johnston, D.T., Farquhar, J., Knoll, A.H., Butterfield, N.J., Rainbird, R., 2006. Environmental Change in the Prelude to a Neoproterozoic Ice Age: Sulfur Isotope Evidence from the Shaler Supergroup, Northwest Territories, Canada, in: AGU Spring Meeting Abstracts.
Kennedy, M.J., Christie-Blick, N., Prave, A.R., 2001a. Carbon isotopic composition of Neoproterozoic glacial carbonates as a test of paleoceanographic models for snowball Earth phenomena. Geology 29, 1135–1138.
Kennedy, M.J., Christie-Blick, N., Sohl, L.E., 2001b. Are Proterozoic cap carbonates and isotopic excursions a record of gas hydrate destabilization following Earth's coldest intervals? Geology 29, 443–446.
Kenny, R., Knauth, L.P., 2001. Stable isotope variations in the Neoproterozoic Beck Spring Dolomite and Mesoproterozoic Mescal Limestone paleokarst: Implications for life on land in the Precambrian. Geol. Soc. Am. Bull. 113, 650–658.
Key, R.M., Liyungu, A.K., Njamu, F.M., Somwe, V., Banda, J., Mosley, P.N., Armstrong, R.A., 2001. The western arm of the Lufilian Arc in NW Zambia and its potential for copper mineralization. J. Afr. Earth Sci. 33, 503–528.
Kilner, B.R., 2005. Low latitude Neoproterozoic glaciation: palaeomagnetic investigations of the Precambrian sequences of Oman and East Greenland. University of Oxford.
Kirschvink, J.L., 1992. Late Proterozoic low-latitude global glaciation: the snowball earth. In: Schopf, J.W., Klein, C. (Eds.), The Proterozoic Biosphere. Cambridge University Press, pp. 51–52. Knauth, L.P., Kennedy, M.J., 2009. The late Precambrian greening of the Earth. Nature 460, 728–732.
Knoll, A.H. 2014. Paleobiological perspectives on early eukaryotic evolution. Cold Spring Harb. Perspect. Biol. 6, 1–14 Knoll, A., Walter, M., Narbonne, G., Christie-Blick, N., 2006. The Ediacaran Period: a new addition to the geologic time scale. Lethaia 39, 13–30.
Knoll, A.H., 2000. Learning to tell Neoproterozoic time. Precambrian Res. 100, 3–20.
Knoll, A.H., 1994. Proterozoic and Early Cambrian protists: evidence for accelerating evolutionary tempo. Proc. Natl. Acad. Sci. 91, 6743–6750.

Knoll, A.H., Hayes, J.M., Kaufman, A.J., Swett, K., Lambert, I.B., 1986. Secular variation in carbon isotope ratios from Upper Proterozoic successions of Svalbard and East Greenland. Nature 321, 832–838.
Knoll, A.H., Walter, M.R., 1992. Latest Proterozoic stratigraphy and Earth history. Nature, v. 356, p. 673–678.
Kröner, A., Cordani, U., 2003. African, southern Indian and South American cratons were not part of the Rodinia supercontinent: evidence from field relationships and geochronology. Tectonophysics 375, 325–352.
Kump, L.R., 1991. Interpreting carbon-isotope excursions: Strangelove oceans. Geology, 19(4), pp.299-302.
Kump, L.R., 2014. Hypothesized link between Neoproterozoic greening of the land surface and the establishment of an oxygen-rich atmosphere. Proc. Natl. Acad. Sci. 111, 14062–14065.
Lacis, A.A., Schmidt, G.A., Rind, D. and Ruedy, R.A., 2010. Atmospheric CO_2: Principal control knob governing Earth's temperature. Science, 330(6002), pp.356-359.
Land, L.S., 1998. Failure to Precipitate Dolomite at 25 C from Dilute Solution Despite 1000-Fold Oversaturation after 32 Years. Aquat. Geochem. 4, 361–368.
Le Ber, E., Le Heron, D.P., Winterleitner, G., Bosence, D.W., Vining, B.A. and Kamona, F., 2013. Microbialite recovery in the aftermath of the Sturtian glaciation: Insights from the Rasthof Formation, Namibia. Sedimentary Geology, 294, pp.1-12.
Le Hir, G., Donnadieu, Y., Krinner, G., Ramstein, G., 2010. Toward the snowball Earth deglaciation…. Clim. Dyn. 35, 285–297.
Le Hir, G., Donnadieu, Y., Goddéris, Y., Pierrehumbert, R.T., Halverson, G.P., Macouin, M., Nédélec, A. and Ramstein, G., 2009. The snowball Earth aftermath: Exploring the limits of continental weathering processes. Earth and Planet. Sci. Lett. 277(3-4), pp.453-463.
Le Hir, G., Ramstein, G., Donnadieu, Y., Goddéris, Y., 2008. Scenario for the evolution of atmospheric pCO_2 during a snowball Earth. Geology 36, 47–50.
Leather, J., Allen, P.A., Brasier, M.D., Cozzi, A., 2002. Neoproterozoic snowball Earth under scrutiny: Evidence from the Fiq glaciation of Oman. Geology 30, 891–894.
Li, C.-W., Chen, J.-Y., Hua, T.-E., 1998. Precambrian sponges with cellular structures. Science 279, 879–882.
Li, Z.-X., Bogdanova, S.V., Collins, A.S., Davidson, A., De Waele, B., Ernst, R.E., Fitzsimons, I.C.W., Fuck, R.A., Gladkochub, D.P., Jacobs, J., 2008. Assembly, configuration, and break-up history of Rodinia: a synthesis. Precambrian Res. 160, 179–210.
Li, Z.X., Evans, D.A. and Halverson, G.P., 2013. Neoproterozoic glaciations in a revised global palaeogeography from the breakup of Rodinia to the assembly of Gondwanaland. Sedimentary Geology, 294, pp.219-232.
Love, G.D., Grosjean, E., Stalvies, C., Fike, D.A., Grotzinger, J.P., Bradley, A.S., Kelly, A.E., Bhatia, M., Meredith, W., Snape, C.E. and Bowring, S.A., 2009. Fossil steroids record the appearance of Demospongiae during the Cryogenian period. Nature, 457(7230), p.718.
Lynch-Stieglitz, J., Stocker, T.F., Broecker, W.S., Fairbanks, R.G., 1995. The influence of air-sea exchange on the isotopic composition of oceanic carbon: Observations and modeling. Glob. Biogeochem. Cycles 9, 653–665.

Macdonald, F.A., Schmitz, M.D., Crowley, J.L., Roots, C.F., Jones, D.S., Maloof, A.C., Strauss, J.V., Cohen, P.A., Johnston, D.T., Schrag, D.P., 2010a. Calibrating the Cryogenian. Science 327, 1241–1243.
Macdonald, F.A., Strauss, J.V., Rose, C.V., Dudás, F. \HO, Schrag, D.P., 2010b. Stratigraphy of the Port Nolloth Group of Namibia and South Africa and implications for the age of Neoproterozoic iron formations. Am. J. Sci. 310, 862–888.
Macdonald, F.A., Schmitz, M.D., Strauss, J.V., Halverson, G.P., Gibson, T.M., Eyster, A., Cox, G., Mamrol, P. and Crowley, J.L., 2017. Cryogenian of Yukon. Precambrian Research. https://doi.org/10.1016/j.precamres.2017.08.015
Macdonald, F.A., Wordsworth, R., 2017. Initiation of Snowball Earth with volcanic sulfur aerosol emissions. Geophys. Res. Lett. 44, 1938–1946.
Mahon, R.C., Dehler, C.M., Link, P.K., Karlstrom, K.E., Gehrels, G.E., 2014. Geochronologic and stratigraphic constraints on the Mesoproterozoic and Neoproterozoic Pahrump Group, Death Valley, California: A record of the assembly, stability, and breakup of Rodinia. Geol. Soc. Am. Bull. 126, 652–664.
Martin, M.W., Grazhdankin, D.V., Bowring, S.A., Evans, D.A.D., Fedonkin, M.A. and Kirschvink, J.L., 2000. Age of Neoproterozoic bilatarian body and trace fossils, White Sea, Russia: Implications for metazoan evolution. Science, 288(5467), pp.841-845.
Martin, H. and Porada, H., 1977a. The intracratonic branch of the Damara Orogen in South West Africa I. Discussion of geodynamic models. Precambrian Res. 5(4), pp.311-338.
Martin, H. and Porada, H., 1977b. The intracratonic branch of the Damara orogen in South West Africa II. Discussion of relationships with the Pan-African mobile belt system. Precambrian Res. 5(4), pp.339-357.
McKirdy, D.M., Burgess, J.M., Lemon, N.M., Yu, X., Cooper, A.M., Gostin, V.A., Jenkins, R.J. and Both, R.A., 2001. A chemostratigraphic overview of the late Cryogenian interglacial sequence in the Adelaide Fold-Thrust Belt, South Australia. Precambrian Research, 106(1-2), pp.149-186.
Meert, J.G., Lieberman, B.S., 2008. The Neoproterozoic assembly of Gondwana and its relationship to the Ediacaran–Cambrian radiation. Gondwana Res. 14, 5–21.
Meert, J.G., van der Voo, R., Ayub, S., 1995. Paleomagnetic investigation of the Neoproterozoic Gagwe lavas and Mbozi complex, Tanzania and the assembly of Gondwana. Precambrian Res. 74, 225–244.
Melezhik, V.A., Gorokhov, I.M., Kuznetsov, A.B., Fallick, A.E., 2001. Chemostratigraphy of Neoproterozoic carbonates: implications for 'blind dating.' Terra Nova 13, 1–11.
Miller, N.R., Alene, M., Sacchi, R., Stern, R.J., Conti, A., Kröner, A., Zuppi, G., 2003. Significance of the Tambien Group (Tigrai, N. Ethiopia) for Snowball Earth events in the Arabian–Nubian Shield. Precambrian Res. 121, 263–283.
Miller, R.M., 2008. The geology of Namibia. Neoproterozoic Low. Palaeoz. Windhoek Namib. Minist. Mines Energy Geol. Surv.
Miller, R.M., 1983. The Pan-African Damara Orogen of South West Africa/Namibia. Geol. Soc. S. Afr. Spec. Publ., 11: 431-515. Miller, R.M., 1980. Geology of a portion of central Damaraland, South West Africa/Namibia. Memoirs of the Geological Survey of SW Africa/Namibia, 6, pp.1-78.
Miller, R.M., 1974. The stratigraphic significance of the Naauwpoort Formation of east central Damaraland, South West Africa. South African Journal of Geology, 77(3), pp.363-367.

Milton, J.E., Hickey, K.A., Gleeson, S.A. and Friedman, R.M., 2017. New U-Pb constraints on the age of the Little Dal Basalts and Gunbarrel-related volcanism in Rodinia. Precambrian Res. 296, pp.168-180.
Moczydlowska, M., 2008. The Ediacaran microbiota and the survival of Snowball Earth conditions. Precambrian Res. 167, 1–15.
Mook, W.G., Bommerson, J.C., Staverman, W.H., 1974. Carbon isotope fractionation between dissolved bicarbonate and gaseous carbon dioxide. Earth Planet. Sci. Lett. 22, 169–176.
Morse, J.W., Arvidson, R.S., 2002. The dissolution kinetics of major sedimentary carbonate minerals. Earth-Sci. Rev. 58, 51–84.
Morse, J.W., Wang, Q., Tsio, M.Y., 1997. Influences of temperature and Mg: Ca ratio on $CaCO_3$ precipitates from seawater. Geology 25, 85–87.
Mustard, P.S., Roots, C.F., 1997. Rift-related volcanism, sedimentation, and tectonic setting of the Mount Harper Group, Ogilvie Mountains, Yukon Territory. Geol. Surv. Can. Bull. 492, 92 p.
Nascimento, D.B., Ribeiro, A., Trouw, R.A.J., Schmitt, R.S., Passchier, C.W., 2016. Stratigraphy of the Neoproterozoic Damara Sequence in northwest Namibia: Slope to basin sub-marine mass-transport deposits and olistolith fields. Precambrian Res. 278, 108–125.
Oriolo, S., Oyhantçabal, P., Wemmer, K. and Siegesmund, S., 2017. Contemporaneous assembly of Western Gondwana and final Rodinia break-up: Implications for the supercontinent cycle. Geoscience Frontiers, 8(6), pp.1431-1445.
Parfrey, L.W., Lahr, D.J., Knoll, A.H. and Katz, L.A., 2011. Estimating the timing of early eukaryotic diversification with multigene molecular clocks. Proc. Natl. Acad. Sci. 108(33), pp.13624-13629.
Partin, C.A. and Sadler, P.M., 2016. Slow net sediment accumulation sets snowball Earth apart from all younger glacial episodes. Geology, 44(12), pp.1019-1022.
Pardue, J.W., Scalan, R.S., Van Baalen, C., Parker, P.L., 1976. Maximum carbon isotope fractionation in photosynthesis by blue-green algae and a green alga. Geochim. Cosmochim. Acta 40, 309–312.
Peltier, W.R., Tarasov, L., Vettoretti, G., Solheim, L.P., 2004. Climate dynamics in deep time: modeling the “snowball bifurcation” and assessing the plausibility of its occurrence. Extreme Proterozoic Geol. Geochem. Clim. 107–124.
Peucker-Ehrenbrink, B., Waters, C.A., Kurz, M.D. and Hoffman, P.F., 2016. No evidence of extraterrestrial noble metal and helium anomalies at Marinoan glacial termination. Earth and Planetary Science Letters, 437, pp.76-88.
Pierre, C., 1989. Sedimentation and diagenesis in restricted marine basins. Handb. Environ. Isot. Geochem. 3, 257–315.
Pierrehumbert, R.T., 2004. High levels of atmospheric carbon dioxide necessary for the termination of global glaciation. Nature 429, 646–649.
Pisarevsky, S.A., Wingate, M.T., Powell, C.M., Johnson, S., Evans, D.A., 2003. Models of Rodinia assembly and fragmentation. Geol. Soc. Lond. Spec. Publ. 206, 35–55.
Plumb, K.A., 1991. New Precambrian time scale. Episodes 14, 139–140.
Porter, S.M., 2004. The fossil record of early eukaryotic diversification. Paleontol. Soc. Pap. 10, 35.
Prave, A.R., 1999. Two diamictites, two cap carbonates, two δ13C excursions, two rifts: the Neoproterozoic Kingston Peak Formation, Death Valley, California. Geology 27, 339–342.

Prave, A.R., Condon, D.J., Hoffmann, K.H., Tapster, S., Fallick, A.E., 2016. Duration and nature of the end-Cryogenian (Marinoan) glaciation. Geology 44, 631–634.
Prave, A.R., Fallick, A.E., Thomas, C.W., Graham, C.M., 2009. A composite C-isotope profile for the Neoproterozoic Dalradian Supergroup of Scotland and Ireland. J. Geol. Soc. 166, 845–857.
Prave, A.R., 1996. Tale of three cratons: Tectonostratigraphic anatomy of the Damara orogen in northwestern Namibia and the assembly of Gondwana. Geology, 24(12), pp.1115-1118.
Prince, J.K., 2014. Sequence stratigraphic, lithostratigraphic and stable isotopic analysis of the Minto Inlet Formation and Kilian Formation of the Shaler Supergroup, Northwest Territories [MS thesis]. Ott. Carlet. Univ.
Rainbird, R.H., 1991. Stratigraphy, Sedimentology and Tectonic Setting of the Upper Shaler Group, Victoria Island, Northwest Territories. in Current Research 1994-C: Canadian Shield: Ottawa, Geological Survey of Canada Paper 92-01C, p. 61–70
Ramanathan, V., Cess, R.D., Harrison, E.F., Minnis, P., Barkstrom, B.R., Ahmad, E., Hartmann, D., 1989. Cloud-radiative forcing and climate- Results from the Earth Radiation Budget Experiment. Science 243, 57–63.
Remane, J., Bassett, M.G., Cowie, J.W., Gohrbandt, K.H., Lane, H.R., Michelsen, O., Naiwen, W., 1996. Revised guidelines for the establishment of global chronostratigraphic standards by the International Commission on Stratigraphy (ICS). Episodes-Newsmag. Int. Union Geol. Sci. 19, 77–81.
Riding, R., 2006. Microbial carbonate abundance compared with fluctuations in metazoan diversity over geological time. Sedimentary Geology, 185(3-4), pp.229-238.
Rooney, A.D., Macdonald, F.A., Strauss, J.V., Dudás, F.Ö., Hallmann, C., Selby, D., 2014. Re-Os geochronology and coupled Os-Sr isotope constraints on the Sturtian snowball Earth. Proc. Natl. Acad. Sci. 111, 51–56.
Rooney, A.D., Strauss, J.V., Brandon, A.D., Macdonald, F.A., 2015. A Cryogenian chronology: Two long-lasting synchronous Neoproterozoic glaciations. Geology 43, 459–462.
Rose, C.V., Swanson-Hysell, N.L., Husson, J.M., Poppick, L.N., Cottle, J.M., Schoene, B., Maloof, A.C., 2012. Constraints on the origin and relative timing of the Trezona δ 13 C anomaly below the end-Cryogenian glaciation. Earth Planet. Sci. Lett. 319, 241–250.
Rothman, D.H., Hayes, J.M., Summons, R.E., 2003. Dynamics of the Neoproterozoic carbon cycle. Proc. Natl. Acad. Sci. 100, 8124–8129.
Rubinson, M., Clayton, R.N., 1969. Carbon-13 fractionation between aragonite and calcite. Geochim. Cosmochim. Acta 33, 997–1002.
SACS, South Africa Committee for Stratigraphy, 1980. Stratigraphy of South Africa. Kent, L.E. (comp); Part 1. Lithostratigraphy of the Republic of South Africa, South West Africa/Namibia, and the Republics of Bophuthatswana, Transkei and Venda. Handb. geol. Surv. S. Afr., 8, 690 pp.
Sawaki, Y., Kawai, T., Shibuya, T., Tahata, M., Omori, S., Komiya, T., Yoshida, N., Hirata, T., Ohno, T., Windley, B.F., 2010. 87 Sr/86 Sr chemostratigraphy of Neoproterozoic Dalradian carbonates below the Port Askaig glaciogenic formation, Scotland. Precambrian Res. 179, 150–164.
Schidlowski, M., Eichmann, R., Junge, C.E., 1975. Precambrian sedimentary carbonates: carbon and oxygen isotope geochemistry and implications for the terrestrial oxygen budget. Precambrian Res. 2, 1–69.

Schmitt, R.S., Trouw, R.A., Passchier, C.W., Medeiros, S.R. and Armstrong, R., 2012. 530 Ma syntectonic syenites and granites in NW Namibia—Their relation with collision along the junction of the Damara and Kaoko belts. Gondwana Research, 21(2-3), pp.362-377.
Scholle, P.A., Arthur, M.A., 1980. Carbon isotope fluctuations in Cretaceous pelagic limestones: potential stratigraphic and petroleum exploration tool. AAPG Bull. 64, 67–87.
Schrag, D.P., Berner, R.A., Hoffman, P.F., Halverson, G.P., 2002. On the initiation of a snowball Earth. Geochem. Geophys. Geosystems 3, 1–21. https://doi.org/10.1029/2001GC000219
Schrag, D.P., Higgins, J.A., Macdonald, F.A., Johnston, D.T., 2013. Authigenic carbonate and the history of the global carbon cycle. Science 339, 540–543.
Sellers, W.D., 1969. A global climatic model based on the energy balance of the earth-atmosphere system. J. Appl. Meteorol. 8, 392–400.
Shaw, A.M., Hilton, D.R., Fischer, T.P., Walker, J.A., Alvarado, G.E., 2003. Contrasting He–C relationships in Nicaragua and Costa Rica: insights into C cycling through subduction zones. Earth Planet. Sci. Lett. 214, 499–513.
Shields, G., Veizer, J., 2002. Precambrian marine carbonate isotope database: Version 1.1. Geochem. Geophys. Geosystems 3.
Shields, G.A., Mills, B.J., 2017. Tectonic controls on the long-term carbon isotope mass balance. Proc. Natl. Acad. Sci. 201614506.
Shields-Zhou, G.A., Porter, S., Halverson, G.P., 2016. A new rock-based definition for the Cryogenian Period (circa 720-635 Ma). Episodes 39, 3–8.
Smith, E.F., MacDonald, F.A., Crowley, J.L., Hodgin, E.B., Schrag, D.P., 2016. Tectonostratigraphic evolution of the c. 780–730 Ma Beck Spring Dolomite: Basin Formation in the core of Rodinia. Geol. Soc. Lond. Spec. Publ. 424, 213–239.
Sohl, L.E., Christie-Blick, N. and Kent, D.V., 1999. Paleomagnetic polarity reversals in Marinoan (ca. 600 Ma) glacial deposits of Australia: implications for the duration of low-latitude glaciation in Neoproterozoic time. Geological Society of America Bulletin, 111(8), pp.1120-1139.
Spencer, A.M., 1971. Late pre-Cambrian glaciation in Scotland. Geological Society of London.
Stanistreet, I.G., Kukla, P.A. and Henry, G., 1991. Sedimentary basinal responses to a late Precambrian Wilson cycle: The Damara orogen and Nama foreland, Namibia. Journal of African Earth Sciences (and the Middle East), 13(1), pp.141-156.
Stern, R.J., 1994. Arc assembly and continental collision in the Neoproterozoic East African Orogen: implications for the consolidation of Gondwanaland. Annu. Rev. Earth Planet. Sci. 22, 319–351.
Stern, R.J., Avigad, D., Miller, N.R., Beyth, M., 2006. Evidence for the snowball Earth hypothesis in the Arabian-Nubian Shield and the East African Orogen. J. Afr. Earth Sci. 44, 1–20.
Stowe, C.W., Hartnady, C.J.H., Joubert, P., 1984. Proterozoic tectonic provinces of southern Africa. Precambrian Res. 25, 229–231.
Strauss, J.V., MacDonald, F.A., Halverson, G.P., Tosca, N.J., Schrag, D.P., Knoll, A.H., 2015. Stratigraphic evolution of the Neoproterozoic Callison Lake Formation: Linking the break-up of Rodinia to the Islay carbon isotope excursion. Am. J. Sci. 315, 881–944.
Strauss, J.V., Rooney, A.D., Macdonald, F.A., Brandon, A.D., Knoll, A.H., 2014. 740 Ma vase-shaped microfossils from Yukon, Canada: Implications for Neoproterozoic chronology and biostratigraphy. Geology 42, 659–662.

Sumner, D.Y., Grotzinger, J.P., 1996. Were kinetics of Archean calcium carbonate precipitation related to oxygen concentration? Geology 24, 119–122.
Sun, X., Turchyn, A.V., 2014. Significant contribution of authigenic carbonate to marine carbon burial. Nat. Geosci. 7, 201.
Swanson-Hysell, N.L., Maloof, A.C., Condon, D.J., Jenkin, G.R., Alene, M., Tremblay, M.M., Tesema, T., Rooney, A.D., Haileab, B., 2015. Stratigraphy and geochronology of the Tambien Group, Ethiopia: Evidence for globally synchronous carbon isotope change in the Neoproterozoic. Geology 43, 323–326.
Swanson-Hysell, N.L., Rose, C.V., Calmet, C.C., Halverson, G.P., Hurtgen, M.T., Maloof, A.C., 2010. Cryogenian glaciation and the onset of carbon-isotope decoupling. Science 328, 608–611.
Swart, P.K., Kennedy, M.J., 2012. Does the global stratigraphic reproducibility of δ13C in Neoproterozoic carbonates require a marine origin? A Pliocene–Pleistocene comparison. Geology 40, 87–90.
Teixeira, W., Figueiredo, M.C.H., 1991. An outline of Early Proterozoic crustal evolution in the São Francisco craton, Brazil: a review. Precambrian Res. 53, 1–22.
Thomson, D., Rainbird, R.H., Planavsky, N., Lyons, T.W., Bekker, A., 2015. Chemostratigraphy of the Shaler Supergroup, Victoria Island, NW Canada: A record of ocean composition prior to the Cryogenian glaciations. Precambrian Res. 263, 232–245.
Toteu, S.F., Van Schmus, W.R., Penaye, J., Nyobe, J.B., 1994. U-Pb and Sm-N edvidence for Eburnian and Pan-African high-grade metamorphism in cratonic rocks of southern Cameroon. Precambrian Res. 67, 321–347.
Trenberth, K.E., 1999. Conceptual framework for changes of extremes of the hydrological cycle with climate change. In Weather and Climate Extremes (pp. 327-339). Springer, Dordrecht.
Trindade, R.I.F., Font, E., D'Agrella-Filho, M.S., Nogueira, A.C.R., Riccomini, C., 2003. Low-latitude and multiple geomagnetic reversals in the Neoproterozoic Puga cap carbonate, Amazon craton. Terra Nova 15, 441–446.
Trindade, R.I., Macouin, M., 2007. Palaeolatitude of glacial deposits and palaeogeography of Neoproterozoic ice ages. Comptes Rendus Geosci. 339, 200–211.
Tucker, M.E., 1982. Precambrian dolomites: petrographic and isotopic evidence that they differ from Phanerozoic dolomites. Geology 10, 7–12.
Tyrrell, T., 1999. The relative influences of nitrogen and phosphorus on oceanic primary production. Nature, 400(6744), p.525.
Tziperman, E., Halevy, I., Johnston, D.T., Knoll, A.H., Schrag, D.P., 2011. Biologically induced initiation of Neoproterozoic snowball-Earth events. Proc. Natl. Acad. Sci. 108, 15091–15096.
van Acken, D., Thomson, D., Rainbird, R.H. and Creaser, R.A., 2013. Constraining the depositional history of the Neoproterozoic Shaler Supergroup, Amundsen Basin, NW Canada: Rhenium-osmium dating of black shales from the Wynniatt and Boot Inlet Formations. Precambrian Res. 236, pp.124-131.
Van Iten, H., de Moraes Leme, J., Simões, M.G., Marques, A.C. and Collins, A.G., 2006. Reassessment of the phylogenetic position of conulariids (? Ediacaran-Triassic) within the subphylum medusozoa (phylum cnidaria). Journal of Systematic Palaeontology, 4(2), pp.109-118.

Vincent, W.F., Gibson, J.A.E., Pienitz, R., Villeneuve, V., Broady, P.A., Hamilton, P.B., Howard-Williams, C., 2000. Ice shelf microbial ecosystems in the high Arctic and implications for life on Snowball Earth. Naturwissenschaften 87, 137–141.
Vogel, J.C., Grootes, P.M., Mook, W.G., 1970. Isotopic fractionation between gaseous and dissolved carbon dioxide. Z. Für Phys. Hadrons Nucl. 230, 225–238.
Weiss, R., 1974. Carbon dioxide in water and seawater: the solubility of a non-ideal gas. Mar. Chem. 2, 203–215.
Wood, R.A., Grotzinger, J.P., Dickson, J.A.D., 2002. Proterozoic modular biomineralized metazoan from the Nama Group, Namibia. Science 296, 2383–2386.
Wu, H., Jiang, X., Wang, J., 2013. Ages and Provenance of the Neoproterozoic Dajiangbian Formation and Aiqiling Formation in Southeast Hunan Province: U-Pb Geochronological Evidence of Detrital Zircons. Geol. Rev. 59, 853–868.
Yang, J., Jansen, M.F., Macdonald, F.A., Abbot, D.S., 2017. Persistence of a freshwater surface ocean after a snowball Earth. Geology 45, 615–618.
Zeebe, R.E., Wolf-Gladrow, D.A., 2001. CO_2 in seawater: equilibrium, kinetics, isotopes. Gulf Professional Publishing.
Zhang, Q., Chu, X., Feng, L., 2009. Discussion on the Neoproterozoic glaciations in the South China Block and their related paleolatitudes. Chin. Sci. Bull. 54, 1797–1800.
Zhuravlev, A.Y., Liñán, E., Vintaned, J.A.G., Debrenne, F. and Fedorov, A.B., 2012. New finds of skeletal fossils in the terminal Neoproterozoic of the Siberian Platform and Spain. Acta Palaeontologica Polonica, 57(1), pp.205-224.
Ziegler, A.M., Hulver, M.L., Lottes, A.L., Schmachtenberg, W.F., 1984. Uniformitarianism and palaeoclimates: inferences from the distribution of carbonate rocks. Geol. J. Spec. Issue 3–25.

Appendices

K1607	Ugab subgroup		86 samples	
	Rondehoek farm, Khorixas District, Kunene Region, Namibia			
	Summas Mountains, Northern Damara Zone			
	Ugab Subgroup, Otavi Group			
	S20˚28.557' E015˚19.950' (at base of section)			
	Base: first non-volcanic exposure past rhyolitic ashflow tuff; Top: last exposure before Chuos Fm outcrops			
	late Tonian			
	dolostone			
Unit	Sample	d13C	d18O	Composite height (m)
	332.9	5.36	-3.87	511.5
	330.3	5.86	-3.32	508.5
	325.5	5.88	-2.06	503.0
	322.5	5.91	-2.2	499.6
	320.0	5.73	-2.35	496.8
	317.2	5.40	-2.55	493.6
	314.1	5.71	-2.55	490.1
	311.0	4.86	-5.78	486.5
	248.8	4.29	-2.06	363.7
	245.8	4.30	-2.45	357.2
	242.4	4.44	-2.31	349.9
	239.5	4.55	-1.46	343.6
	236.7	3.72	-3.14	337.5
	233.4	4.05	-2.66	330.4
	230.4	4.44	-2.00	323.9
	228.5	3.93	-3.51	319.8
	226.8	4.21	-3.06	316.1
	224.0	4.08	-3.02	310.0
	220.9	4.34	-2.22	303.3
	217.9	4.40	-2.77	296.8
	214.8	4.42	-2.39	290.1
	211.6	4.70	-1.84	283.2
	208.2	4.52	-2.31	275.8
	204.6	4.52	-2.42	268.1
	201.7	4.69	-2.19	261.8
	198.9	4.59	-2.34	255.7

	195.8	4.94	-1.41	249.0
	192.8	4.56	-1.91	242.5
	190.0	4.07	-3.76	236.5
	186.9	4.13	-3.27	229.8
	183.8	4.57	-2.58	223.0
	180.1	2.68	-3.08	215.0
	177.2	4.81	-1.16	208.8
	174.2	3.26	-2.04	202.3
	171.0	3.33	-4.03	195.3
	152.8	0.00	-3.67	147.8
	143.9	0.35	-5.85	142.2
	136.8	-0.21	-10.80	137.7
	132.7	-1.37	-12.99	135.1
	128.2	-1.12	-12.47	132.2
	125.2	-0.70	-10.65	130.3
	122.0	-0.20	-6.86	128.3
	115.9	-1.99	-9.72	124.5
	103.0	-2.97	-14.26	116.3
	101.8	-2.47	-14.24	115.5
	93.5	-0.24	-7.49	110.2
	92.2	-0.73	-6.13	109.4
	90.8	-0.09	-4.79	108.4
	88.8	-0.07	-5.18	107.1
	86.1	0.32	-9.75	105.3
	84.0	1.49	-11.83	103.9
	82.5	0.24	-10.01	102.9
	79.6	1.59	-9.54	100.9
	76.7	1.82	-10.01	99.0
	75.1	-0.49	-11.27	97.9
	73.4	0.27	-8.75	96.8
	71.8	1.57	-8.63	95.7
	70.1	1.11	-9.85	94.6
	68.2	-0.84	-18.51	93.3
	66.0	0.94	-9.4	91.9
	64.4	0.39	-11.73	90.8
	59.9	0.69	-9.47	87.8
	58.5	0.36	-9.68	86.8
	56.4	0.1	-10.74	85.4
	55.6	-0.14	-11.95	84.9
	54.3	-0.77	-7.69	84.0
	52.8	1.16	-4.85	83.0
	51.6	-0.48	-10.1	82.2
	50.2	-0.4	-4.96	81.3

	48.8	0.32	-7.89	80.4
	42.3	-0.61	-15.81	76.0
	38.6	-1.2	-11.52	73.6
	35.5	-1.03	-7.3	71.5
	34.2	-0.29	-8.82	70.6
	33.6	-0.57	-7.08	70.2
	30.1	-0.71	-2.54	67.9
	29.1	0.06	-8.84	67.2
	27.8	-0.21	-9.16	66.3
	26.8	-1.11	-8.91	65.7
	22.4	-2.55	-7.96	62.7
	21.2	0.07	-8.57	61.9
	20.6	-2.11	-8.9	61.5
	19.3	-1.62	-9.4	60.7
	18.7	-1.18	-8.59	60.3
	17.8	-1.02	-8.52	59.7

Appendix 1: Carbon and oxygen isotope data from section K1607.

G1532	Ugab subgroup		87 samples	
	Vrede farm, lower Huab River, southern Kunene Region, Namibia			
	Vrede South Dome, Northern Zone, Damara Belt			
	Ugab subgroup, Otavi Group			
	S20°23'35.4" E14°09'30.2" (base of section)			
	Base: first not-too-deformed bed closest to center of dome; Top: ? (contact with Rasthoff Fm?)			
	late Tonian			
	limestone and dolostone			
Unit	Sample	d13C	d18O	Composite height (m)
	440.3	-2.19	-4.76	972.6
	436.0	-0.84	-5.24	969.4
	428.0	-0.73	-2.58	963.5
	422.6	-0.72	-3.76	959.5
	420.0	-3.97	-6.08	957.6
	416.0	-2.31	-4.27	954.7
	412.0	-2.20	-3.14	951.8
	408.0	-2.90	-1.66	948.8
	404.0	-1.68	-2.77	945.9

	399.9	-1.15	-3.53	942.9
	395.5	-2.26	-2.74	939.6
	392.0	-2.06	-3.47	937.1
	387.0	-1.23	-4.31	933.4
	382.0	-0.28	-4.79	929.7
	376.0	-0.66	-4.54	925.3
	371.3	-0.33	-2.85	921.8
	365.0	0.62	-2.75	917.2
	356.9	-0.65	-3.48	911.3
	354.4	-1.09	-3.66	909.4
	350.0	-0.31	-2.33	906.2
	345.0	1.11	-2.63	902.5
	341.0	1.53	-1.92	899.6
	336.9	1.68	-0.91	896.6
	332.1	1.92	-1.28	893.0
	328.2	2.07	-1.46	890.2
	324.0	0.18	-1.10	887.1
	319.2	0.93	-0.58	883.5
	310.1	1.50	0.23	876.9
	304.9	0.38	-8.92	873.0
	300.3	0.95	-4.26	869.6
	279.5	-0.29	-6.02	854.4
	268.9	1.44	-2.16	846.6
	265.3	3.72	0.30	843.9
	261.0	2.89	0.04	840.8
	256.4	2.33	0.06	837.4
	252.7	1.83	-0.22	834.7
	248.6	4.06	-0.83	831.6
	244.3	2.19	-1.71	828.5
	240.2	1.64	-2.38	825.5
	236.3	1.81	-2.58	822.6
	232.4	2.30	-0.05	819.7
	228.0	2.32	-1.22	816.5
	223.5	3.08	-1.76	813.2
	220.7	1.77	-3.03	811.1
	217.0	2.48	-1.06	808.4
	213.3	1.73	-2.53	805.7
	209.6	2.28	-0.86	803.0
	207.0	1.48	-3.07	801.1
	200.0	0.66	-2.85	795.9
	196.2	0.69	-7.29	793.1
	194.0	-1.09	-10.68	791.5
	162.8	1.15	-7.94	768.6

	160.6	1.60	-8.70	767.0
	156.7	-1.39	-12.81	764.1
	155.1	1.65	-9.34	762.9
	128.8	1.46	-9.08	743.6
	124.5	2.31	-8.31	740.4
	120.0	2.71	-5.97	737.1
	115.5	2.17	-6.50	733.8
	110.0	1.11	-5.92	729.8
	106.5	1.72	-6.15	727.2
	100.7	1.61	-7.59	722.9
	96.5	1.47	-7.18	719.8
	91.7	1.23	-8.18	716.3
	86.6	2.06	-6.07	712.6
	81.6	2.49	-6.75	708.9
	78.8	2.34	-6.69	706.8
	75.3	1.97	-6.81	704.3
	70.6	2.07	-7.10	700.8
	66.7	1.80	-7.19	697.1
	62.3	2.61	-6.35	692.3
	59.7	1.89	-8.24	689.4
	56.0	2.80	-6.92	685.4
	51.5	2.90	-7.18	680.5
	48.4	3.54	-5.36	677.1
	42.2	2.85	-6.83	670.4
	38.9	4.14	-7.30	666.8
	34.8	3.81	-8.30	662.3
	30.0	4.58	-7.91	657.1
	26.2	4.42	-8.88	652.9
	22.7	2.25	-2.64	649.1
	19.8	3.80	-4.39	645.9
	16.0	4.02	-7.35	641.8
	12.0	5.48	-6.02	637.4
	7.8	5.87	-5.82	632.9
	4.6	5.50	-5.79	629.4
	1.4	5.42	-5.19	625.9

Appendix 2: Carbon and oxygen isotope data from section G1532.

P1607	**Ugab subgroup**		21 samples	
	Vrede farm, lower Huab River, southern Kunene Region, Namibia			
	Vrede South Dome (NW), Northern Zone, Damara Belt (Note: samples are from P1607 566.0 - 655.0)			
	Ugab Subgroup, Otavi Group, Damara Supergroup			
	20.3880 S, 14.1511 E (base of uppermost ribbonite unit)			
	Base: base of the uppermost ribbonite unit of the Ugab Sbgp; Top:			
	late Tonian			
	dolostone			
Unit	Sample	d13C	d18O	Composite height (m)
	88.8	-1.15	-3.74	973.5
	85.5	-1.18	-0.05	971.1
	81.0	-2.45	-7.14	967.7
	76.5	-1.49	-3.46	964.4
	72.3	-0.31	-2.96	961.4
	67.5	-1.32	-6.63	957.8
	63.0	-0.71	-4.35	954.5
	58.5	-0.64	-5.54	951.2
	54.1	-0.71	-3.90	948.0
	49.5	-1.29	-5.63	944.6
	45.0	-1.51	-5.08	941.3
	40.5	-1.94	-0.10	938.0
	36.0	-1.50	-1.22	934.7
	31.5	-1.35	-2.34	931.4
	26.9	-2.04	-3.43	928.0
	22.5	-1.52	-4.16	924.7
	18.0	-2.24	-4.86	921.4
	13.5	-1.59	-5.39	918.1
	9.0	-1.01	-8.19	914.8
	4.6	0.10	-5.91	911.6
	0.4	-0.61	-4.36	908.5

Appendix 3: Carbon and oxygen isotope data from section P1607.